

A Kinetic and Mechanistic Study of Cyclic Amine Functionalized Platinum(II) Complexes with Bio-Relevant Nitrogen Nucleophiles

By

Mthobisi Ian Nxumalo

BSc. (Hons.) (University of KwaZulu-Natal)



School of Chemistry and Physics

University of KwaZulu-Natal

Pietermaritzburg

3209

**A Kinetic and Mechanistic Study of Cyclic
Amine Functionalized Platinum(II) Complexes
with Bio-Relevant Nitrogen Nucleophiles**

By

Mthobisi Ian Nxumalo

A thesis submitted in fulfilment of the requirements for the degree

of

Master of Science

School of Chemistry and Physics

University of KwaZulu-Natal

Pietermaritzburg

3209

Table of Contents

<i>Declaration</i>	i
<i>Abstract</i>	iii
<i>Acknowledgements</i>	v
<i>Abbreviations</i>	vi
<i>Ligands</i>	vi
<i>Other Abbreviations</i>	vi
<i>List of Figures</i>	viii
<i>List of Tables</i>	x
<i>List of Schemes</i>	xi
Chapter 1 - Introduction	1
1.1 Platinum Chemistry	1
1.2 Properties Displayed By Recent Complexes Of Interest	2
1.3 Current Findings on Anticancer Platinum(II) Drugs	3
1.4 Aim Of This Study	11
1.5 References	16
Chapter 2 – Substitution Reactions	22
2.1 Introduction	22
2.2 Mechanism of Ligand Substitution of Square-Planar Complexes	24
2.2.1 Stoichiometric and Intimate mechanisms.....	24
2.2.2 The Dissociative Mechanism (D).....	26
2.2.3 The Associative Mechanism (A).....	27
2.2.4 The Interchange Mechanism (I).....	28
2.3 Substitution Reactions of Square-Planar Complexes	29
2.3.1 Kinetics and Mechanism of Ligand Substitution at Square-Planar Centres	30
2.4 Factors Influencing the Rate of Substitution Reactions	34
2.4.1 The Effect of the Non-Labile Ligand.....	34
2.4.1.1 The <i>trans</i> Effect.....	35
2.4.2 The Molecular Orbital Theory.....	41
2.4.2.1 σ - <i>trans</i> effect.....	41
2.4.2.2 π - <i>trans</i> effect.....	43

2.4.2.3	The <i>Cis</i> Effect.....	44
2.4.2.4	The Steric Effect.....	45
2.4.3	The Effect of the Entering Nucleophile.....	47
2.4.4	The Effect of the Leaving Group.....	51
2.4.5	The Effect of the Solvent.....	52
2.5	References.....	54

Chapter 3 - Reaction Kinetics.....58

3.1	Introduction.....	58
3.2	The Rate Law.....	60
3.3	Integrated Rate Expressions.....	61
3.3.1	Irreversible First-Order Reactions.....	61
3.3.2	Reversible First-Order Reactions.....	62
3.3.3	Irreversible Second-Order Reactions.....	63
3.3.4	Reversible Second-Order Reactions.....	65
3.4	Activation Parameters and Temperature Dependence.....	67
3.4.1	The Arrhenius Equation.....	67
3.4.2	Transition-State Theory.....	68
3.4.3	Effect of Pressure on the Rate Constant.....	68
3.5	Instrumental Techniques Associated with the Study of Chemical Kinetics.....	69
3.5.1	UV/Visible Spectrophotometry.....	71
3.5.2	Flow Methods.....	73
3.6	References.....	75

Chapter 4: Experimental.....78

4.1	Materials and Procedures.....	78
4.2	Instrumentation and Physical Measurements.....	79
4.2.1	Characterization.....	79
4.2.2	Computational Modelling.....	79
4.2.3	Kinetic Analyses.....	80
4.3	Synthesis of the Ligand Systems (L1 - L4).....	81

4.3.1	Synthesis of ligands (4'-[2-(1-Piperidinyloxy)]-2,2':6',2''-terpyridine (L1S1), (4'-[2-(1-Pyrrolidino)ethoxy]-2,2':6',2''-terpyridine (L2S1) and (4'-[2-(1-Morpholino)ethoxy]-2,2':6',2''-terpyridine (L3S1)).	81
4.3.2	Synthesis of 2,6-Di(2-pyridyl)- β -(aminoethoxy)pyridine (L4S1).	83
4.4	Synthesis of Platinum(II) Complexes	85
4.4.1	Synthesis of [Pt(L1S1)Cl]·BF ₄ (C1S1).	85
4.4.2	Synthesis of Dichloro(1,5-cyclooctadiene)platinum(II), [Pt(COD)Cl ₂].	86
4.4.3	Platination of L1S1 , L2S1 , L3S1 and L4S1 .	87
4.5	Kinetic Measurements	89
4.5.1	Preparation of Platinum Complexes for Kinetic Analyses	89
4.5.2	Preparation of Nucleophile Solutions for Kinetic Analysis	89
4.6	References	91

Chapter 5: Results and Discussion..... 93

5.1	Synthesis and Characterization of the Terpyridyl Ligands	93
5.2	Synthesis and Characterization of the Platinum Complexes	94
5.3	Kinetic Measurements	95
5.4	Kinetic results	101
5.5	Computational Analysis	102
5.6	Discussion	105
5.6.1	Reactivity of the Platinum(II) complexes	105
5.6.2	Reactivity of the Nucleophiles	110
5.7	Conclusions	111
5.8	References	113
Appendix A - Synthesis Supporting Information		115
Appendix B - Kinetic and Thermodynamic Data		137

Declaration

I, Mthobisi Ian Nxumalo hereby declare that this thesis present results and observations from the original work investigated in the School of Chemistry and Physics, University of KwaZulu-Natal, Pietermaritzburg, South Africa, under the supervision of Dr. Desigan Reddy and has not been submitted for the fulfilment of any degree or diploma at any University.

.....
Mthobisi Ian Nxumalo

I hereby certify that this statement is correct.

.....
Dr. Desigan Reddy
(Supervisor)

School of Chemistry and Physics
University of KwaZulu-Natal
Pietermaritzburg
October 2018

The financial assistance of the National Research Foundation (NRF) towards this research is hereby acknowledged.

*Dedicated with lots of love to my late Father, Vincent Fana Nxumalo
and wonderful Mother Gladys Fisani Nxumalo who has always been
there for me and the entire family.*

Abstract

In this study, four square-planar platinum(II) complexes were synthesized namely **C1S1**, **C2S1**, **C3S1** and **C4S1**. The novel platinum(II) complex (**C4S1**) was synthesized using methods detailed in **Chapter 4** and characterized using NMR spectroscopy, mass spectroscopy and elemental analysis.

The kinetics of the chloride ligand substitution from a series of square-planar platinum(II) complexes named above were investigated using a series of five-membered heterocyclic neutral nitrogen-donor nucleophiles: Imidazole (**Im**), Pyrazole (**Pyz**), 1-methylimidazole (**1-MIm**) and L-Histidine (**His**) in an aqueous solution of constant ionic strength.

The kinetics of chloride substitution were investigated as a function nucleophile concentration and temperature under *pseudo* first-order conditions using UV/Visible spectrophotometry and stopped-flow spectrophotometric techniques. The observed *pseudo* first-order rate constants obeyed the simple rate law, $k_{\text{obs}} = k_2[\text{Nu}]$. The observed rate constants along with activation parameters obtained i.e. low activation enthalpies and large, negative activation entropies support an associative mechanism. The data obtained shows that the reactivity of these complexes are influenced by both electronic and steric effects with steric effects being the dominant factor contributing to the overall trend. The kinetic results also show that appended cyclic amine pendant, *trans* to the leaving chloride group acts as a σ -donor into the terpyridine chelate ligand and is effective only up to the first cyclic amine. The change of the appended cyclic amine to another e.g. from pyrrolidine of **C2S1** to piperidine of **C1S1** shows that the inductive σ -donor ability of the cyclic amine pendant no longer controls the reactivity of the metal centre. The substitution reactivity of the complexes with cyclic amines pendant (**C1S1**, **C2S1** and **C3S1**) are controlled by the steric influence of the appended cyclic amine which decreases as the cyclic amine pendant gets larger in size, **C3S1** < **C1S1** < **C2S1**. This in turn blocks the metal center hence lowering the affinity for the incoming azole nucleophile. The results further support that, the slightest modifications to the terpy moiety leads to changes in the reactivity. The overall trend in the rate of chloride substitution is: **C4S1** > **C2S1** > **C1S1** > **C3S1**. The observed reactivity trends were

supported by density functional theory (DFT) calculation (dipole moment, HOMO-LUMO energy gap, electrophilicity index etc.). In addition, the substitution kinetics was influenced solely by the basicity of the incoming azole nucleophile. The order of reactivity of the nucleophiles with the complexes is in the form, **1-MIm** > **Im** > **His** > **Pyz**.

Acknowledgements

I would like to express my sincere gratitude to Dr. D. Reddy for his enthusiastic supervision of this project, his endless patience and most of all, the many hours of invaluable time that he has invested in guiding this research.

A huge thanks goes to my Mother, Gladys Fisani Nxumalo for her continuous support throughout this MSc. Your love, kindness and more importantly your faith and support to keep on going is highly appreciated.

I am grateful towards the School of Chemistry and Physics at the University of KwaZulu-Natal (Pietermaritzburg) as well Dr. D. Reddy for providing laboratory space and equipment, and to the National Research Foundation (NRF) for their financial assistance.

I will also like to thank the following people:

1. Mrs. Caryl Janse van Rensburg and Mr. Craig Grimmer for helping out with the instrumentation (NMR and Mass Spectroscopy) and giving fruitful advice.
2. The SCP technical staff as a whole.
3. Mr. Shawn Ball for his services at the Chemical Stores.
4. Mr. Clarence Mortlock and Mr. Banzi Sikwekwe at the Glassblowing Workshop.
5. The academic staff in chemistry for their continued support especially, Dr. B. A Xulu, Dr. A Mambanda and Prof. F. R. Van Heerden.
6. ChemBurg and all chemistry postgraduates for endless support and laughter.

Finally, and most importantly, I would like to thank God for helping through and guiding me until the end.

Abbreviations

Ligands

L1S1	4'-[2-(1-Piperidinyloxy)ethoxy]-2,2':6',2''-terpyridine
L2S1	4'-[2-(1-Pyrrolidino)ethoxy]-2,2':6',2''-terpyridine
L3S1	4'-[2-(1-Morpholino)ethoxy]-2,2':6',2''-terpyridine
L4S1	2,6-Di(2-pyridyl)- β -(aminoethoxy)pyridine

Other Abbreviations

A	Absorbance or Arrhenius pre-exponential factor (as indicated)
A	Associative mechanism
CDCl ₃	Deuterated chloroform
°C	Celsius
COD	1,5-cyclooctadiene
Dien	Diethylenetriamine
D	Dissociative
d	Doublet
dd	Doublet of doublets
DFT	<u>D</u> ensity <u>F</u> unctional <u>T</u> heory
DMSO	Dimethyl Sulfoxide
<i>E_a</i>	Arrhenius activation energy
ΔE	Energy gap between the HOMO and LUMO
<i>E</i>	Extinction coefficient
ESI	Electron spray ionisation
FTIR	Fourier Transform Infrared
ΔG	Gibbs free energy of activation
<i>h</i>	Planck's constant
ΔH^\ddagger	Change in enthalpy of activation
His	L-Histidine
HOMO	<u>H</u> ighest <u>O</u> ccupied <u>M</u> olecular <u>O</u> rbital
<i>I</i>	Ionic strength
I	Interchange mechanism
I _a	Associatively activated interchange mechanism
I _d	Dissociatively activated interchange mechanism

<i>I</i>	Intensity
Im	Imidazole
IR	Infrared
<i>k</i>	Rate constant
K	Kelvin
K_{eqm}	Equilibrium constant
k_b	Boltzmann's constant
k_{obs}	Observed pseudo first-order rate constant
<i>l</i>	Pathlength
LC-MS	Liquid Chromatography Mass Spectrometry
LFER	<u>L</u> inear <u>F</u> ree <u>E</u> nergy <u>R</u> elationship
LUMO	<u>L</u> owest <u>U</u> noccupied <u>M</u> olecular <u>O</u> rbital
1-MIm	1-methylimidazole
n°_{Pt}	Nucleophilicity of the incoming group Pt
NBO	Natural Bond Orbital
NMR	<u>N</u> uclear <u>M</u> agnetic <u>R</u> esonance
Nu	Nucleophile
ppm	Parts per million
Pyz	Pyrazole
<i>R</i>	Gas constant
RMS	<u>R</u> oot <u>M</u> ean <u>S</u> quares
RMSD	<u>R</u> oot <u>M</u> ean <u>S</u> quares <u>D</u> eviation
S	Nucleophilic discrimination factor
s, d, t	(NMR) singlet, double, triplet
ΔS^{\ddagger}	Change in entropy of activation
<i>T</i>	Transmittance
Terpy	2,2':6',2''-terpyridine

List of Figures

Figure:	Title
Figure 1.1	Platinum(II) complexes comprising the π -acceptor pyridine ligands investigated by van Eldik <i>et al.</i>
Figure 1.2	Platinum(II) complexes investigated by Jaganyi <i>et al.</i> and Reddy <i>et al.</i>
Figure 1.3	Platinum(II) complexes studied by Ongoma <i>et al.</i> (PtCl , CH₃PhPtCl , CH₃PhisoqPtCl and pyPhenPtCl) and Nkabinde <i>et al.</i> (PtCl , PtL3)
Figure 1.4	4'-functionalised monoclear Pt(II) terpyridine complexes studied by Shaira <i>et al.</i>
Figure 1.5	View of the inclination angle, α , for the pendant unit attached at the 4'-position of the terpy backbone, for the Ptppyeg and Ptppyteg complexes studied by Shaira <i>et al.</i>
Figure 1.6	(a) Hydrogen-bonding interactions with a metal ion located centrally in a guanine quartet; (b) schematic view of an intramolecular quadruplex DNA structure.
Figure 1.7	Structures of the terpyridyl complexes employed by Teulade-Fichou <i>et al.</i> to investigate the relationship between the metal centre geometry and quadruplex DNA binding affinity.
Figure 1.8	4'-functionalized Anthracene-Terpyridine complexes reported by Gama <i>et al.</i>
Figure 1.9	4'-functionalized terpyridines reported by Vilar <i>et al.</i>
Figure 2.1	The potential energy profile diagrams showing the various substitution mechanisms occurring at square-planar complexes as proposed by Langford-Gary.
Figure 2.2	Energy profiles for an associative substitution mechanism showing the relationship between the intermediate and the transition states: (a) shows the bond-breaking transition state at a higher energy, whereas (b) shows the bond-making transition state at a higher energy.
Figure 2.3	Plot of reaction rates of <i>trans</i> -Pt(py) ₂ Cl ₂ against concentration of different nucleophiles in methanol at 30 °C.

Figure 2.4:	Diagram showing both associative k_2 (direct nucleophilic attack) and k_1 (solvolysis) pathways for square planar complexes.
Figure 2.5	Illustration of the changes in energy and stereochemistry that occur during the act of associative substitution of the leaving group, X, by the entering group, Y, of a square-planar complex: Energy levels at 2 , 4 , 6 , and 8 indicate the different transition states whilst the remaining levels show energies of the reaction intermediates.
Figure 2.6	Schematic diagram showing the labilization of the leaving group (X) by the <i>trans</i> ligand (T).
Figure 2.7	(a) σ -donation from the filled ligand p_x orbital to vacant metal $5d_{x^2-y^2}$ orbital. (b) π -back-donation from the filled metal d_{xz} orbital to the antibonding linear combination of carbons' p_x orbitals in C_2H_4 .
Figure 2.8	Distribution of charge in induced dipoles in the L–Pt–Cl coordinate of <i>trans</i> -[PtA ₂ LX] due to polarization
Figure 2.9	Illustration of the R ₃ P–Pt double bond. If ligands PR ₃ and X are in the xy plane and the d -orbitals shown are either d_{xy} or d_{yz} .
Figure 2.10	Activated trigonal bipyramidal complex for the <i>trans</i> -PtA ₂ LXY.
Figure 2.11	The Molecular Orbital Diagram of [PtCl ₄].
Figure 2.12	Diagram showing the ground state σ -bonding of L–Pt–X using the σ_x MO. (a) The equal σ - bond strengths of L and X . (b) The σ -bonding strength of the <i>trans</i> -ligand, L is greater than that of X thus weakening the Pt–X bond.
Figure 2.13	The σ - <i>trans</i> -effect due to the stabilization of the trigonal bipyramidal intermediate. (a) Only the p_x orbital is available for σ -bonding of ligands L and X (b) p_x and the p_z orbitals are available for σ -bonding of ligands L , X and Y in a trigonal plane.
Figure 2.14	The steric effect of the aryl square-planar complex and trigonal bipyramidal intermediate of the <i>cis</i> isomer and <i>trans</i> isomer.
Figure 2.15	Rates of Pt(II) complexes correlated with <i>trans</i> -[Pt(py) ₂ Cl ₂] as reference, for different entering nucleophiles: • = <i>trans</i> -[Pt(PEt ₃) ₂ Cl ₂] in methanol at 30 °C; ▲ = [Pt(en)Cl ₂] in water at 35 °C.

Figure 3.1	A summary of reaction techniques and their associated time scales available for the monitoring chemical kinetics.
Figure 3.2	A schematic diagram of a UV/Visible spectrophotometer set-up.
Figure 3.3	The spectrum obtained from Cary UV/Visible spectrophotometer for the substitution of Cl ⁻ from [Pt{4'-(<i>o</i> -tolyl)-2,2':6',2''-terpyridine}Cl]CF ₃ SO ₃ (2.50 x 10 ⁻⁵ mol dm ⁻³) with 1-methylimidazole (5.00 x 10 ⁻⁴ mol dm ⁻³) in methanol solution (<i>I</i> = 0.10 M (0.09 M LiCF ₃ SO ₃ + 0.01 M NaCl)) at 333 nm and 298.15K.
Figure 3.4	A schematic diagram of a <i>stopped-flow</i> spectrophotometer apparatus
Figure 5.1	Absorbance spectra of C2S1 (2.50x10 ⁻⁴ M) and His (2.50x10 ⁻³ M) at an aqueous ionic strength of 0.01 M (0.009 M LiCF ₃ SO ₃ and 0.001 M LiCl) at 298.15 K
Figure 5.2	Corresponding kinetic trace and the fit of C2S1 (2.50x10 ⁻⁴ M) and His (2.50x10 ⁻³ M) at 390 nm at an ionic strength of 0.01 M (0.009 M LiCF ₃ SO ₃ and 0.001 M LiCl) at 298.15 K.
Figure 5.3	Kinetic trace for the reaction of C4S1 (2.5 X10 ⁻⁴ M) and His (5.0 x10 ⁻³ M) obtained from stopped-flow spectrophotometry in ultrapure water (<i>I</i> = 0.01 M, 0.009 M LiCF ₃ SO ₃ + 0.001 M LiCl) at 380.0 nm and 298.15 K
Figure 5.4	Dependence of the <i>pseudo</i> first-order rate constant (<i>k</i> _{obs}) on the concentrations of the azole nucleophiles for the chloride substitution from C1S1 in an aqueous solution of constant ionic strength (<i>I</i> = 0.01 M (0.009 M LiCF ₃ SO ₃ + 0.001 M LiCl)) at 298.15 K).
Figure 5.5	Eyring plots used to calculate the activation parameters for the direct nucleophilic substitution reaction for C1S1 with the four azole nucleophiles at various temperatures (ranging between 15 – 35 °C).

List of Tables

Table 1.1	Second-order rate constants, <i>k</i>₂ (±Std. Error), M⁻¹ s⁻¹ at 25 °C for aqua substitution
Table 2.1	Estimated <i>σ</i> - and <i>π-trans</i> effects of selected ligands.
Table 2.2	The effect of <i>trans</i> ligand, L on the reactivity rate of <i>cis</i> - Pt(PEt ₃) ₂ LCl with <i>py</i> .

Table 2.3	Steric effects on the rate constants for the chloride substitution by pyridine in <i>cis</i> - and <i>trans</i> -[Pt(PEt ₃) ₂ (L)Cl].
Table 2.4	A selection of n°_{pt} values listed according to donor atom for <i>trans</i> -[Pt(py) ₂ Cl ₂].
Table 2.5	Effect of solvent on the rate of chloride exchange from <i>trans</i> -[Pt(<i>py</i>) ₂ Cl ₂] at 25 °C
Table 5.1	Summary of second-order reaction rates (k_2) (\pm standard deviations) and activation parameters for the chloride displacement from the investigated platinum(II) complexes by Im , 1-MIm , Pyz and His in an aqueous solution of constant ionic strength, ($I = 0.010 \text{ M (0.009 M LiCF}_3\text{SO}_3 + 0.001 \text{ M LiCl)}$) at 25.0 °C
Table 5.2	Selected bond lengths (Å) and bond angles(°) for the platinum complexes C1S1 , C2S1 , C3S1 and C4S1 obtained from the computational studies.
Table 5.3	DFT-calculated (B3LYP/LANL2DZ) molecular orbitals diagrams showing the HOMO's and LUMO's and the planarity of the tridentate Pt(II) complexes.
Table 5.4	Energies of HOMO-LUMO gap, the DFT-calculated Dipole moment (D), the calculated parameter and electronic chemical potential, μ obtained for the platinum(II) complexes studied.
Table 5.5	The DFT-calculated NBO charges on the central Pt, the donor nitrogen atoms and the leaving group, Cl.
Table 5.6	The pKa values and the DFT-calculated NBO charges for the donor atoms of the nucleophiles (1-MIm , Im , His and Pyz) used in this study.

List of Schemes

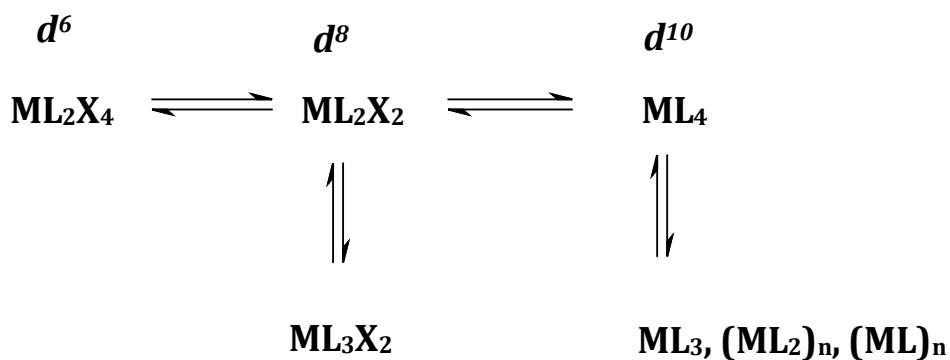
Scheme 1.1	Characteristic reactions for these complexes are ligand substitution, reductive elimination and oxidative addition reactions.
Scheme 2.1	The modes of bond-breaking in substitution reactions.
Scheme 2.2	Heterolytic bond-making process via a two-electron oxidative addition.

Scheme 2.3	Heterolytic bond-breaking process via a two-electron reductive elimination.
Scheme 2.4	The reaction pathways proposed by Langford and Gray.
Scheme 2.5	Reaction pathway following an associative mode of substitution.
Scheme 2.6	Schematic illustration for ligand substitution in d^8 square-planar complexes.
Scheme 2.7	Direct replacement of the leaving ligand (X) by an incoming ligand (Y).
Scheme 2.8	The approximate order of decreasing the <i>trans-effect</i> in platinum(II) complexes.
Scheme 2.9	Schematic representation for the preparation of <i>cis</i> -Pt(NH ₃) ₂ Cl ₂ from the treatment of [Pt(Cl) ₄] ²⁻ with neutral NH ₃ .
Scheme 2.10	Schematic representation for the preparation of <i>trans</i> -Pt(NH ₃) ₂ Cl ₂ from treatment of [Pt(NH ₃) ₄] ²⁺ with chloride ions.
Scheme 5.1	Proposed mechanism of chloride substitution from the 4'-substituted terpy platinum(II) complexes byazole ligands.

Chapter 1 - Introduction

1.1 Platinum Chemistry

Platinum is one of the most versatile and most studied transition metals.¹⁻² It is recognisably different in nature compared to other transition metals due to its ability to form a wide range of complexes and the relative ease with which it takes part in different reactions.² Platinum is mainly extracted from platinum bearing ores such as sperrylite (PtAs₂) and platinum(II) sulfide (PtS). It is usually found in the +2 and +4 oxidation states with the +2 species being the best studied.³ Moreover, the +2 and +4 oxidation states form a wide range of kinetically and thermodynamically stable complexes.² In the +2 oxidation state, the metal has 8 *d*-orbital electrons and importantly adopts a square planar geometry because of the vacant *d*_(x²-y²) orbitals. In addition, it was previously noted that a change in the oxidation state of the platinum often results in a change in the coordination chemistry adopted by the metal centre. This change is either by reductive elimination or oxidative addition (**Scheme 1.1**).²



L = neutral ligand, X = anionic ligand

Scheme 1.1: Characteristic reactions for these complexes are ligand substitution, reductive elimination and oxidative addition reactions.²

Platinum also has a variety of possible applications in industry. It can be used as a catalyst in the chemical industry. In the automobile industry, its use is mainly to minimize environmental problems where it oxidizes carbon monoxide, hydrogen and any unburnt

hydrocarbons as well as reducing the oxides in the nitrogen.⁴⁻⁸ In the electronics industry, it is used for temperature measurements and as a corrosion resistant electrical contact for high and low voltage applications, sensors for gas detectors to optical data storage disks and hybridised integrated circuits.³⁻⁸ It can further be used to manufacture jewellery when alloyed with either iridium or ruthenium.⁴⁻⁸ The greatest breakthrough to date on potential platinum applications was the discovery of the biologically active platinum antitumour complex, *cis*-diaminechloroplatinum(II) (cisplatin).⁹ This complex together its structural-activity relationships (SAR) derivatives have been found to be effective against testicular cancer as well as ovarian, head, neck, bladder, lung, prostate and cervical tumours.⁹⁻¹⁵ Regardless of its success, it was found that coordination of certain sulfur containing proteins and amino acids¹⁶⁻¹⁷ to the platinum drug leads to some toxic side effects (neuro- and nephrotoxicity)^{16,18} affecting the biodistribution of the drug and its pharmacokinetics resulting in reduced drug accumulation as well as reduced formation of the required Pt-DNA adducts.^{16, 19} Moreover, the derivatives of cisplatin namely carboplatin, oxaliplatin etc. have been approved in some countries but they did not necessary show a breakthrough in the pharmaceutical industry due to their structural similarities to the parent hence showing a similar cross-resistance.^{11, 20-25}

1.2 Properties Displayed By Recent Complexes Of Interest

In the past decade, research has focused on platinum complexes with more bulky chelating ligands examining the effects of labile and non-labile groups on substitution reactions.²⁶ These bulky ligands result in compounds with higher tumour growth inhibitory²⁶ and reduces the kinetic instability by slowing down the substitution reaction of the leaving group.²⁶ This type of complex is said to be inert due to the slow rates in which complex formation with DNA nucleobases happens.^{1, 27-30} It is further deduced that the steric and/or electronic properties displayed by the non-leaving ligand bestow some form of a push and/or pull effect on the reactivity of the complexes and are crucial in controlling the lability of the leaving group(s) in square-planar platinum(II) complexes.^{1, 28} On the other hand,

extremely reactive complexes are not ideal as they can be deactivated easily by non-target nitrogen- and sulfur-donor nucleophiles before reaching the nucleus.^{1,27-30} In addition, some of the key aspects highlighting the efficacy (cytotoxicity) of antitumour Pt(II)-based drugs are the kinetic control posed by the lability of the low spin d^8 square-planar complexes as well as the potential for intercalation of the planar spectator-backbone between DNA base pairs.^{12, 31-32} Indeed, several studies have reported and illustrated that the rate of ligand substitution on square-planar complexes is highly dictated by the structure and electronic properties of the chelate ligand backbone.³³⁻³⁹ Furthermore, the kinetic and thermodynamic data affirms that the degree of lability of the leaving group by a *trans*-coordinated ligand is influenced by the σ - and π -structural features of the ancillary groups.¹ Also, the lability of the leaving ligand can be subdivided into the *trans* π -effect or *trans* σ -effect since its substitution rate is dependent on the strength of the σ -donor or π -acceptor ability of the spectator ligand.¹ Therefore, knowledge and complete understanding of these properties, other related traits as well as their substitution behaviour with sulfur and nitrogen containing nucleophiles can be useful in designing future metal-based complexes with predictable reactivity as well as their mode of action binding to DNA base pairs. Particularly, knowledge on their kinetic and mechanistic substitution behaviour would be important in the synthesis of new platinum anticancer drugs. However, interest here will be given mainly on the mononuclear platinum(II) *N*-donor complexes particularly terpyridines with the presence of substituents, primarily in the 4'-position.

1.3 Current Findings on Terpyridine/Tridentate Anticancer Platinum(II) Drugs

Previous studies on platinum(II) complexes with chelating ligands containing pyridine were to precisely understand the mechanism of antitumour action of the platinum drugs.^{33, 40} Those studies were proposed due to the ability of the inert ligands combining different steric and electronic effects and as a result causing different solubility and reactivity in their application as antitumour drugs.³⁵ It has been reported that the π -acceptor groups of these

N⁴C/N⁴N/C tridentate non-leaving ligand induce high lability of the co-ligand of the complex.^{33, 36-37, 40-41} Van Eldik *et al.*^{33-34, 40} studied the effect of increasing the number of π -acceptor pyridine ligands of the aqua platinum(II) tri(N-donor) complexes (**Figure 1.1**), viz. [Pt(diethylenetriamine)OH₂]²⁺ (**aaa**), [Pt(2,6-bis-aminomethylpyridine)OH₂]²⁺ (**apa**), [Pt(N-(pyridyl-2-methyl)-1,2diamino-ethane)OH₂]²⁺ (**aap**), [Pt(*bis*(2-pyridylmethyl)amine)OH₂]²⁺ (**pap**), [Pt(2,2'-bipyridyl)(NH₃)(OH₂)]²⁺ (**app**) and [Pt(terpy)OH₂]²⁺ (**ppp**).

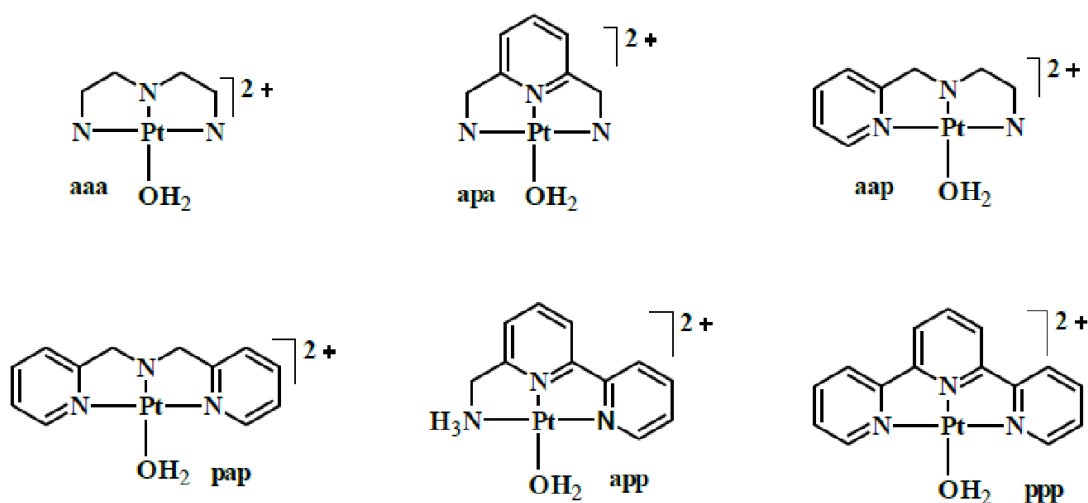


Figure 1.1: Platinum(II) complexes comprising the π -acceptor pyridine ligands investigated by van Eldik *et al.*⁴⁰

Substitution rates of these complexes with some neutral and anionic nucleophiles *i.e.* thiourea (TU), 1,3-dimethyl-2-thiourea (DMTU), 1,1,3,3-tetramethyl-2-thiourea (TMTU), thiocyanate (SCN⁻) and iodide (I⁻) revealed an increase in the rates of substitution reactions with an increase in the π -acceptor pyridine ligands on the metal center. The nucleophilic kinetic substitution data of the aqua leaving group from the metal complexes by TU, TMTU and I⁻ showed increased k_2 values of 5.6×10^3 , 4.8×10^4 , and 3.3×10^4 M⁻¹s⁻¹ respectively, for changing the coordination structure of the complexes from **aaa** to **ppp** (**Table 1.1**).

Table 1.1: Second-order rate constants, k_2 (\pm Std. Error), $M^{-1} s^{-1}$ at 25 °C for aqua substitution.⁴⁰

Complexes	pK_a	k_2 ($M^{-1}s^{-1}$)		
		TU	TMTU	I ⁻
(aaa)	6.26	29 (± 0.4)	3.2 (± 0.04)	6.73 (± 0.05) $\times 10^2$
(aap)	5.71	1.10(± 0.01) $\times 10^2$	2.93 (± 0.02) $\times 10^2$	2.46(± 0.01) $\times 10^2$
(apa)	6.04	1.00(± 0.01) $\times 10^2$	1.23 (± 0.01) $\times 10^2$	1.80(± 0.01) $\times 10^2$
(pap)	5.53	3.93(± 0.02) $\times 10^2$	1.82(± 0.02) $\times 10^2$	8.54(± 0.06) $\times 10^2$
(app)	6.37	1.43(± 0.01) $\times 10^3$	1.20(± 0.03) $\times 10^3$	1.70 (± 0.2) $\times 10^3$
(ppp)	4.62	1.63 (± 0.2) $\times 10^5$	1.53 (± 0.3) $\times 10^4$	2.20 (± 0.4) $\times 10^4$

Essentially, the high reactivity of Pt(**ppp**) relative to Pt(**aaa**) arises from the strong π -acceptor effect of the terpy ligand because of its conjugated nature. This is best explained in terms of the electronic communication with the ligands. Therefore, due to an increased electronic communication within the entire ligand of the three pyridyl rings in terpy, the electrophilicity of Pt(**ppp**) was highest compared to its analogues. It was noted that the strong π -acceptor effect of the terpy enhances the π^* -acceptance of electron density from the metal d -orbitals.

Furthermore, the bond between the metal centre and the incoming nucleophile in the transition state is stabilized by the increased aromaticity around the metal centre. This allows for the spreading of the electron density over the aromatic system thereby increasing the substitution rate. In addition, it was established that the π -effect posed by the tridentate ligand was strongest when the π^* -acceptor pyridine ring is coordinated *trans* to the leaving group. Further studies by Basolo *et al.*¹ and Tobe *et al.*²⁹ also showed that the *trans* effect is dominant over the π -acceptor effect.

Further studies by Jaganyi *et al.*^{34, 39, 42} investigated the influence of the chelate substituent⁴²⁻⁴³, the *cis* σ -effect and the extent of π -backbonding on the ligand substitution to understand the effect of changing the structure of typical strong **N⁺C/N⁺N/C** π -acceptor ligands on the reactivity of their analogous platinum(II) complexes. A series of platinum(II) complexes *viz.*

[PtL(terpy)Cl]⁺ (where L = H or tri-*tert*-butyl), [Pt{4'-phenyl-terpy}Cl]⁺, [Pt{4'-(*o*-R-phenyl)-terpy}Cl]⁺ (where R = CF₃, CH₃ and Cl⁻) and [Pt{4'-(*o*-CF₃-phenyl)-6-phenyl-bipy}Cl]⁺ (**Figure 1.2**) were studied against anionic and neutral sulfur containing nucleophiles (TU, TMTU, DMTU, SCN⁻ and I⁻).

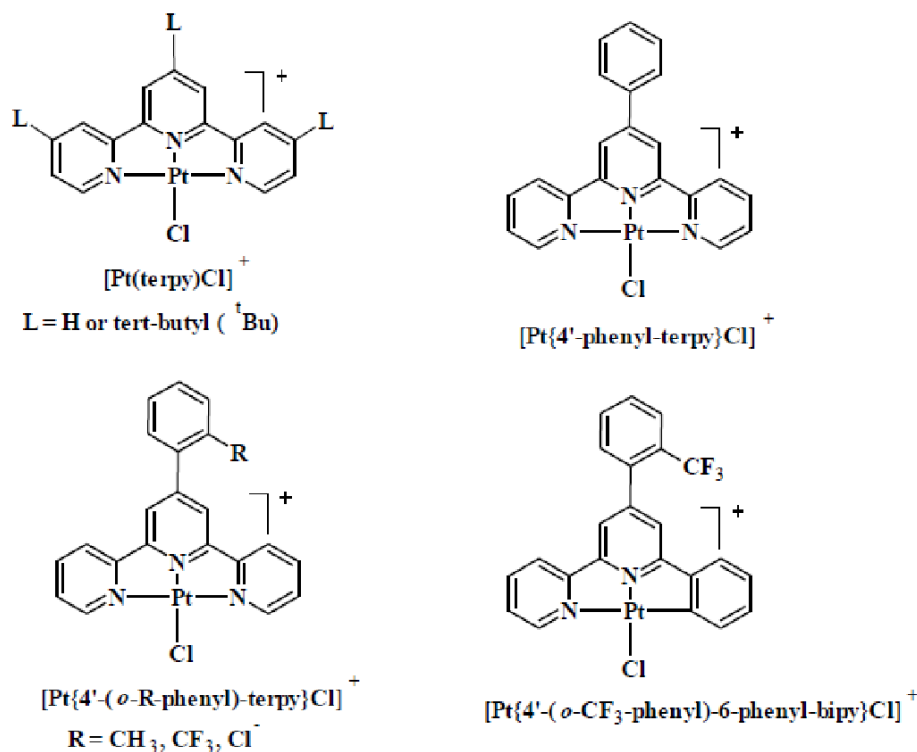


Figure 1.2: Platinum(II) complexes investigated by Jaganyi *et al.*^{39, 43} and Reddy *et al.*⁴⁴

Results on the rate of substitution showed that the effect of replacing the N-donor atom of the terpy with a carbon atom (C) in the *cis*-position to form analogous Pt(N^AN^AC)Cl complexes supported the findings of van Eldik *et al.*³⁴ indicating an unexpected lower reactivity when thiourea was the incoming nucleophile. Moreover, a similar trend of reactivity was observed by Reddy *et al.*⁴⁴ when each complex was reacted with azoles of different basicity and steric hindrance. This decrease in reactivity is attributed to the Pt–C *cis* σ -effect which decelerates the substitution reaction by accumulating electron density along the *cis* bond to the platinum(II) atom due to the stronger σ -donor phenyl ring. This in turn destabilizes the transition state which subsequently decreases the reactivity. However,

when the central pyridyl ring of [Pt(terpy)Cl]⁺ was replaced by a deprotonated phenyl ring to form the analogous Pt(N[^]C[^]N)Cl complex, reactivity with thiourea as the incoming nucleophile increased significantly. This was attributed to the strong *trans* labilization effect caused by the Pt-C bond of the deprotonated phenyl ring *trans* to the leaving group.³⁴ This strong *trans* labilization effect of the Pt (N[^]C[^]N)Cl complex is present both in the ground and transition states.⁴⁵⁻⁴⁷

Furthermore, the effect of the ancillary group on the π -acceptor property of the terpyridine complexes showed that electron donating groups ([PtL(terpy)Cl]⁺ (where L = H or tri-*tert*-butyl)) reduce the π -acceptor property of the ligand and subsequently reduces the electrophilicity of the metal center thereby decreasing the reactivity of the complex.^{39, 42, 48-50} The influence of ligand substitution is also controlled by the extent of the π -back-bonding where the presence of the substituents in the *ortho* position of the ancillary phenyl ring alters the reactivity either by enhancing or reducing the π -back-bonding ability of the terpy moiety.^{39, 43, 47, 51-56} Substituents with π -electron withdrawing effect or σ -inductive donation stabilize the transition state and enhance the rate of chloride substitution which further increases the π -back-bonding of the terpy system thereby increasing the electrophilicity of the platinum center as well as the reactivity of the metal center.^{39, 42, 48-50}

Another study by Pitteri *et al.*⁴¹ investigated the substitution reactions of the platinum(II) terpy complex [Pt(terpy)Cl]⁺, with neutral five-membered nitrogen heterocyclic donors *i.e.* thiazole, oxazole, imidazole, pyrazole and 3,5-dimethylpyrazole of different basicities. Results showed an increase in the rate of substitution with an increase in the basicity of the nucleophiles while increased steric hindrance decreased the substitution rate. Therefore, it can be concluded that substitution reactions of terpyridine complexes with nitrogen heterocyclic donors depend on both the basicity of the nucleophile as well as its steric hindrance.

Other studies by Ongoma *et al.*⁵⁷, Shaira *et al.*⁵⁸ and Nkabinde *et al.*⁵⁹ studied a set of complexes of the platinum(II) complexes with either *cis*-pyridine or *cis*-quinoline and *cis*-2-pyridine or *cis*-2'-quinoline additions on the terpy ligand to understand the effect of the extended π -conjugated systems (**Figure 1.3**).

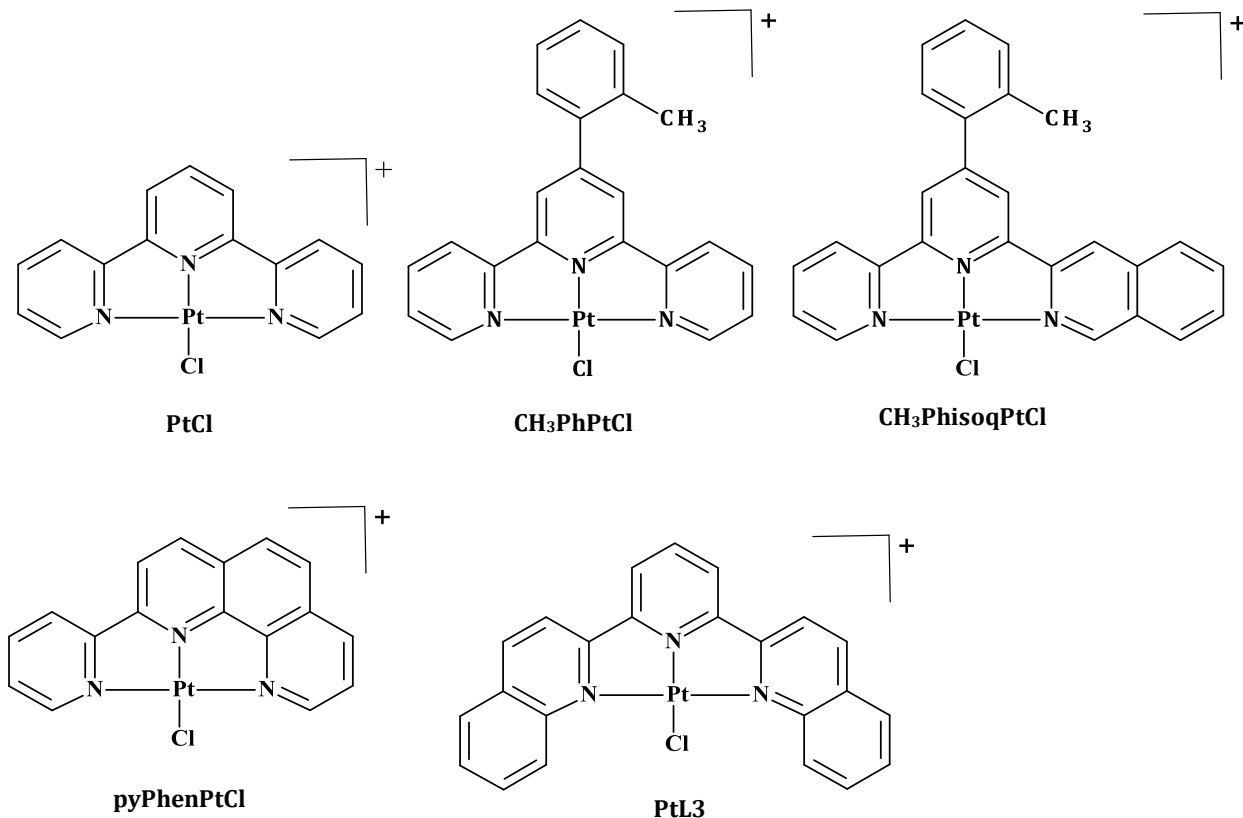


Figure 1.3: Platinum(II) complexes studied by Ongoma *et al.*⁵⁷ (**PtCl**, **CH₃PhPtCl**, **CH₃PhisoqPtCl** and **pyPhenPtCl**) and Nkabinde *et al.*⁵⁹ (**PtCl**, **PtL3**)

Results by Ongoma *et al.*⁵⁷ showed a decrease in the second-rate constants of the complexes with extended π -conjugation. Expectation for extended π -conjugated systems would be an increase in the rate of substitution because it should enhance the π -back-bonding effect. Moreover, similar results have been reported previously but they have been due to the increased *cis*-effect not the decrease in delocalisation of the π -electron density.^{34,42,47} Similar results by Nkabinde *et al.*⁵⁹ using azoles as the incoming nucleophile were observed. This was attributed to a net σ -donor effect that suppresses the π -acceptability of the quinoline bearing Pt(II) complex thereby reducing π -back-bonding. This pumps electron density on the metal center thereby lowering the electrophilicity of the Pt(II) center which further destabilizes the transition state and decreases the reactivity. Other studies by Shaira *et al.*⁵⁸ and Ongoma *et al.*⁵⁷ investigated the effect of extending the π -conjugation on the *cis/trans* position of the platinum(II) terpyridine complex to form (**pyPhenPtCl**) (see **Figure 1.3**).

Azoles and thioureas were used as the incoming nucleophiles. Results on both cases showed an increased substitution rates for **pyPhenPtCl** compared to all the complexes in **Figure 1.3**. This increased reactivity was attributed to the amplified aromaticity on the chelate backbone of **pyPhenPtCl** compared to the terpy moiety **PtCl**. The increased π -conjugation in **pyPhenPtCl** enhances the π -back-bonding ability of the chelate ligand by decreasing the energy of the ligands π^* -orbitals which in turn increases the rates of substitution reactions. This extended π -conjugation effect can be further explained in terms of electronic communications with the π -acceptor ligands. This extended π -conjugation on the chelate backbone of **pyPhenPtCl** increases the π -acceptor ability of the ligand which effectively increases the π -back-bonding from the metal center to the anti-bonding π -orbitals of the ligand system. This results in better electronic communication between the phenanthroline and the pyridine subunit which in turn increases the electrophilicity of the metal center and hence the reactivity.

Shaira *et al.*⁴⁸ functionalized terpyridine at the 4'-position by polyethylene glycoxy groups and further investigated the ligand substitution behaviour of the 4'-functionalised mononuclear Pt(II) terpyridine complexes (**Figure 1.4**) with thiourea (**TU**), 1,3-dimethyl-2-thiourea (**DMTU**), 1,1,3,3-tetramethyl-2-thiourea (**TMTU**) and iodide (**I⁻**). The lengths of the polyethylene glycoxy tail were systematically increased by incorporating 2-3 units to understand the role of flexible poly glycol pendant groups on the substitution reactions of Pt(II) terpyridine.

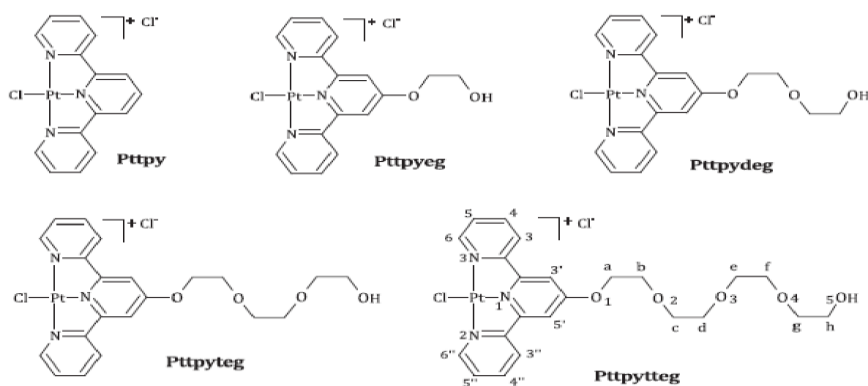


Figure 1.4: 4'-functionalised mononuclear Pt(II) terpyridine complexes studied by Shaira *et al.*⁴⁸

The results showed that when a single ethylene glycoxy pendant group is attached to the 4'-position of the terpyridine chelate ligand forming **Ptptyeg**, the reactivity of the resultant complex decreased significantly to that of **Ptpty**. This showed that the polyethylene glycoxy pendant is acting as a σ -donor.⁴⁸ This also supports earlier findings with regard to electron donating groups on the ancillary position of terpyridine which reduces the positive charge at the metal center thereby lowering the electrophilicity of the metal center hence decreasing reactivity.^{34, 38-39, 42, 60} Furthermore, the DFT calculations revealed a decrease in the electrophilicity index from **Ptpty** to **Ptptyeg**.⁶¹⁻⁶³ This is an indication of decreased ability of the complex to accept electrons from the incoming nucleophile.⁶¹⁻⁶³ This also indicates a reduction of the π -back-bonding ability of the terpy moiety from **Ptpty** to **Ptptyeg** due the addition of the ethylene glycoxy pendants. A similar effect due to the electron donating groups has also been reported by Jaganyi *et al.*^{39, 42} Furthermore, the steric contribution imposed on one side of the Pt(II) coordination sphere of **Ptptyeg** by the inclined appended ethylene glycoxy unit is notable (**Figure 1.5**).

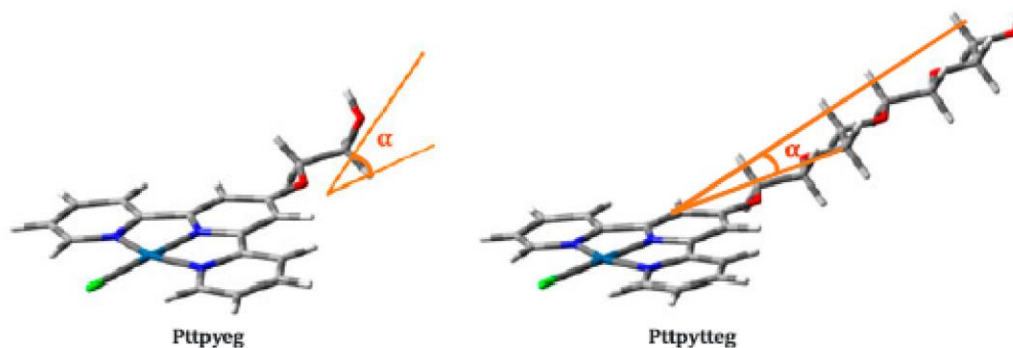


Figure 1.5: View of the inclination angle, α , for the pendant unit attached at the 4'-position of the terpy backbone, for the **Ptptyeg** and **Ptptyteg** complexes studied by Shaira *et al.*⁴⁸

This inclination hindered the approach of the axially incoming nucleophile thereby decreasing the rate of substitution in **Ptptyeg**. The steric influence existed in **Ptptyeg** because of an observed angle of inclination, α , which was absent in **Ptpty**. Therefore, it was concluded that both the steric and electronic effects were contributing factors in the

different rate of substitution between **Pttpy** and **Pttpyeg**. Further analysis of the other having ethylene glycoxy pendants showed a slight increase in the rate of substitution with an increase in the number of ethylene glycoxy units. This observed reactivity from **Pttpyeg** to **Pttpytteg** was attributed to the steric hindrance due to inclination of the ethylene glycoxy pendant group to the plane containing Pt(II).⁶⁴ Also, in all cases, **TU** had the highest rate constant which decreased as the incoming nucleophile got bulkier, i.e. rate constants for **DMTU** and **TMTU** were significantly lower compared to **TU**. This showed that these complexes are sensitive to the steric hindrance of the incoming nucleophiles. This is typical of an associative substitution reaction.

The previously mentioned studies together with other analogous platinum complexes of terpyridine were studied mainly to establish the connection between the structure, kinetics and thermodynamic parameters, stacking in the solid state and in solution. Thorough investigations on the substitution reactions of the platinum(II) complexes with variations in the 4'-position of terpy particularly terpyridine complexes functionalized with flexible linkers at the 4'-position and their substitutional behaviour with neutral nitrogen donors have seldom been studied.

1.4 Aim Of This Study

Kinetic and mechanistic information on platinum(II) complexes of terpyridine with a flexible linker in the 4'-position is scarce in literature. Although there have been several 4'-functionalised mononuclear Pt(II) terpyridine complexes synthesized in the past, these have been tested whether they are good G-quadruplex binders, for their ability to stabilize the quadruplex DNA inhibiting telomerase (which plays an essential role in cancer cell immortalization) or their preference for G-quadruplex DNA over duplex.

Complexes containing the terpyridine backbone can form metal complexes with a variety of transition metals that have been identified for potential applications in fields like macromolecular chemistry, nanoscience, biochemistry and photophysics. Of interest, terpy bearing complexes have been used as building blocks for novel supramolecular structures

such as double helicates,⁶⁵ dendrimers,⁶⁶⁻⁶⁷ micelles,⁶⁸ metallo-supramolecular polymers⁶⁹⁻⁷² and others⁷³⁻⁷⁴ (Figure 1.6).⁷⁵

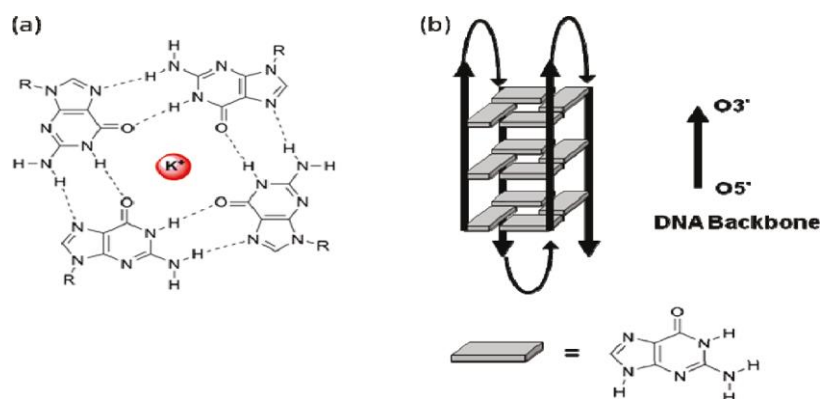


Figure 1.6: (a) Hydrogen-bonding interactions with a metal ion located centrally in a guanine quartet; (b) schematic view of an intramolecular quadruplex DNA structure.⁶²

In biochemical sciences, they can be used as sensors in tumour research⁷⁶ due to their ability to interact with double strand DNA and proteins.⁷⁷⁻⁸⁴ Teulade-Fichou *et al.*⁸⁵ reported terpyridine metal complexes as efficient quadruplex binders and that they improved the stabilization of the human G-quadruplex sequence upon the introduction of an *N*-methylated heteroaromatic side arm (Figure 1.7).

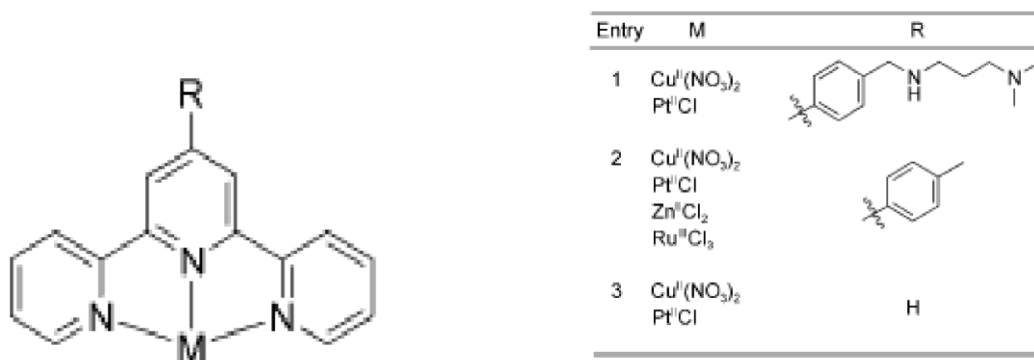


Figure 1.7: Structures of the terpyridyl complexes employed by Teulade-Fichou *et al.*⁸⁵ to investigate the relationship between the metal centre geometry and quadruplex DNA binding affinity.

In addition, it was found that the affinity and selectivity for telomeric quadruplex DNA were dependent on the geometry adopted by the complex. Further studies demonstrated the need for the quadruplex stabilizers to display at least one accessible planar surface to participate in effective π -stacking interactions with the terminal G-tetrads.⁸⁶ Furthermore, another study showed moderate binding enhancement of the platinum(II) terpyridine complex upon addition of side chains with cyclic amine head groups in the 4'-position.⁷⁴ While some terpyridine complexes were found to be cytotoxic against human ovarian cancer⁸⁷⁻⁸⁸ while others showed toxic side effects that were specific to certain biomolecules such as sulfur donors⁸⁹. As a consequence, the search for better agents with improved side effects remains of interest and further calls for investigations in the mechanism of interaction of these molecules with biomolecules and DNA.

Gama *et al.*⁹⁰ reported a new series of 4'-functionalized anthracene-terpyridine metal complexes as new G-Quadruplex DNA binders (**Figure 1.8**). These complexes functionalized at the terpy 4'-position with flexible linkers showed affinity for quadruplex-forming sequences and good selectivity over duplex DNA. Also, the free ligands had little affinity for any of the DNA sequences that were used. This implies that the presence of the metal is essential for high affinity and was more evident for platinum(II) complexes over copper(II) complexes. In addition, the interaction of the metal complex with G-quadruplex-forming sequence showed dependence on the length of a linker between the chelating terpyridine unit and the anthracene moiety. The presence of a longer linker resulted in enhanced interactions of the G-quadruplex-forming sequence. The kinetic and mechanistic studies of these complexes reported by Gama *et al.*⁹⁰ have not yet been reported, hence there is still a lack of understanding in mechanism of antitumour action of these platinum drugs.

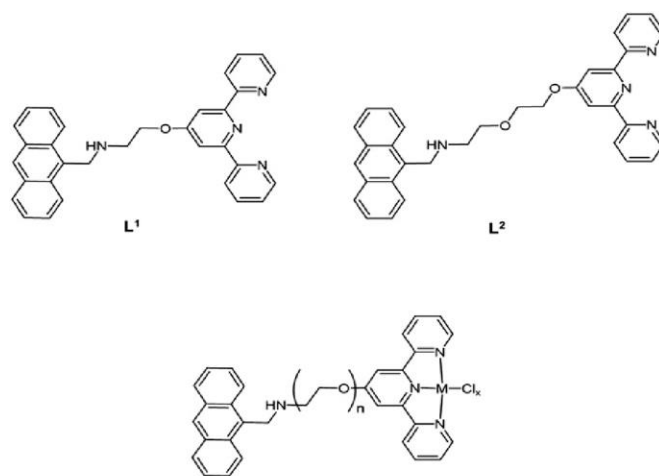


Figure 1.8: 4'-functionalized Anthracene-Terpyridine complexes reported by Gama *et al.*⁹⁰

In this study, we are interested in the series of complexes reported by Vilar *et al.*⁹¹ (**Figure 1.9**). These complexes have a fixed linker length with only variations of the size of the ring as well as addition of an oxygen atom in the *ortho* position. These three complexes bind strongly to HTelo and *c-myc* quadruplex DNA. However, their selectivity for quadruplex versus duplex DNA was not as high as expected. The attachment of the cyclic amine pendant on the terpyridyl backbone enhanced the complexes solubility in water as well as their interaction with DNA. However, the initial goal that these substituents would prevent the terpyridine complexes from interacting with duplex DNA by blocking the possibility of intercalation was not fully achieved.

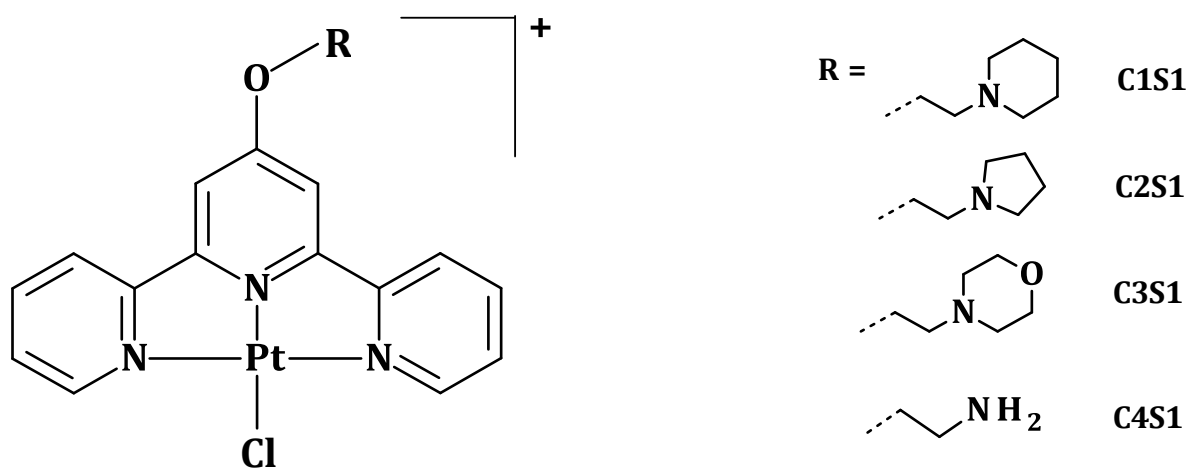


Figure 1.9: 4'-functionalized terpyridines reported by Vilar *et al.*⁹¹

The purpose of this study was to gain insight into the structure-reactivity relationships. We report here the synthesis, kinetics and mechanistic investigation into the substitution reactions of mononuclear Pt(II) complexes (**Figure 1.8**) with azoles as incoming nucleophiles.

The specific aims of this research were to:

1. Synthesize model compounds previously found to mimic metal ion interaction with DNA and proteins.
2. Observe kinetic effects and deduce the mechanism of substitution reactions of these complexes with azoles.
3. Determine the effect of functionalizing the terpy moiety in the 4'-position and further investigate how electronic and steric factors within the metal complex affect its reactivity.

1.5 References

1. Basolo, F.; Pearson, R. G., *Mechanisms of Inorganic Reactions: A study of Metal Complexes in Solution, 2nd Edition*, John Wiley & Sons Inc.: New York, **1967**, p. 11 – 35.
2. Belluco, U., *Organometallic Coordination Chemistry of Platinum*, **1974**, p. 1, 19 - 50, 220 - 221.
3. Shriver, D. F.; Atkins, P. W., *Inorganic Chemistry, 3rd Edition*, Oxford University ,New York, **2002**, p. 88 – 101.
4. Hartley, F. R., *Chemistry of the Platinum Group Metals Recent Developments*. Elsevier, Amsterdam, **1991**, p. 9, 23-30, 547-570.
5. Seymour, R. J.; O'Farrelly, J. I., *Kirk Othmer Encyclopaedia of Chemical Technology*. Platinum-Group Metals, Wiley, **2001**, p. 79 – 83.
6. Loferski, P. J., *Platinum-Group Metals*, United States Geological Survey, **2009**.
7. Xiao, Z.; Laplante, A. R., *Minerals Engineering*, **2004**, 17, p. 961.
8. Cairns, J., *Cancer Science and Society*, W. H. Freeman and Company, US, **1978**, p. 15-31, 35-39.
9. Lippert, B., *Cisplatin: Chemistry and Biochemistry of a Leading Anticancer Drug*, **2005**, p. 1 - 100, 184 - 190.
10. Gieng, M.; Tiekink, E. R. T., *Metallotherapeutic Drugs and Metal-Based Diagnostic Agents: The Use of Metals in Medicine*, **2005**, p. 489 - 502.
11. Chu, G., *Journal of Biological Chemistry*, **1994**, 269 (2), 787-90.
12. Wong, E.; Giandomenico, C. M., *Chemical Reviews*, **1999**, 99 (9), 2451-2466.
13. Jamieson, E. R.; Lippard, S. J., *Chemical Reviews*, **1999**, 99 (9), 2467-2498.
14. Łakomska, I., *Inorganica Chimica Acta.*, **2009**, 362 (3), 669-681.
15. Arnesano, F.; Natile, G., *Pure and Applied Chemistry*, **2008**, 80 (12), 2715-2725.
16. Crider, S. E.; Holbrook, R. J.; Franz, K. J., *Metallomics*, **2010**, 2 (1), 74-83.
17. Peleg-Shulman, T.; Najajreh, Y.; Gibson, D., *Journal of Inorganic Biochemistry*, **2002**, 91 (1), 306-311.

18. Wang, X.; Guo, Z., *The role of sulfur in platinum anticancer chemotherapy*, *Anti-Cancer Agents in Medicinal Chemistry (Formerly Current Medicinal Chemistry-Anti-Cancer Agents)*, **2007**, *7* (1), 19-34.
19. Vinje, J.; Sletten, E., *NMR spectroscopy of anticancer platinum drugs*, *Anti-Cancer Agents in Medicinal Chemistry (Formerly Current Medicinal Chemistry-Anti-Cancer Agents)*, **2007**, *7* (1), 35-54.
20. Lippert, B., *Cisplatin: Chemistry and Biochemistry of a Leading Anticancer Drug*, John Wiley & Sons: **1999**, p. 13 – 27.
21. Lokich, J., What is the “best” platinum: cisplatin, carboplatin, or oxaliplatin? *Cancer investigation*, **2001**, *19* (7), 756-760.
22. Su, W.-C.; Chang, S.-L.; Chen, T.-Y.; Chen, J.-S.; Tsao, C.-J., *Japanese Journal of Clinical Oncology*, **2000**, *30* (12), 562-567.
23. Bower, M.; Newlands, E.; Holden, L.; Rustin, G.; Begent, R., *Annals of Oncology*, **1997**, *8* (5), 477-483.
24. Lévi, F.; Metzger, G.; Massari, C.; Milano, G., *Clinical Pharmacokinetics*, **2000**, *38* (1), 1-21.
25. Mellish, K. J.; Qu, Y.; Scarsdale, N.; Farrell, N., *Nucleic Acids Research*, **1997**, *25* (6), 1265-1271.
26. Hambley, T. W., *Coordination Chemistry Reviews*, **1997**, *166*, 181-223.
27. Jansen, B. A.; Brouwer, J.; Reedijk, J., *Journal of Inorganic Biochemistry*, **2002**, *89* (3-4), 197-202.
28. Hubbard, C. D.; Van Eldik, R., *Journal of Coordination Chemistry*, **2007**, *60* (1), 1-51.
29. Tobe, M. L.; Burgess, J., *Inorganic Reaction Mechanisms*, Longman: Harlow, Essex, England; New York, **1999**, p. 87 – 89.
30. Bogojeski, J., *Chronic Lymphocytic Leukaemia*, InTechOpen: Europe, **2012**, p. 339-366.
31. Reedijk, J., *Proc Natl Acad Sci U S A*, **2003**, *100* (7), 3611-6.
32. Reedijk, B. J., *Platinum Metals Review*, **2008**, *52* (1), 2-11.
33. Jaganyi, D.; Hofmann, A.; van Eldik, R., *Angewandte Chemie International Edition*, **2001**, *40* (9), 1680-1683.
34. Hofmann, A.; Dahlenburg, L.; van Eldik, R., *Inorganic Chemistry*, **2003**, *42* (20), 6528-6538.

35. Cummings, S. D., *Coordination Chemistry Reviews*, **2009**, 253 (3-4), 449-478.
36. Pitteri, B.; Marangoni, G.; Cattalini, L.; Bobbo, T., *Journal of the Chemical Society, Dalton Transactions*, **1995**, (23), 3853-3859.
37. Czap, A.; Heinemann, F. W.; van Eldik, R., *Inorganic Chemistry*, **2004**, 43 (24), 7832-7843.
38. Pantoja, E.; Gallipoli, A.; van Zutphen, S.; Komeda, S.; Reddy, D.; Jaganyi, D.; Lutz, M.; Tooke, D. M.; Spek, A. L.; Navarro-Ranninger, C.; Reedijk, J., *Journal of Inorganic Biochemistry*, **2006**, 100 (12), 1955-1964.
39. Reddy, D.; Jaganyi, D., *Dalton Transactions*, **2008**, (47), 6724-6731.
40. Hofmann, A.; Jaganyi, D.; Munro, O. Q.; Liehr, G.; van Eldik, R., *Inorganic Chemistry*, **2003**, 42 (5), 1688-1700.
41. Pitteri, B.; Bortoluzzi, M., *Polyhedron*, **2006**, 25 (14), 2698-2704.
42. Jaganyi, D.; Reddy, D.; Gertenbach, J.; Hofmann, A.; van Eldik, R., *Dalton Transactions*, **2004**, (2), 299-304.
43. Jaganyi, D.; Boer, K. L. D.; Gertenbach, J.; Perils, J., *International Journal of Chemical Kinetics*, **2008**, 40 (12), 808-818.
44. Reddy, D.; Akerman, K. J.; Akerman, M. P.; Jaganyi, D., *Transition Metal Chemistry*, **2011**, 36 (6), 593-602.
45. Eldik, R., *Journal of the Chemical Society, Dalton Transactions*, **1994**, (8), 1257-1263.
46. Schmülling, M.; Grove, D. M.; van Koten, G.; van Eldik, R.; Veldman, N.; Spek, A., *Organometallics*, **1996**, 15 (5), 1384-1391.
47. Romeo, R.; Plutino, M. R.; Monsù Scolaro, L.; Stoccoro, S.; Minghetti, G., *Inorganic Chemistry*, **2000**, 39 (21), 4749-4755.
48. Shaira, A.; Jaganyi, D., *Journal of Coordination Chemistry*, **2014**, 67 (17), 2843-2857.
49. Chipangura, M.; Mambanda, A.; Jaganyi, D., *Transition Metal Chemistry*, **2015**, 40 (1), 109-115.
50. Mambanda, A.; Jaganyi, D., *Dalton Transactions*, **2011**, 40 (1), 79-91.
51. Basolo, F.; Chatt, J.; Gray, H. B.; Pearson, R. G.; Shaw, B. L., *Journal of the Chemical Society, Dalton Transactions*, **1961**, 2207-2215.
52. Gray, H. B., *Journal of the American Chemical Society*, **1962**, 84 (9), 1548-1552.

53. Schmulling, M.; Ryabov, A. D.; Vaneldik, R., *Journal of the Chemical Society, Chemical Communications*, **1992**, (21), 1609-1611.
54. Deubel, D. V., *Journal of the American Chemical Society*, **2002**, *124* (20), 5834-5842.
55. Pitteri, B.; Marangoni, G.; Cattalini, L.; Visentin, F.; Bertolasi, V.; Gilli, P., *Polyhedron*, **2001**, *20* (9-10), 869-880.
56. Annibale, G.; Brandolisio, M.; Pitteri, B., *Polyhedron*, **1995**, *14* (3), 451-453.
57. Ongoma, P.; Jaganyi, D., *Dalton Transactions*, **2012**, *41* (35), 10724-10730.
58. Shaira, A.; Reddy, D.; Jaganyi, D., *Dalton Transactions*, **2013**, *42* (23), 8426-8436.
59. Nkabinde, S. N., *MSc Dissertation, Tuning the Reactivity of Mononuclear Tridentate Platinum (II) Complexes: A detailed Kinetic and Mechanistic Approach using Azole Nucleophiles*, University of KwaZulu-Natal, South Africa. **2014**, p. 154 – 162.
60. Reddy, D.; Jaganyi, D., *International Journal of Chemical Kinetics*, **2011**, *43* (4), 161-174.
61. Parr, R. G.; Pearson, R. G., *Journal of the American Chemical Society*, **1983**, *105* (26), 7512-7516.
62. Chattaraj, P. K.; Maiti, B., *Journal of the American Chemical Society*, **2003**, *125* (9), 2705-2710.
63. Mebi, C. A., *Journal Chemical Sciences*, **2011**, *123* (5), 727-731.
64. Mambanda, A.; Jaganyi, D.; Hochreuther, S.; van Eldik, R., *Dalton Transactions*, **2010**, *39* (15), 3595-3608.
65. Lehn, J.-M., *Supramolecular chemistry Volume 1*. Vch, Weinheim Germany: **1995**, p. 12, 33 - 40.
66. Newkome, G. R.; He, E.; Godínez, L. A., *Macromolecules*, **1998**, *31* (13), 4382-4386.
67. Schubert, U.; Weidl, C.; Moorefield, C.; Baker, G.; Newkome, G., *Abstr Pap Amer Chemical Soc.*, **1999**; p. U473-U473.
68. Gohy, J.-F.; Lohmeijer, B. G.; Varshney, S. K.; Schubert, U. S., *Macromolecules*, **2002**, *35* (19), 7427-7435.
69. Schubert, U. S.; Eschbaumer, C., *Angewandte Chemie International Edition*, **2002**, *41* (16), 2892-2926.
70. Lohmeijer, B. G.; Schubert, U. S., *Angewandte Chemie International Edition*, **2002**, *41* (20), 3825-3829.

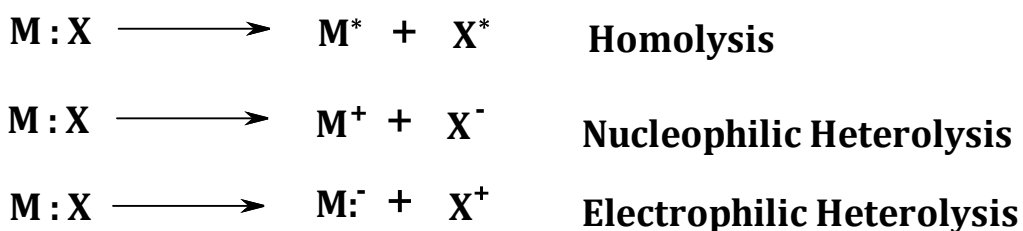
71. Kelch, S.; Rehahn, M., *Macromolecules*, **1999**, 32 (18), 5818-5828.
72. Khatyr, A.; Ziessel, R., *The Journal of Organic Chemistry*, **2000**, 65 (10), 3126-3134.
73. Ziener, U.; Lehn, J. M.; Mourran, A.; Möller, M., *Chemistry—A European Journal*, **2002**, 8 (4), 951-957.
74. Figgemeier, E.; Merz, L.; Hermann, B.; Zimmermann, Y.; Housecroft, C.; Güntherodt, H.-J.; Constable, E., *The Journal of Physical Chemistry B*, **2003**, 107 (5), 1157-1162.
75. Ziessel, R.; Douce, L.; El-ghayoury, A.; Harriman, A.; Skoulios, A., *Angewandte Chemie*, **2000**, 112 (8), 1549-1553.
76. Zhang, Y.; Murphy, C. B.; Jones, W. E., *Macromolecules*, **2002**, 35 (3), 630-636.
77. Carter, P. J.; Cheng, C.-C.; Thorp, H. H., *Journal of the American Chemical Society*, **1998**, 120 (4), 632-642.
78. Daniher, A.; Bashkin, J., *Chemical Communications*, **1998**, (10), 1077-1078.
79. Field, J. S.; Haines, R. J.; McMillin, D. R.; Summerton, G. C., *Journal of the Chemical Society, Dalton Transactions*, **2002**, (7), 1369-1376.
80. Bonse, S.; Richards, J. M.; Ross, S. A.; Lowe, G.; Krauth-Siegel, R. L., *Journal of Medicinal Chemistry*, **2000**, 43 (25), 4812-4821.
81. Messori, L.; Abbate, F.; Marcon, G.; Orioli, P.; Fontani, M.; Mini, E.; Mazzei, T.; Carotti, S.; O'Connell, T.; Zanello, P., *Journal of Medicinal Chemistry* **2000**, 43 (19), 3541-3548.
82. Peyratout, C. S.; Aldridge, T. K.; Crites, D. K.; McMillin, D. R., *Inorganic Chemistry*, **1995**, 34 (17), 4484-4489.
83. Cusumano, M.; Di Pietro, M. L.; Giannetto, A., *Inorganic Chemistry*, **1999**, 38 (8), 1754-1758.
84. Howe-Grant, M.; Wu, K. C.; Bauer, W. R.; Lippard, S. J., *Biochemistry*, **1976**, 15 (19), 4339-4346.
85. Bertrand, H.; Bombard, S.; Monchaud, D.; Talbot, E.; Guédin, A.; Mergny, J.-L.; Grünert, R.; Bednarski, P. J.; Teulade-Fichou, M.-P., *Organic & Biomolecular Chemistry*, **2009**, 7 (14), 2864-2871.
86. Bertrand, H.; Monchaud, D.; De Cian, A.; Guillot, R.; Mergny, J.-L.; Teulade-Fichou, M.-P., *Organic & Biomolecular Chemistry*, **2007**, 5 (16), 2555-2559.
87. Lowe, G.; Droz, A. S.; Vilaivan, T.; Weaver, G. W.; Park, J. J.; Pratt, J. M.; Tweedale, L.; Kelland, L. R., *Journal of Medicinal Chemistry*, **1999**, 42 (16), 3167-3174.

88. Lowe, G.; Droz, A. S.; Vilaivan, T.; Weaver, G. W.; Tweedale, L.; Pratt, J. M.; Rock, P.; Yardley, V.; Croft, S. L., *Journal of Medicinal Chemistry*, **1999**, *42* (6), 999-1006.
89. Bugarcic, Z. D.; Liehr, G.; van Eldik, R., *Journal of the Chemical Society, Dalton Transaction*, **2002**, (14), 2825-2830.
90. Gama, S.; Rodrigues, I.; Mendes, F.; Santos, I. C.; Gabano, E.; Klejevskaia, B.; Gonzalez-Garcia, J.; Ravera, M.; Vilar, R.; Paulo, A., *Journal of Inorganic Biochemistry*, **2016**, *160*, 275-286.
91. Suntharalingam, K.; White, A. J. P.; Vilar, R., *Inorganic Chemistry*, **2009**, *48* (19), 9427-9435.

Chapter 2 – Ligand Substitution

2.1 Introduction

In general, substitution can be defined as a process whereby an ion or a molecule from the coordination sphere of a reactive centre is replaced by another from the environment.¹⁻⁴ The importance of understanding the ligand substitution behaviour of the platinum drug with the target DNA arises from the fact that the majority of transition metal complexes that display anticancer activity are found in the d^8 electronic configuration hence their ligand substitution reveal more about their anticancer properties. A substitution in which the replacement of the ligand involves only a change in coordination number of the reaction centre but no temporal change in oxidation state is termed *simple* substitution.^{1,4} In addition, a simple substitution is further categorized by bond-breaking and bond-making with a temporary change in the coordination number in the transition state.⁴ Ingold and Hughes⁵ were able to further classify the substitution (bond-breaking) of carbon as either homolytic or heterolytic (**Scheme 2.1**).^{1, 4-5}

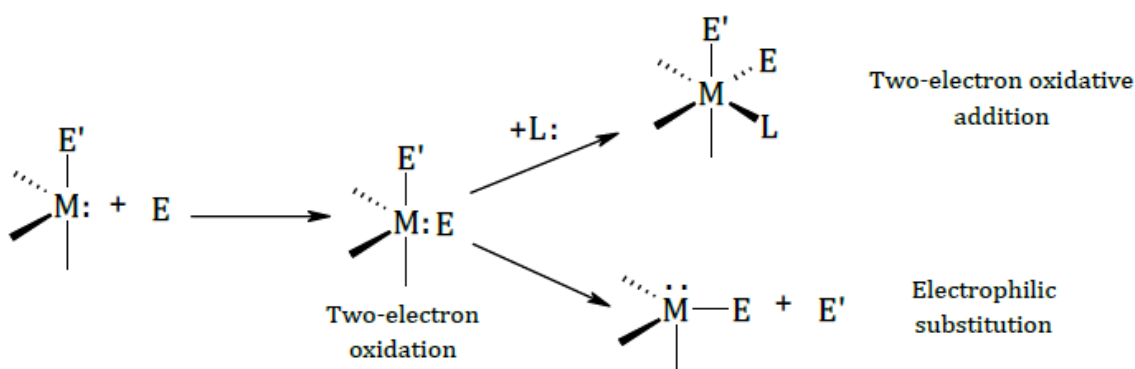


Scheme 2.1: The modes of bond-breaking in substitution reactions.^{1, 4-5}

When a homolytic bond-breaking process occurs, electrons are shared equally.¹ However, the heterolytic substitution process can be further divided into two (2) subgroups, namely electrophilic heterolysis or nucleophilic heterolysis.⁴ In a nucleophilic process, the electrons of the broken bond remain with the leaving group while the incoming ligand(s) provides a pair of replacement electrons.⁴ In an electrophilic process, the electrons remain with the reaction centre with the incoming ligand acting as an electron pair acceptor.⁴ Therefore, the heterolytic process can be regarded as a Lewis acid-base reaction since the reaction centre

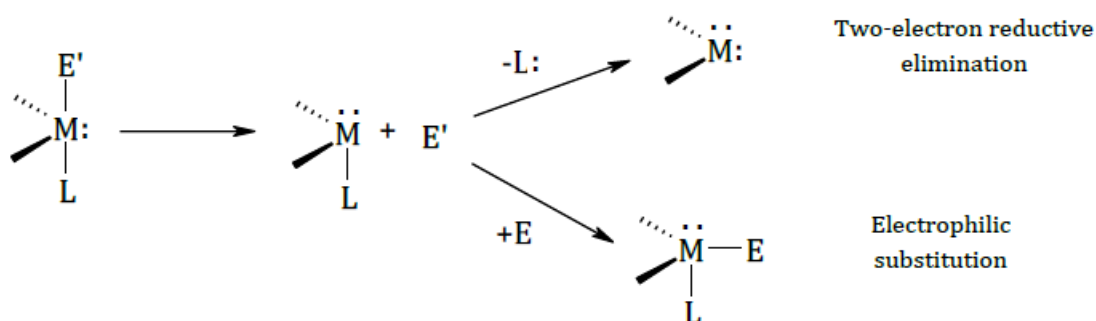
acts as a Lewis acid (during nucleophilic processes) and as a Lewis base (during electrophilic processes).³

Furthermore, the change in the number of ligands in a nucleophilic process does not result in a temporary change in the oxidation state of the reaction centre thereby termed a simple substitution. However, the addition of an electrophile is accompanied by a two-electron oxidation (bonding of the two previously non-bonding electrons).³ In addition, if the ligand departs as a Lewis acid, the reaction is an electrophilic substitution (S_E). Also, an oxidative addition reaction may occur if the ligand acting as a Lewis base attaches itself to the metal centre leading to the stabilization of the high oxidation state intermediate (**Scheme 2.2**).³



Scheme 2.2: Heterolytic bond-making process via a two-electron oxidative addition.³

In an electrophilic reaction, the reaction centre acts as a base whereby a dissociative two-electron reduction occurs leading to a bonding pair of electrons to become non-bonding. The loss of a Lewis base leads to reductive elimination whereas the gain of an electron pair acceptor completes the substitution by restoring the oxidation state (**Scheme 2.3**).³



Scheme 2.3: Heterolytic bond-breaking process via a two-electron reductive elimination.³

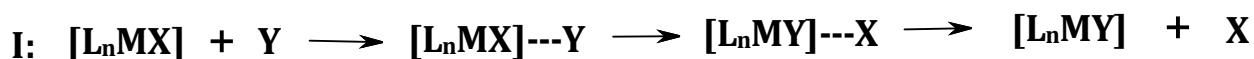
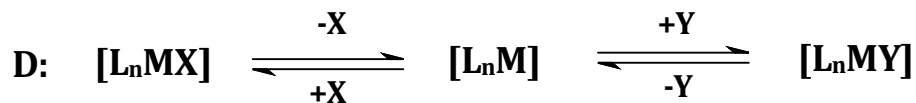
Nucleophilic substitution reactions (S_N1 or S_N2)^{1,4,6-7} are seldom used in inorganic reactions since they do not describe substitution reaction mechanisms in sufficient detail, i.e. this method is based on the substitution on carbon centres, albeit most kinetic substitution reactions of inorganic complexes undergo S_N1 or S_N2 mechanisms.⁴

2.2 Ligand Substitution for Metal Complexes

2.2.1 Stoichiometric and Intimate Mechanisms

The concept of the stoichiometric and intimate mechanism was introduced by Langford and Gray⁸ in an attempt to classify inorganic substitution reactions. The stoichiometric mechanism was further categorised into three simple pathways depending on the intermediate species (**Scheme 2.4**),^{2-3, 8-11} namely:

- Dissociative (D):** This process is similar to an S_N1 mechanism in which the leaving group is lost in the first step forming an intermediate with reduced coordination number.^{1-3,9,12-13}
- Associative (A):** This process is similar to an S_N2 mechanism in which the entering ligand adds in the first step forming an intermediate of increased coordination number.^{1-3,9,12-13}
- Interchange (I):** This process involves no detectable intermediate as bond-breaking and bond formation occurs simultaneously or within a pre-formed aggregate.^{1-3, 9, 12-13}



where, Y = nucleophile or solvent molecule

Scheme 2.4: The reaction pathways proposed by Langford and Gray.⁸

Furthermore, it can be deduced that the type of activation mechanism depends on the detection of an intermediate species.³ In addition, the stoichiometric interchange (I) mechanism can be further subcategorised into two groups based on intimate mechanism because it has a variety of transition states, (**Figure 2.1**).^{1, 3-4}

- (i) Dissociatively activated intimate mechanism (**I_d**): The transition state formed here shows no direct interaction between the reactive centre and the entering ligand thus there is only minimal effect of the entering ligand on the reaction rate. Therefore, the reaction is more sensitive to the nature of the leaving ligand.^{1-3, 9,12-13}
- (ii) Associatively activated intimate mechanism (**I_a**): This mechanism is associative in nature hence there is substantial bonding of the reactive centre to both the entering and leaving ligand before the leaving ligand bond is weakened in the transition state. Therefore, the reaction is more sensitive to the nature of the incoming ligand.^{1-3,9,12-13}

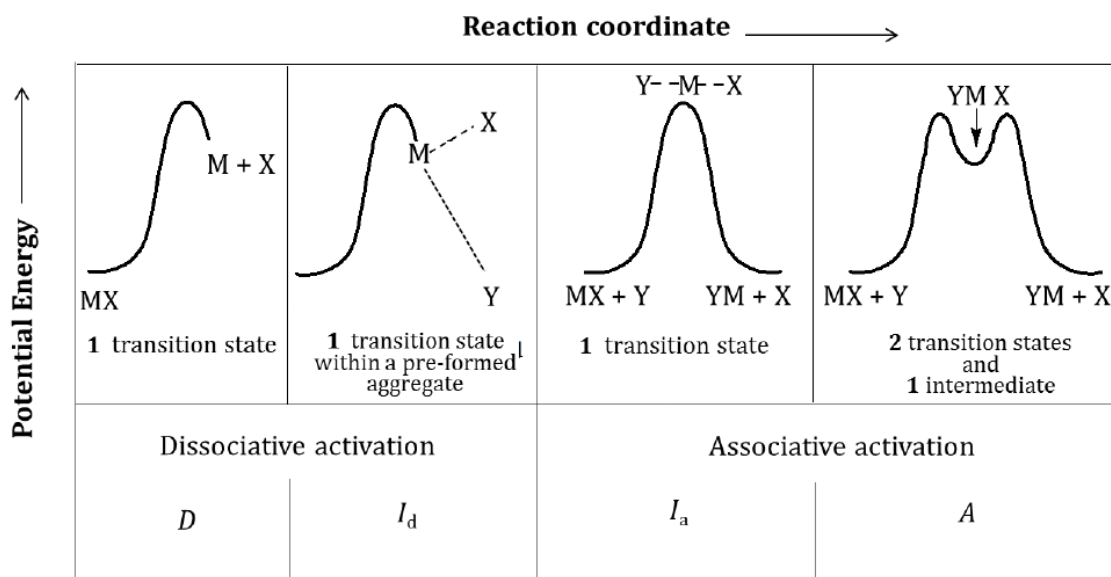


Figure 2.1: The potential energy profile diagrams showing the various substitution mechanisms occurring at square-planar complexes as proposed by Langford-Gary.^{3,8}

2.2.2 The Dissociative Mechanism (D)

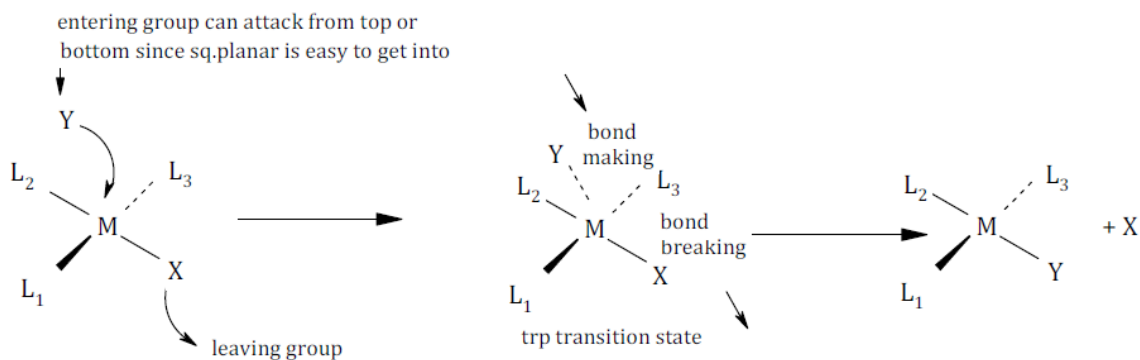
As illustrated by the diagram above (**Figure 2.1**), bond (**M---X**) breaks completely resulting in an intermediate of lower coordination number (14-electron) before the incoming ligand attaches itself to the metal centre (**M---Y**).^{3,11} The reaction profile of a dissociative mechanism consists of one transition state and one intermediate. The intermediate species is assumed to last for a sufficiently long time allowing it to equilibrate with its environment before coordinating the incoming ligand.^{3,13}

Accordingly, the rate of reaction is solely dependent on the nature of the leaving group and independent of the nature and concentration of the incoming ligand.^{3,8,14} Also, the incoming ligand can dominate if it is present in large excess hence the consumption of the intermediate may occur when the leaving group is in close proximity to the metal centre.³ Moreover, solvent attack is also favoured when the leaving group moves from the coordination shell to the solvation. This results in reduced ability of the metal complex to discriminate which

enables the solvent (usually present in excess) to dominate the substitution process.⁹ In addition, the dissociative mechanism is non stereoselective.¹⁵

2.2.3 The Associative Mechanism (A)

In this mechanism, bond formation ($M\cdots Y$) takes place before bond ($M-X$) breaks resulting in an increase in the coordination number around the metal centre. Here, the intermediate of higher coordination number is formed via two transition states (**Figure 2.1, Scheme 2.4**) namely, the bond-making transition state and the bond-breaking transition state.³ In this mechanism, the rate determining step is the bond formation (between the metal centre and incoming ligand (Y)). However, it has been well researched and reported that for an associative mode of substitution, all the ligands involved can influence the stability and activation energy of the five-coordinate activated complex (**Scheme 2.5**).^{13,16}



Scheme 2.5: Reaction pathway following an associative mode of substitution. ^{13,16}

When the incoming ligand (Y) and the leaving group (X) are chemically identical, the two transition states will have the same potential energy whereas a net chemical change will result in one transition state to be at a higher potential energy level than the other. Furthermore, the more stable transition state will have a deeper potential energy well (**Figure 2.2**).^{13,16}

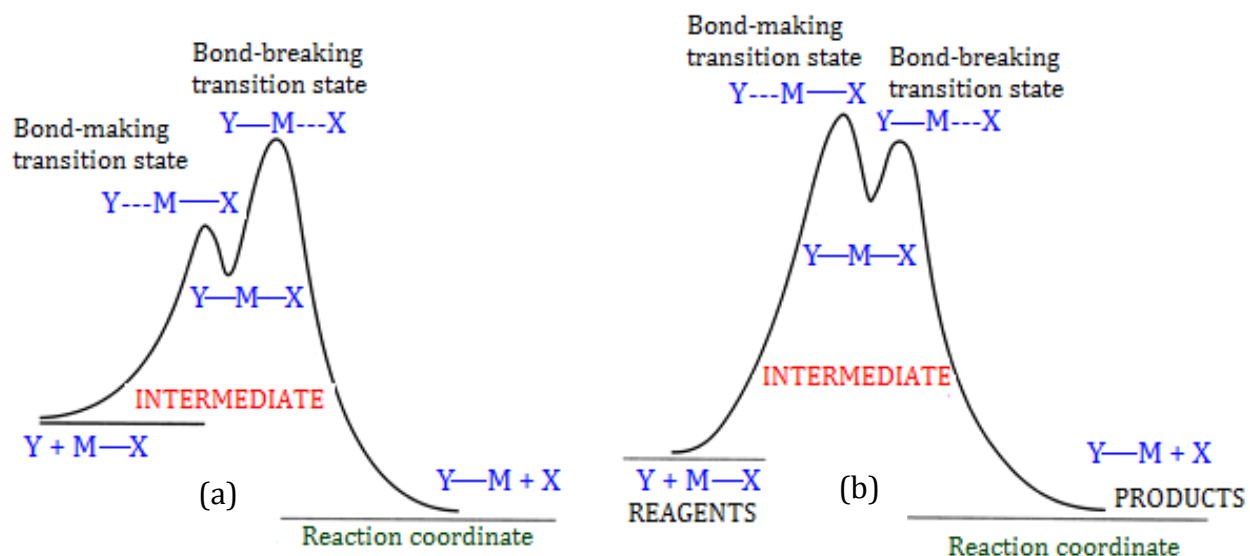


Figure 2.2: Energy profiles for an associative substitution mechanism showing the relationship between the intermediate and the transition states: (a) shows the bond-breaking transition state at a higher energy, whereas (b) shows the bond-making transition state at a higher energy.^{13, 16}

2.2.4 The Interchange Mechanism (I)

The interchange mechanism can be further divided into two groups, i.e. the associative interchange mechanism (**I_a**) and the dissociative interchange mechanism (**I_d**).^{3,11} In the former, the bond-making step is more noticeable than the bond-breaking step hence this mechanism accounts for differences between the interchange mechanism and the associative mechanism.^{3,11} Therefore, the reaction rate is more dependent on the nature of the incoming ligand and the leaving group leaves the metal centre only when the incoming ligand is tightly bound to the metal centre.¹⁻³ In the latter, the mechanism covers the differences between the interchange mechanism and the dissociative mechanism meaning the bond-breaking step is more prominent in the transition state formation.^{1-3,9} Also, the leaving group moves from the inner coordination sphere to the outer coordination sphere while the entering group moves from the outer coordination sphere to the inner coordination, hence the reason why the transition state formed consists of two very weak bonds between the metal centre with both the leaving group and the entering group.^{1-3,9}

In addition, the possibility of the solvent bonding the reactive metal centre is higher only if there is a reagent with a concentration much less than that of the solvent, which is already in the inner coordination sphere where the dissociation takes place.

2.3 Ligand Substitution at Square-Planar Platinum (II) Complexes

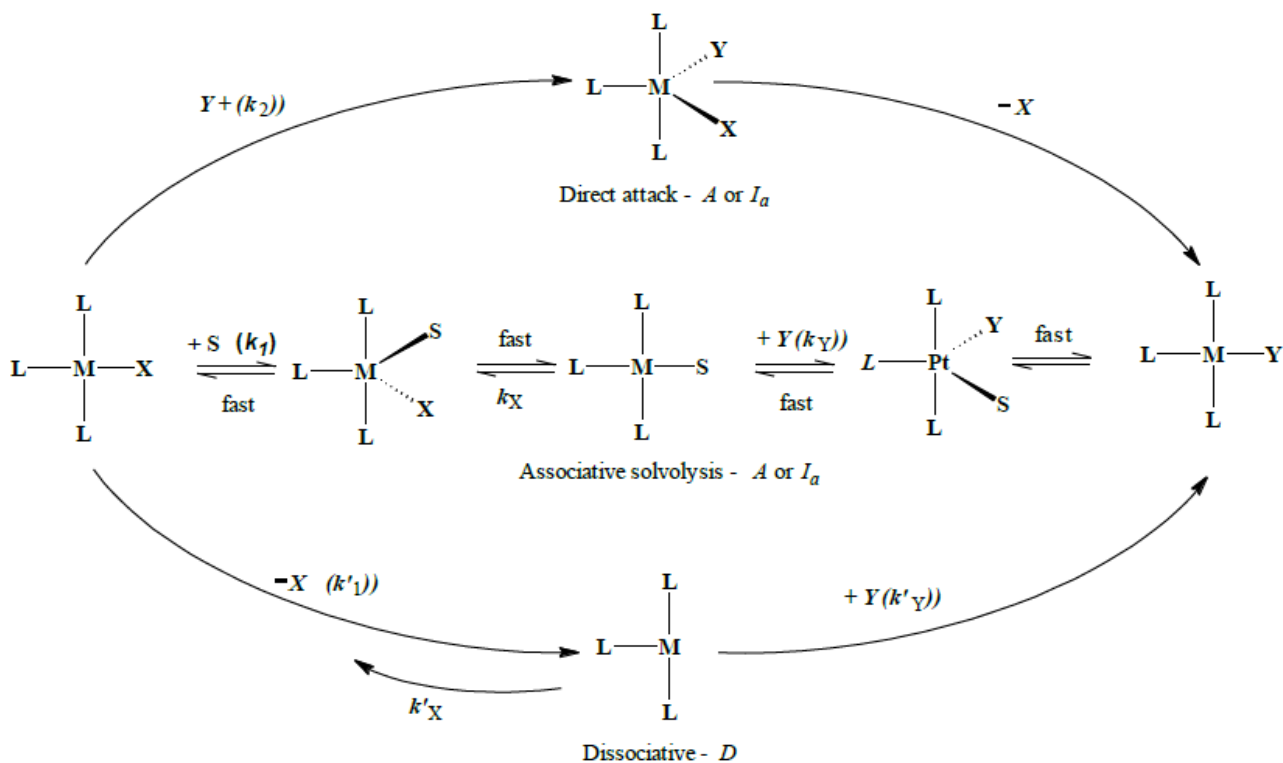
The term square-planar generally refers to most four coordinate complexes with low-spin d^8 configuration, such as nickel(II), palladium(II), iridium(I), rhodium(I), gold(III) and platinum(II).^{1-3,9,12-13,17} Studies on the ligand substitution behaviour of square-planar complexes dates back to the 1950s.¹¹ Although ligand substitution at square-planar centres are well investigated and among the most widely understood in inorganic reaction mechanisms, several studies have reported that not all reaction centres with a d^8 configuration are relevant for square-planar substitution.^{6, 12, 18-21}

For example, the square-planar complexes of Rh(I) and Ir(I) are inclined to oxidative additions while Ni(II) complexes consisting of a wider range of spin multiplicities, coordination numbers and geometries tend to favour other geometries such as octahedral over square-planar.^{1, 3, 13} In addition, square-planar Ni(II) and Pd(II) complexes react *via* the same mechanism as that of Pt(II) complexes but at rates which are at least five orders of magnitude higher than those of Pt(II) complexes therefore their substitution reactions are difficult to fully analyse and as a result, they are less attractive.²² Moreover, the square-planar complexes of Au(III) can be formed but they are easily reduced to lower oxidation state such as Au(I) and Au(0) hence they are not stable.

Platinum(II) complexes on the other hand have dominated the studies on the substitution behaviour owing to their stable redox behaviour and relatively low reactivity.^{13,16} This allows for the synthesis of a variety of platinum(II) complexes and for the relative ease of studying and interpreting the mechanistic and kinetic behaviour of these complexes.^{3,11-13}

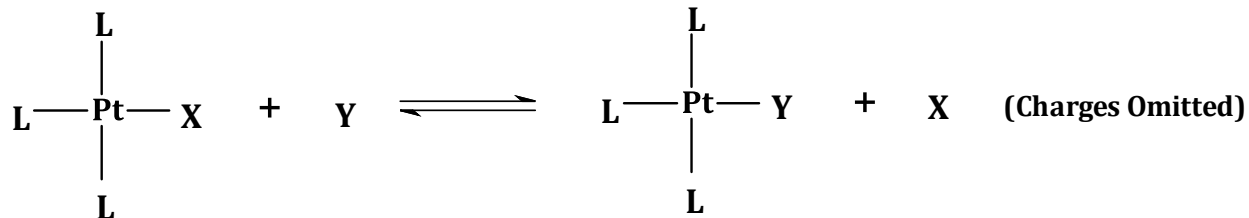
2.3.1 Kinetics and Mechanism of Ligand Substitution

A detailed mechanistic pathway for a square-planar substitution requires an understanding of how the nature of reactants and/or solvent used affect the kinetics and mechanism of the reaction.³ The substitution kinetics may occur through any one of the three pathways, depending on the nature of the reactants and/or solvent (**Scheme 2.6**).³ There are two possible associative pathways: one involving a direct attack of the incoming ligand and the other involving a solvated complex. The third is a dissociative pathway involving a three-coordinate intermediate.



Scheme 2.6: Schematic illustration for ligand substitution in d^8 square-planar complexes.³

However, most studied substitution reactions of square-planar platinum(II) complexes are often represented by a direct replacement of a leaving ligand (X) by an incoming nucleophile (Y), which can be illustrated as follows.^{6-7,9}



Scheme 2.7: Direct replacement of the leaving ligand (X) by an incoming ligand (Y).^{6-7, 9}

The substitution can be described by a rate law consisting of two terms, one being first-order with respect to the complex (PtL₃X) and the other being first-order in each of the metal complex (PtL₃X) and the entering ligand (Y) (*Equation 2.1*).^{1, 3, 6, 13}

$$\begin{aligned}
 \text{Rate} &= -\frac{d[\text{PtL}_3\text{X}]}{dt} = k_1[\text{PtL}_3\text{X}] + k_2[\text{PtL}_3\text{X}][\text{Y}] \\
 &= (k_1 + k_2[\text{Y}])[\text{PtL}_3\text{X}] \qquad \qquad \qquad (2.1)
 \end{aligned}$$

where k_1 and k_2 represents the first- and second-order rate constants respectively. k_1 is the rate constant that is independent of the incoming nucleophile, (Y) and k_2 is the rate constant that is dependent on the Y (for a given solvent at a fixed temperature).^{1, 3, 6, 13}

Equation 2.1 clearly shows the typical bimolecular substitution mechanism for a square-planar complex which depends on both the metal complex and the incoming nucleophile.⁶ The kinetic substitution reactions are however done usually under *pseudo* first-order conditions, where the entering nucleophile is present in at least a 10-fold excess with respect to the metal complex. This is to force the substitution process to completion while its kinetics remains first-order.

Accordingly, the rate equation simplifies to that of a first-order process, (*Equation 2.2*):

$$\text{Rate} = k_{obs}[\text{PtL}_3\text{X}], \qquad k_{obs} = k_1 + k_2[\text{Y}] \qquad (2.2)$$

where k_{obs} = the observed first-order or observed pseudo first-order rate constant.

Hence, a plot of k_{obs} against concentration of the Y, [Y], will give k_2 as a slope and k_1 as the y-intercept. Therefore, as mentioned above, the value of the k_1 is independent of the entering

nucleophile while k_2 depends on the reactivity of the entering nucleophile. A typical example of such a plot is represented by **Figure 2.3** for the substitution reaction of $trans\text{-Pt}(\text{py})_2\text{Cl}_2$ with different nucleophiles.^{6-7, 13, 16}

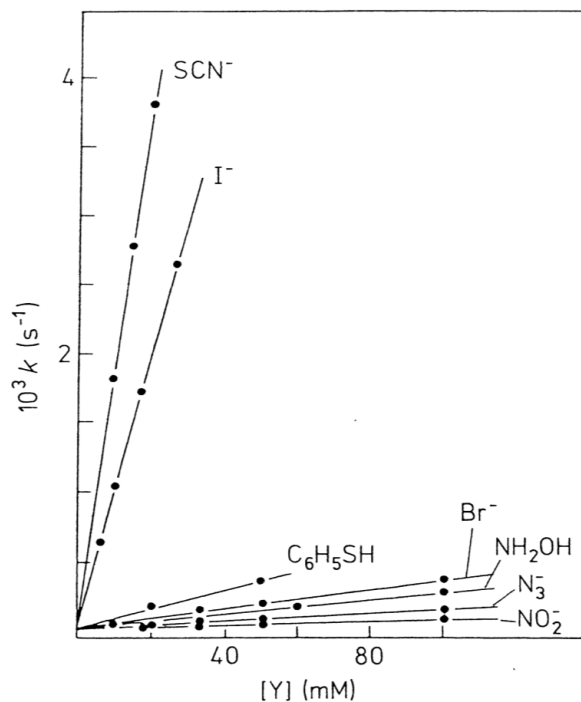


Figure 2.3: Plot of reaction rates of $trans\text{-Pt}(\text{py})_2\text{Cl}_2$ against concentration of different nucleophiles in methanol at 30 °C.^{13, 16, 23}

As illustrated by **Figure 2.3**, the value of k_1 is the same for all the nucleophiles studied for the same metal complex underlining the independence of k_1 to the nature of the entering nucleophiles, while k_2 (slope) differs with the entering nucleophile as this is a nucleophile dependent path.^{6, 11-13} In addition, most ligand substitutions are carried out in coordinating solvents such as water and methanol thus the k_1 term can be attributed to the associative solvolysis pathway, which is a slow displacement of the leaving group (**X**) by the solvent (**S**) *i.e.* rate-determining step, followed by a rapid replacement of (**S**) by the entering nucleophile (**Y**).¹¹⁻¹³

However, positive k_1 values can also be representative of the reverse reaction or a parallel solvolysis.²⁴⁻²⁵ The pathway dependent of the (**Y**) is characterised by k_2 whose rate-

determining step is the direct nucleophilic attack along the z -axis (**Figure 2.4**).^{1, 3, 6, 13} The extra electrons contributed by the entering nucleophile to the square-planar complex results in a saturated 18-electron five-coordinate intermediate.^{1, 3, 6, 13}

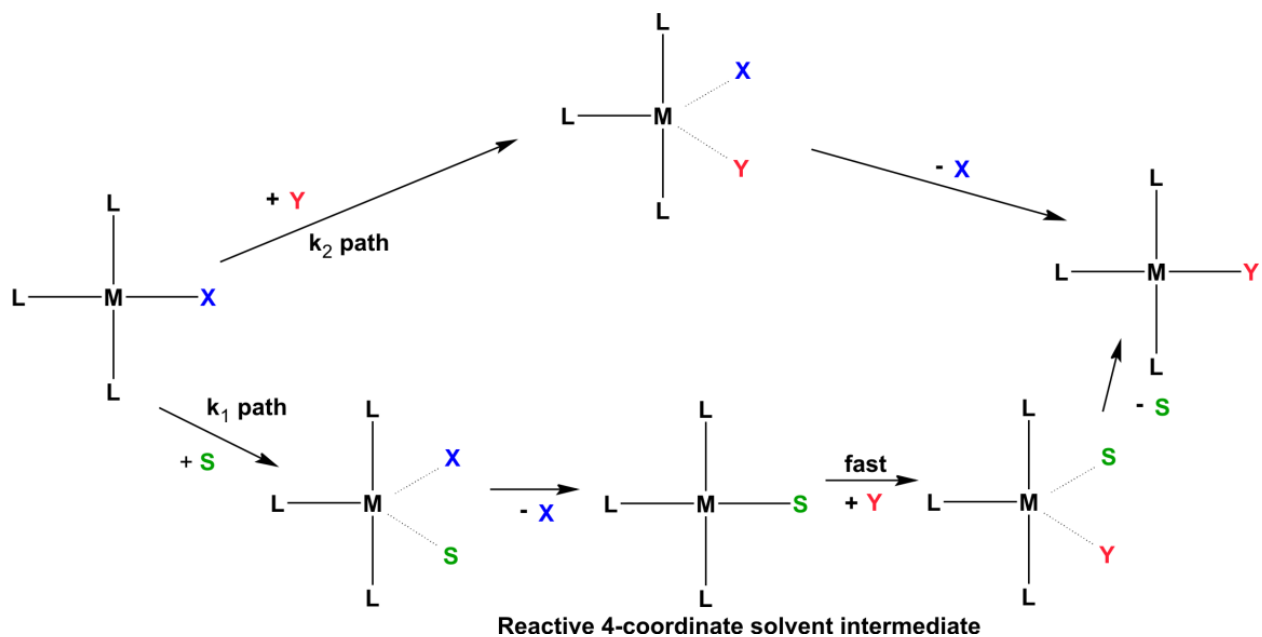


Figure 2.4: Diagram showing both associative k_2 (direct nucleophilic attack) and k_1 (solvolysis) pathways for square planar complexes.^{1, 3, 6, 13}

Square-planar d^8 metal complexes have an unsaturated 16-electron coordinate valence shell hence often follow an associative pathway involving an 18-electron transition state.^{1,3} In general, platinum(II) d^8 systems have a relatively low energy, vacant p_z orbital, which allows the metal centre to extend its coordinate number from four to five by accepting an extra pair of electrons from the entering ligand resulting in a trigonal bipyramidal transition state geometry (**Figure 2.5**).^{2-3,8, 11, 13} This extended coordination is possible since the four coordinate square-planar complexes are not sterically hindered therefore the incoming ligand can attack the metal centre from both above and below the square-plane.^{9, 12} General considerations of the shape and the available orbitals support only the formation of a trigonal bipyramidal geometry.^{9, 12} However, both trigonal bipyramidal and square pyramidal geometries have been found during the process of substitution.^{9, 12}

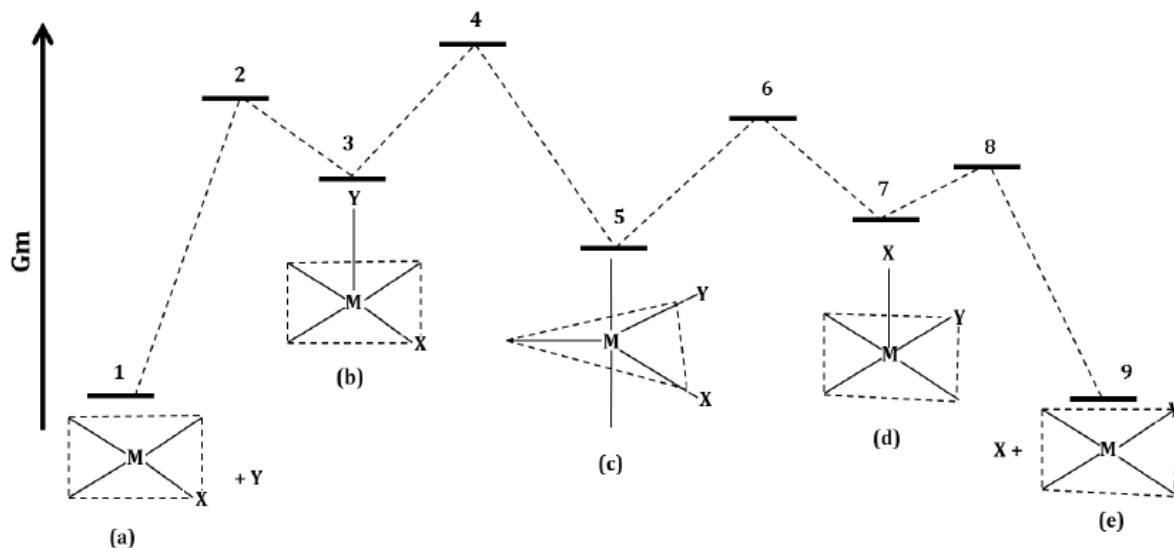


Figure 2.5: Illustration of the changes in energy and stereochemistry that occur during the act of associative substitution of the leaving group, X, by the entering group, Y, of a square-planar complex: Energy levels at **2, 4, 6, and 8** indicate the different transition states whilst the remaining levels show energies of the reaction intermediates.^{8,11-13}

2.4 Factors Influencing the Rate of Ligand Substitution

The substitution kinetics of square-planar complexes involving an associative pathway depends on several factors and as a result, all the ligands in the five coordinate transition state have the ability to affect the stability and the activation energies of the process. The following factors influence and play a critical role on the reactivity of square-planar complexes.

2.4.1 The Effect of the Non-Labile Ligands

Besides the expected influence of the entering (Y) and leaving (X) groups, the substitution behaviour of square-planar complexes are also affected by the nature of the non-labile ligands positioned *cis* and *trans* to the leaving group.^{1, 3, 6, 26-27} The effect that these ligands have on the metal centre is known as the *cis*- and *trans*-effects.²⁸ In an associative type

mechanism, the transition state formed involves a trigonal bipyramidal intermediate with the leaving group (**X**), the entering group (**Y**) and the *trans* ligand all in the trigonal plane.^{1,3,6,21} The two *cis* ligands are in the axial positions hence they remain symmetrically distinct due to the T-shaped relationship between the *trans* ligand and the two *cis* ligands.^{1,3,6,21} Moreover, the influence due to the *trans* ligand is more pronounced than the two *cis* ligands.^{1,3,6,21}

2.4.1.1 The *trans*-Effect

One of the most important factors is the influence of the coordinated ligand on the substitution rate of ligands opposite to it in a metal complex.^{6-7,12} This influence was first observed by Werner in the early 20th century^{13,29-30} and was later understood by Chernyaer and co-workers in 1926 when they introduced the concept of *trans*-effect to understand reactions of square-planar platinum(II) complexes.^{3,6} The *trans*-effect is universally defined as ‘the effect of a coordinated ligand on the rate of replacement of a ligand *trans* to itself’⁷, i.e., the tendency of the spectator ligand to direct an incoming ligand (**Y**) to the position *trans* to itself.¹² This happens because the spectator ligand labilizes the ligand *trans* to it in order to facilitate substitution.^{6,18} **Figure 2.6** illustrates the effect of the *trans* ligand (**T**) on the leaving group (**X**).^{6,18}

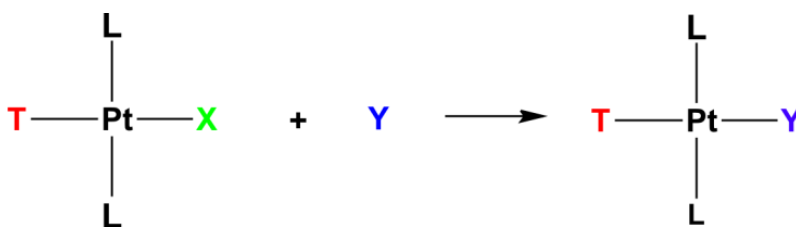
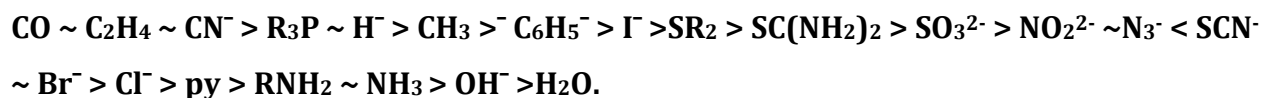


Figure 2.6: Schematic diagram showing the labilization of the leaving group (**X**) by the *trans* ligand (**T**).^{6,18}

In addition, labilization of the leaving group (**X**) is dependent on the *trans* ligand (**T**), i.e. the greater the *trans* effect of a specific ligand, the greater the *trans*-labilization of the leaving group and the larger the rate constant for the substitution reaction.^{6,12} In platinum(II) complexes, the generally accepted order of *trans* effect established from extensive

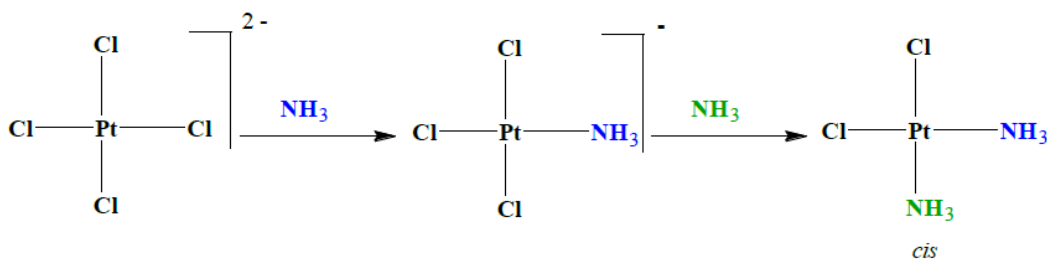
investigations on the effect of the ligand on substitution reactivity at the platinum(II) centre (using different nucleophiles) is as follows:^{3, 6, 12-13}



Scheme 2.8: The approximate order of decreasing the *trans*-effect in platinum(II) complexes. ^{3, 6, 12-13}

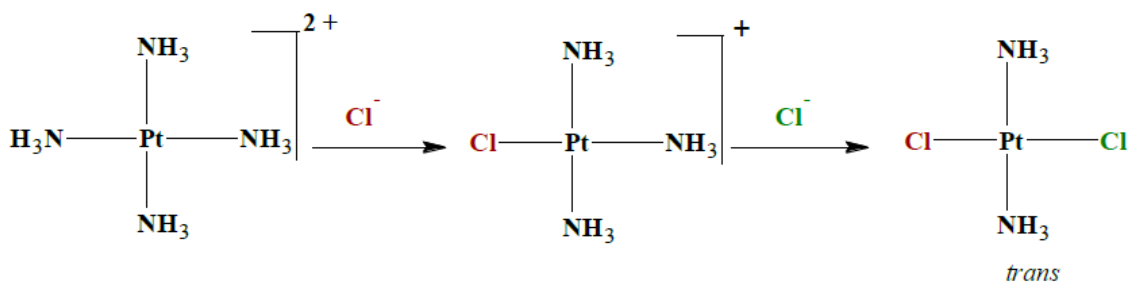
It is worth noting that kinetically the *trans*-effect can be significantly large i.e. up to six orders of magnitude greater or more for inert ligands with high *trans*-effect compared to ligands with low *trans*-effect.⁶ The above sequence covers the rate effects in the range 10^6 to 10^{11} -fold increase on the lability of the complex when a strong labilizing ligand is attached.^{7, 31-32} Since the *trans*-effect is a kinetic phenomenon affecting the rate of substitution of the leaving group positioned *trans* to it, its origin is an increase or decrease in the rate arising from the *trans*-effect of a ligand due to reactant destabilization and/or in the transition state stabilization.^{6, 13}

In addition, the *trans*-effect has been useful in rationalizing the synthetic procedures of square-planar complexes of the desired geometry.¹² An example of this empirically established trend is the synthesis of the *cis* and *trans* isomers of $\text{PtCl}_2(\text{NH}_3)_2$.⁶ The second NH_3 (**Scheme 2.9**) is substituted in the *cis* position by the negatively charged Cl^- since it has a larger *trans*-effect than the neutral NH_3 ligand.⁶ Furthermore, the least reactive chloride group in the formed $[\text{Pt}(\text{NH}_3)\text{Cl}_3]^-$ is the chloride ligand opposite to the NH_3 group, which upon substitution, forms *cis*- $\text{PtCl}_2(\text{NH}_3)$.⁶



Scheme 2.9: Schematic representation for the preparation of *cis*- $\text{Pt}(\text{NH}_3)_2\text{Cl}_2$ from the treatment of $[\text{PtCl}_4]^{2-}$ with neutral NH_3 .⁶

The *trans* isomer is prepared by treating $[\text{Pt}(\text{NH}_3)_4]^{2+}$ with chloride ions (**Scheme 2.10**), where the first chloride replaces any NH_3 ligand.⁷ The now coordinated chloride group replaces the most labile ligand in $[\text{Pt}(\text{NH}_3)\text{Cl}_3]^-$ - which is the NH_3 ligand opposite to the chloride ligand thereby forming *trans*- $\text{Pt}(\text{NH}_3)_2\text{Cl}_2$.⁶



Scheme 2.10: Schematic representation for the preparation of *trans*- $\text{Pt}(\text{NH}_3)_2\text{Cl}_2$ from treatment of $[\text{Pt}(\text{NH}_3)_4]^{2+}$ with chloride ions.⁶

Another phenomenon closely related to the *trans*-effect but characteristically different is the *trans* influence, which is purely thermodynamic. It is important to note that ligands with the highest *trans* effect such as H^- , CH_3^- and SnCl_3^- normally form either unusually strong σ -bonds (**Figure 2.7(a)**) or unusually strong π -bonds (**Figure 2.7(b)**) for ligands such as C_2H_4 , CO and CN^- when considering the *trans*-effect in substitution reactions of platinum(II) complexes.³³

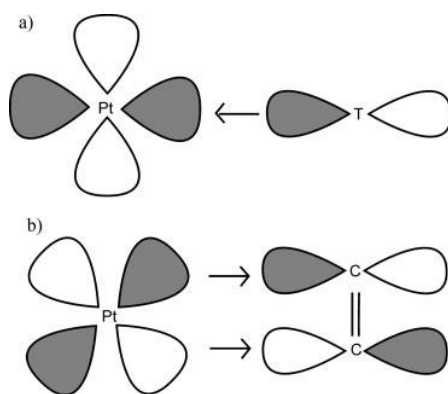


Figure 2.7: (a) σ -donation from the filled ligand p_x orbital to vacant metal $5d_{x^2-y^2}$ orbital. (b) π -back-donation from the filled metal d_{xz} orbital to the antibonding linear combination of carbons' p_x orbitals in C_2H_4 .³³

Therefore it is essential to differentiate between the *trans*-effect and the *trans*-influence of a ligand and further understand both the σ - and π -bonding effects hence the *trans*-effect. These effects involve the ground state orbitals shared by the metal, the leaving group and the *trans* ligand.² The *trans*-effect known to be the effect of the ligand on the rate of substitution of the *trans* ligand involves both the ground and transition state whereas the *trans* influence is the effect of the *trans*-ligand only on the ground state properties like bond lengthening (X-ray determinations) and vibrational bond stretches (IR frequencies) *i.e.* an equilibrium phenomenon.^{6, 13, 34} If there is no transition state differences, the *trans*-influence order and the *trans*-effect order would be the same. In addition, several studies have been conducted to explain the *trans*-effect with the π -bonding theory and the polarization theory being the two common theories used to explain it.^{7, 35-38}

a. The Polarization Theory

This theory was postulated by Grinberg³⁹ and it is based on polarization focusing more on the **Pt–X** bond weakening due to the strong *trans*-effect caused by **L** in **PtA₂LX**.⁶ Postulated by Grinberg,³⁹ Meerwein⁴⁰ further studied in detail the influence of ligand polarization on the rate of substitution. It was explained using charge distribution in induced dipoles in the **L–Pt–X** coordinate, where **X** is the leaving group and **L** is the *trans* ligand (**Figure 2.8**).^{6, 40}

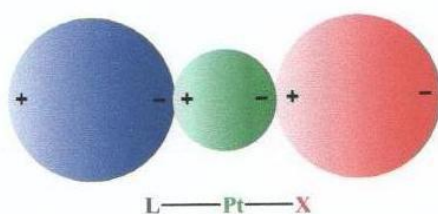


Figure 2.8: Distribution of charge in induced dipoles in the L–Pt–Cl coordinate of *trans*-[PtA₂LX] due to polarization.⁶

Grinberg's theory states that the primary charge on the platinum(II) induces a dipole in **L** (the *trans* ligand) which then induces a dipole in the platinum metal.⁶ This second dipole repels the negative charge in the leaving group, **X**, hence the force of attraction of **X–Pt** is reduced causing the **Pt–X** bond to lengthen and weaken.⁶ The weakening of the **Pt–X** bond

accelerates the rates of substitution at the square-planar platinum(II) centre.^{6, 41} Therefore, ligands with a stronger *trans*-influence weaken the **Pt-L** bond to be easily displaced hence increasing the energy of the ground state.⁴²⁻⁴³ In addition, it was noted that for this theory to fully support the *trans*-effect series, the effect of covalent bonding needs to be considered. Ligands of high polarizability are expected to form the most covalent bonds with platinum(II).⁴⁴

b. The π -Bonding Theory

The π -bonding effect in metal complexes was made known by Pauling⁴⁵ to justify the short Ni-C bond distances in Ni(CO)₄.⁴⁵ This theory deals solely with ligands high in the *trans*-effect series⁶ and further states that these ligands with π -bonds such as CO, CN⁻, C₂H₄ and PR₃ stabilize the transition state during the course of a substitution reaction which is the reason they are high in the *trans*-effect series.^{6, 34} These ligands have strong π -acceptor abilities and are regarded strong *trans* directors thus stabilizes the transition five-coordinate transition state by removing the increased electron density from the metal centre. **Figure 2.9** below shows the bonding of phosphorus to the platinum(II) metal centre.^{6, 34}

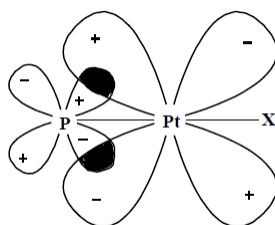


Figure 2.9: Illustration of the R₃P-Pt double bond. If ligands PR₃ and X are in the *xy* plane and the *d*-orbitals shown are either *d*_{*xy*} or *d*_{*yz*}.^{6, 18, 34}

A σ -bond is formed when a pair of electrons is donated from the phosphorus to the platinum metal centre whereas the corresponding π -bond is formed by the overlap of a filled *d*-orbital of the platinum centre with a vacant orbital of the ligand.^{6, 11}

The removal of electrons from the platinum centre to the vacant orbitals of the ligands weakens the **Pt-X** bond in the presence of most good *trans* directors with the exception of olefins in which electron donation (σ -bonding) is more important than electron withdrawing (π -bonding).⁶ However, there is no clarity on whether bond weakening in the ground state is always adequate to account for the effect of good *trans* activation, i.e. the removal of electrons from the platinum metal in the ground state by the π -bonding would actually appear to strengthen bonds of other ligands instead of weakening the **Pt-X** bond.⁶

Chatt *et al.*⁴⁶ and later Orgel⁴⁷ proposed that the *trans*-effect is due to π -bonding stabilizing the activated trigonal bipyramidal intermediate in the transition state. Independently, they proposed a π -bonding stabilization mechanism of the activated complex for the substitution reaction of *trans*-PtA₂LX with Y to form *trans*-PtA₂LY where **X** is the leaving group, **Y** is the entering group and **L** is the *trans* π -bonding ligand (**Figure 2.10**).⁴⁶⁻⁴⁷

Chatt *et al.*⁴⁶ stated that the incoming group brings additional electron density in the transition state and removal of this added charge from the platinum(II) *via* π -bonding of the *trans* ligand, **L**, enhances the addition of the entering group, **Y**, thereby increasing the rate of an associative substitution reaction as the activation energy is lowered.⁴⁶ Orgel⁴⁷ supported this by emphasizing that the stability of the transition state is increased due to π -bonding which reduces the electron density on platinum(II) along the **Pt-X** and **Pt-Y** direction leading to the retention of configuration.⁴⁷ This is well known as the π -*trans*-effect.⁶

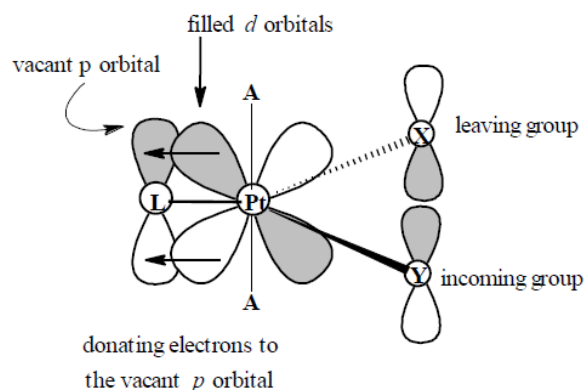


Figure 2.10: Activated trigonal bipyramidal complex for the *trans*-PtA₂LXY. ^{6, 34}

2.4.2 Molecular Orbital Theory

This theory supports the π -*trans*-effects and further best describes and explains the σ - and π -*trans* effect as it explains the bonding in square-planar platinum(II) systems.^{6, 34}

2.4.2.1 σ -*trans* effect

A simplified MO diagram of PtCl_4^{2-} is shown in **Figure 2.11**.^{6, 48} The most stable orbitals are the σ -bonding orbitals and the second most stable orbitals are the π -bonding molecular orbitals.^{6, 48} These orbitals are mainly located on the chloride ligands.^{6, 48} Following them in stability are the anti-bonding of the σ - and π -orbitals, π^*_{xz} , π^*_{yz} , $\pi^*_{z^2}$, $\sigma^*_{z^2}$ and π^*_{xy} and the comparatively unstable $\sigma^*_{x^2-y^2}$.^{6, 48} All these orbitals come from the 5d atomic orbitals of the platinum(II) and contain four probable MO of which π^*_{xy} is the most stable and the $\sigma^*_{x^2-y^2}$ relatively the least stable MO.^{6, 34, 48} The anti-bonding σ -orbitals; σ^*_s , σ^*_x , σ^*_y and σ^*_z are located at higher energies and are relatively the least stable from them all.^{6, 48} These higher energy p_z valence orbitals are not involved in any σ -bond formation.^{6, 48}

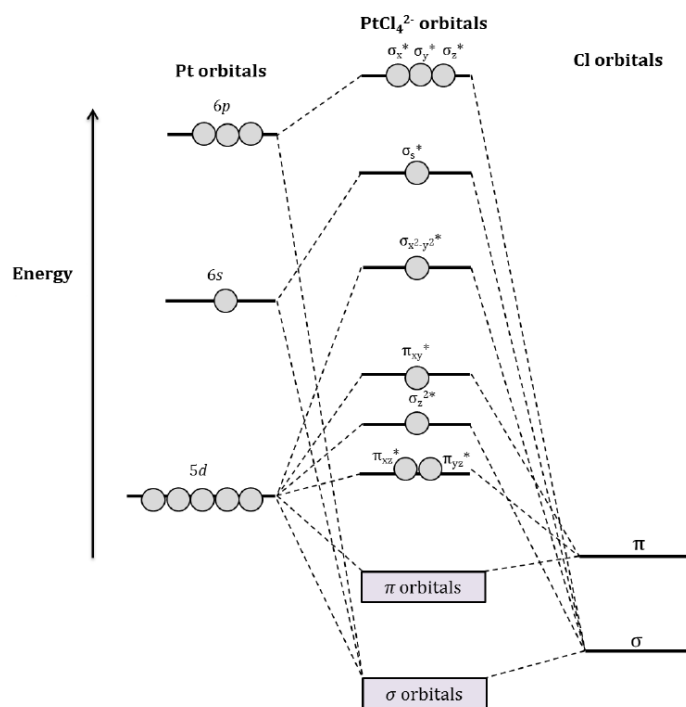


Figure 2.11: The Molecular Orbital Diagram of $[\text{PtCl}_4]^{2-}$.^{2-6, 34}

In square-planar complexes, $d_{x^2-y^2}$, s , p_x , p_y and $5d_{z^2}$ metal valence orbitals are the only four orbitals used for the σ -bond formation.^{7,40} However, only two orbitals (p -orbitals) are effective *trans* directors since they have the correct geometry for *trans* directing properties.^{6,34} Therefore in *trans*-PtA₂LX, the *trans* ligand, **L** and the leaving group, **X** share the same (d_{sp^2}) σ_x orbital in the overall MO arrangement.⁶ If as expected that the σ -donor ability of the *trans* ligand, **L** is large then the **Pt-L** bond is strengthened hence has a larger portion of the shared MO orbital.⁶ This in turn weakens the ground state **Pt-X** bond due to a smaller share of the electrons available for bonding enhancing the substitution reaction of **X** by **Y** (**Figure 2.12**).^{13, 62}

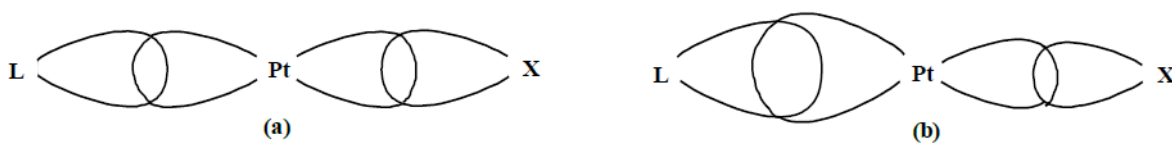


Figure 2.12: Diagram showing the ground state σ -bonding of **L-Pt-X** using the σ_x MO. (a) The equal σ -bond strengths of **L** and **X**. (b) The σ -bonding strength of the *trans*-ligand, **L** is greater than that of **X** thus weakening the **Pt-X** bond.^{2,6, 13}

The stronger of the two (the *trans* ligand, **L** or the leaving group, **X**) contributes more electron density towards the shared orbital.⁷ For example, a good σ -donor (covalent ligand) such as H^- and CH_3^- will donate a large amount of electron density to the p_x orbital of the metal creating repulsion between the σ -electrons of the *trans* ligand and the electrons of the metal in the same p_x orbital.⁶ This in turn strengthens the **Pt-L** bond and weakens the **Pt-X** bond subsequently enhancing the reaction rate.⁶

Langford and Gray⁸ provided an additional explanation to rate enhancement due to σ -donation. They suggested that such good σ -donors as H^- and CH_3^- stabilize the trigonal bipyrimidal intermediate by a process called σ -*trans* effect.⁸ In the ground state of a square planar complex, there is only a single p -orbital (p_x) used to bond **L-Pt-X**.^{3, 6}

However, during an associative substitution reaction, addition of the entering group, **Y** *trans* to the *xy* plane causes **X** to shift out of plane into a trigonal plane containing **Pt**, **L**, **X** and **Y** (**Figure 2.13**).^{3, 6} This newly formed trigonal plane has two *p*-orbitals (p_x and p_z) for three bonding ligands.⁷ This leads to an increased stability of the transition state since two orbitals for three bonding ligands are better than one orbital shared by two ligands in the ground state.⁶ Furthermore, this means that good σ -bonding ligands which can donate into the extra *p*-orbital can stabilize the σ -structure in the transition state hence will have higher *trans*-effect.⁸

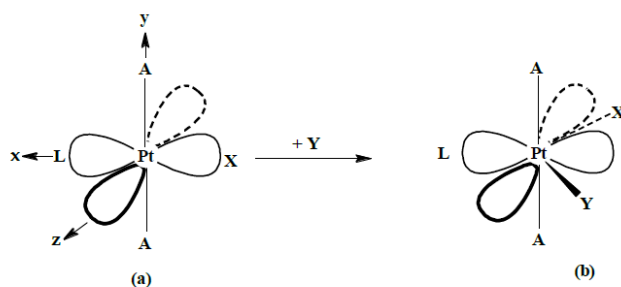


Figure 2.13: The σ -*trans*-effect due to the stabilization of the trigonal bipyramidal intermediate. (a) Only the p_x orbital is available for σ -bonding of ligands **L** and **X** (b) p_x and the p_z orbitals are available for σ -bonding of ligands **L**, **X** and **Y** in a trigonal plane.^{3, 6, 8}

2.4.2.2 π -*trans* effect

Strong π -bonds are given by good *trans* directing groups such as C_2H_4 , CO and CN^- .⁶ In square-planar complexes, only three MO's (π^*_{xz} , π^*_{yz} and π^*_{xy}) have the correct orientation to form π -bonding.⁴⁹ There is a formation of the trigonal bipyramidal intermediate when there is an addition of the entering nucleophile, **Y**.⁶ Formation of this five coordinate intermediate results in an additional MO ($\pi^*_{x^2-y^2}$) which is also in the correct orientation for π -bonding.⁶ These four MO's in the trigonal plane are shared in π -bonding with the three ligands (**L**, **X** and **Y**). The *trans* ligand can greatly stabilize the transition state if it is capable of bonding to the π^* orbitals which results in delocalization of the electronic charge to the ligands which further lowers the energy of the system.^{2,6} Therefore it can be said that the

primary purpose of a good *trans* π -acceptor ligand will be to stabilize the transition state by lowering the activation energy of the reaction.^{6, 13,26, 50-51}

For example, studies by Jaganyi *et al.*^{26, 52} have shown that *trans* π -accepting ligands can cause an increase in the substitution reaction of platinum(II) complexes. This *trans*-effect was related to the π -accepting ability of the ligands which withdraw electron density from the metal centre thus stabilizing the trigonal bipyrimidal intermediate. A number of studies on the assessment of the σ - and π -*trans* effect of several ligands have been done and the qualitative results obtained are tabulated below (**Table 2.1**).⁶

Table 2.1: Estimated σ - and π -*trans* effects of selected ligands.⁶

Ligand	σ -effect*	π - effects*
C₂H₄	w	vs
CO	m	vs
CN⁻	m	s
PR₃	s	m
H⁻	vs	vw
I⁻	m	m
CH₃⁻	s	w
Pyridine	w	w

* vs, very strong; s, strong; m, medium; w, weak; vw, very weak

2.4.2.3 The *Cis* Effect

There are few reports on the *cis* effect with results obtained often being contradictory.^{29, 58-59} The substitution reactions are sensitive to the *cis* ligand though to a smaller extent when compared to the *trans* ligand.^{1, 3, 13} The *trans*-effect has been shown to be 10³-10⁶ orders of magnitude greater than that of *cis* effect.^{9, 50} The *cis* effect is quite significant in the presence of steric hindrance in the *cis* position.³ Also, investigating the *cis* effect requires the varying of the *trans* ligand as it is more difficult to study the *cis* effect by varying the *cis*

ligand.³ The effect of the steric hindrance from the *cis* position is more significant in the trigonal bipyramidal transition state as the *trans* group (**L**) shares the equatorial trigonal plane and is 120° away from the entering and leaving group while the axial *cis* ligand is 90° away from the equatorial groups.¹³ Therefore, for square planar complexes undergoing an associative mechanism, an increase in the size of the entering group would destabilize the trigonal bipyramidal intermediate hence decreasing the rate of the substitution reaction.³ For example, a kinetic study performed with *cis*-Pt(Et₃)₂LCl with pyridine (*Equation 2.3*) had the same trend as its isomeric complex, *trans*-Pt(Et₃)₂LCl with pyridine when the *trans* ligand (**L**) was changed.⁵⁴ It was noted that the order of the reaction with *cis* complex increased by factor of three (**Table 2.2**)¹³ while the *trans* complex had an order much higher.^{7, 35}

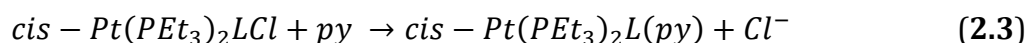


Table 2.2: The effect of *trans* ligand, **L** on the reactivity rate of *cis*-Pt(PEt₃)₂LCl with *py*.⁵⁴

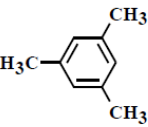
L	k₁ (10² s⁻¹)
Cl⁻	1.7
C₆H₆⁻	3.8
CH₃⁻	6

2.4.2.4 The Steric Effect

Steric effects are generally space-filling effects⁵⁵ categorised as steric bulky and steric hindrance. The latter is due to mutual repulsion of electron densities of a group of atoms around the metal centre while the former is the shielding of the reaction site from direct attack by an entering group.^{54, 56} The transition state of an associated-type mechanism involves an increase in the steric hindrance since it comprises of a five-coordinate intermediate.¹ This slows down the substitution reaction because the transition state is destabilized by increased steric interactions.^{1-3, 6, 9} However, the associative substitution reaction of a specific platinum(II) complex can be retarded if the ligands are sterically bulky.^{1-3, 6, 9} This results in acceleration of a dissociative-type mechanism due to steric strain being relieved by bond dissociation.^{1, 2, 6, 9} The retardation effect is more prominent on the reaction

rate if the sterically hindered groups are in the *cis* positions relative to the leaving group.^{1, 3} The influence of the steric bulk on the reaction rate can be either due to the steric bulk in the spectator ligand or in the incoming nucleophile.^{1, 3} In addition, the use of sterically hindered ligands in square-planar complexes is useful in changing the substitution mechanism from associative to dissociative.^{1-3, 6, 9, 11} For instance, the steric effect exerted in *cis*-/*trans*-Pt(PEt₃)₂LCl was studied, (L = phenyl, *o*-tolyl, mesityl). The rate constant data obtained is shown in **Table 2.3**.^{3, 13, 54}

Table 2.3: Steric effects on the rate constants for the chloride substitution by pyridine in *cis*- and *trans*-[Pt(PEt₃)₂(L)Cl].^{3, 13, 54}

Ligand, L		<i>k</i> _{obs} , s ⁻¹	
		<i>cis</i> -Pt(PEt ₃) ₂ LCl (0 °C)	<i>trans</i> -Pt(PEt ₃) ₂ LCl (25 °C)
L = phenyl		8.0x10 ⁻²	1.2x10 ⁻⁴
L = <i>o</i> -tolyl		2.0x10 ⁻⁴	1.7x10 ⁻⁵
L = mesityl		1.0x10 ⁻⁶ (25 °C)	3.4x10 ⁻⁶

An increase in the steric bulk results in a decrease of the reaction rate from phenyl to mesityl. However, there is larger decrease in the reaction rate for the *cis* complex in comparison to the *trans* complex.^{6, 13} The large decrease in the *cis* complex results from the fact that the L is in the axial position in the transition state (90° away from the equatorial groups) thus there is greater steric repulsion between the *cis* ligands and the leaving group compared to L in the equatorial position (120° away from the entering and leaving group) for the *trans* complex (**Figure 2.14**).²

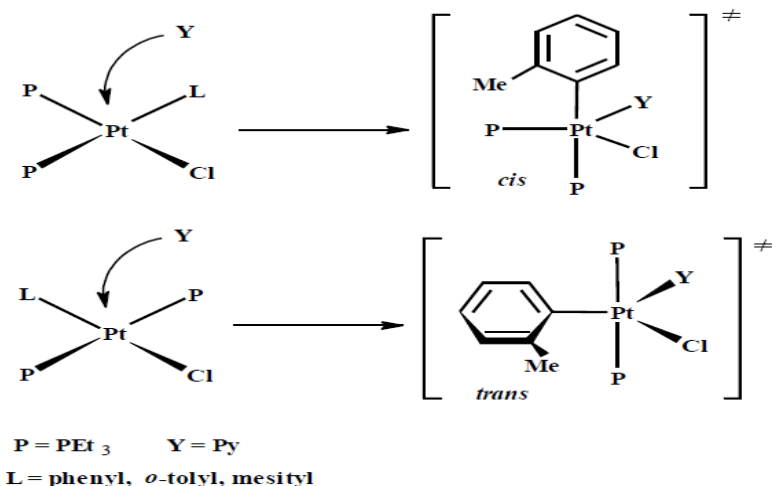
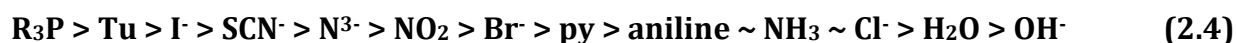


Figure 2.14: The steric effect of the aryl square-planar complex and trigonal bipyramidal intermediate of the *cis* isomer and *trans* isomer.²

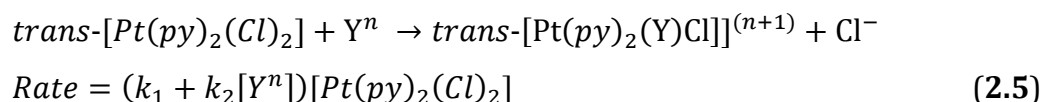
2.4.3 The Effect of the Entering Nucleophile

As mentioned previously, an associative substitution reaction is largely dependent on the nucleophilicity of the entering nucleophile.⁹ Nucleophilicity is a measure of the reactivity of the nucleophile towards an electron-deficient atom (platinum metal centre in this case).^{1, 3} The stronger the nucleophile, the greater the second order rate constant (k_2) for that specific Pt(II) complex.¹⁻³ The nucleophilicity of an entering nucleophile is usually influenced by several factors such as basicity, polarizability, oxidability, solvation energy and the nature of the metal centre.⁹ Studies performed on platinum(II) complexes with various nucleophiles showed that the nucleophilic reactivity order is, (*Series 2.4*):^{6, 18, 23, 57}



The reactivity trend (*Equation 2.4*) is mostly dependent on the polarizability (softness) of the entering nucleophiles than it is on their base strength.^{6, 13, 55} Polarizability is best explained using the “Hard Soft Acid Base” theory (HSAB), discovered by Pearson in 1963.^{29, 58} This theory suggests that “soft” (polarizable) nucleophiles prefer soft metals as their substrate, such as platinum and gold, whereas “hard” (non-polarizable) nucleophiles prefer hard substrates.^{2, 9, 29, 58} Hard acids (metal ions) are small and highly charged and possess a

valence electron shell which is not easily distorted while soft acids (metal ions) are large and possess low charge and have a valence electron shell which is easy to distort or remove.^{9, 29, 58} Therefore, the high tendency of larger donors to be effective nucleophiles towards platinum(II) complexes indicates that platinum(II) is a soft centre thus platinum(II) is more effective towards large donors.^{2,9, 29} In order to correlate an empirical scale of the nucleophilicity, a comprehensive study on the relative reactivity and nucleophilicity was conducted by Belluco²³ using *trans*-[Pt(py)₂Cl₂] in methanol at 30 °C (*Equation 2.5*).^{3, 59}



When *trans*-[Pt(py)₂Cl₂] was used as the standard, the nucleophilicity constant of the incoming nucleophile, n°_{pt} , is defined as follows, (*Equation 3.6*):^{1, 3, 6, 13}

$$n^{\circ}_{pt} = \log\left(\frac{k_y}{k^{\circ}_s}\right) \quad (2.6)$$

where, k_y = the measured second-order rate constant for the reaction of the entering nucleophile, k°_s is the second-order rate constant for attack of the solvent (methanol) in an associative mechanism and is equal to $\{k_s/[\text{MeOH}]\}$ and k_s = the rate constant for attack of the solvent, MeOH, on the complex.

At 30 °C, the concentration of pure methanol is assumed to be 24.3 M and the equation simplifies to *Equation 2.7*:^{1, 3, 6, 13}

$$n^{\circ}_{pt} = n_{pt} + \log(24.3) = n_{pt} + 1.39 \quad (2.7)$$

A summary of the typical n°_{pt} data obtained for *Equation 2.7* is given in **Table 2.4** for different entering nucleophiles (**Y**).

Table 2.4: A selection of n°_{pt} values listed according to donor atom for *trans*-[Pt(py)₂Cl₂].^{6, 23, 60}

Nucleophile	Donor Atom	n°_{pt}
CH ₃ OH	O	0
Imidazole	N	3.44
C ₅ H ₅ N	N	3.13
NH ₃	N	3.06
(C ₆ H ₅) ₂ S	S	4.38
S=C(NH ₂) ₂	S	7.17
SO ₃ ²⁻	S	5.79
Cl ⁻	Cl (Halogen)	3.04
I ⁻	I (Halogen)	5.46
(C ₂ H ₅) ₃ P	P	8.79
(C ₆ H ₅ CH ₂) ₂ Se	Se	5.53
CN ⁻	C	7.14

The nucleophilic reactivity constant measures the reactivity of the entering nucleophile towards the platinum(II) centre.⁶ From **Table 2.4** above, a number of interesting trends can be observed. The nucleophilicity of the halogens follow the decreasing trend, I⁻ > Br⁻ > Cl⁻ hence decreases down the order. Furthermore, phosphine and sulfur-donor groups have the most reactive nucleophiles towards platinum(II) centre due to their high nucleophilicity constant values. In addition, most reactive nucleophiles are soft (species which are large, have low charge states and are strongly polarizable) which is why sulfur is a better donor than oxygen and nitrogen. The nucleophilic reactivity constant correlates other properties in the ligand and this correlation is termed linear free energy relationship (LFER), (*Equation 2.8*).^{6, 15} Plots of log k_y for a given nucleophile versus the n°_{pt} value for many platinum(II) complexes were found to be linear signifying a linear free energy relationship (LFER) of the form (**Figure 2.15**):^{6, 15}

$$\log k_y = S. n^{\circ}_{pt} + C \quad (2.8)$$

where, S is the *nucleophilic discrimination factor* and depends on the complex.

C is the *intrinsic reactivity*.

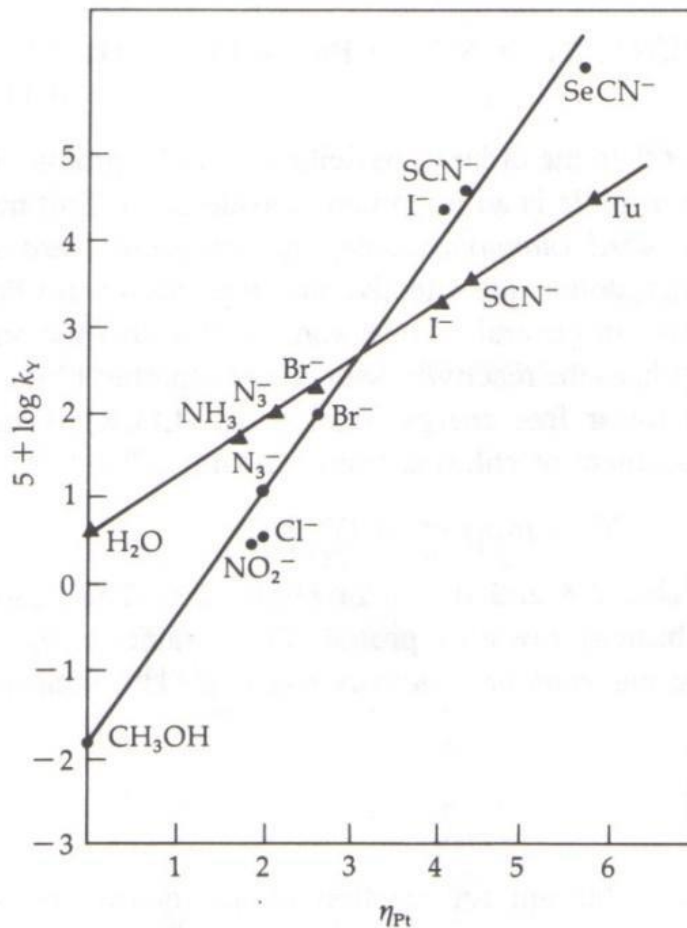


Figure 2.15: Rates of Pt(II) complexes correlated with *trans*-[Pt(py)₂Cl₂] as reference, for different entering nucleophiles: ● = *trans*-[Pt(PEt₃)₂Cl₂] in methanol at 30 °C; ▲ = [Pt(en)Cl₂] in water at 35 °C.^{6, 23, 34, 62}

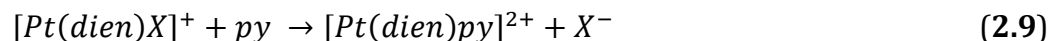
The nucleophilic discrimination factor (*S*) measures the sensitivity of the platinum(II) centre to the nucleophilicity of the entering nucleophile. The intercept (*C*) is equivalent to log *k_s* where *k_s* represents the rate constant of the weakest nucleophile in a solution.^{1, 3, 6} A smaller value for *k_s* is reflective of a complex which is more sensitive to the changes in the nucleophile.⁶ From **Figure 2.15**, the *trans*-Pt(py)₂Cl₂ complex is regarded as the reference complex with *S* equal to 1.¹⁵ Values of *S* > 1 imply higher sensitivity of the reaction rate to changes in the nucleophilic nature relative to the reference complex.¹⁵ In addition, certain nucleophiles such as NO₂⁻ and SeCN⁻ do not follow the LFER as seen in **Figure 2.15**.^{1, 3, 23} These nucleophiles have better π-accepting abilities which increase the reactivity by lowering the energy of the transition state through metal to ligand π-interactions.^{1, 3, 60} These

ligands having good π -accepting abilities tend to be more reactive towards better π -donating metal complexes such as $[\text{PtCl}_4]^{2-}$ and less reactive to poor π -donating complexes such as $[\text{Pt}(\text{dien})\text{Br}]^+$ relative to the reference *trans*- $[\text{Pt}(\text{py})_2\text{Cl}_2]$.

2.4.4 The Effect of the Leaving Group

The effect of the leaving group has a smaller impact on the rate of substitution in associatively activated square planar complexes and are considered less important.^{1, 13} The entering group (**Y**) and the leaving group (**X**) are closely connected, i.e. occupy equivalent positions in the transition state hence it is very difficult to qualify the effect of the leaving group.^{1, 13} The leaving group is also closely related to the nature of the reaction centre, the nature of the *trans* ligand and the solvent polarity.^{1, 3} In order to investigate and understand the effect of the leaving group, the *cis* and *trans* ligands must be the same.

The reaction below has been studied in depth, (*Equation 2.9*).⁶²⁻⁶³



From the kinetic data, it was established that the rate of substitution of the leaving group decreases in the order:



This series shows that the strongly bound ligands dissociate more slowly from the five-coordinate intermediate thus leaving groups with lower nucleophilicity are easily replaced.^{3, 6, 15} The series also highlights that for an associative-type mechanism, a large amount of metal ligand (**Pt-X**) bond breaking occurs in the transition state which depends on a specific reaction.^{6, 13}

2.4.5 The Effect of the Solvent

The solvent effects can play at least two important roles in the substitution reactions of square-planar complexes.^{3, 6} It can be the reaction medium and it can also influence the energy of the activation process through solvation of the ground and activated states.^{3, 6} As mentioned before, the solvolysis pathway results in a second order rate law for substitution reactions of square-planar complexes (also see Chapter 3). In addition, studies have shown that the contribution of the solvent to the overall reaction rate is proportional to the coordinating ability of the solvent.¹⁵ This is shown by the experimental data (**Table 2.5**) obtained for the chloride exchange reaction with radio-labelled ³⁶Cl⁻ for *trans*-[Pt(py)₂Cl₂] (*Equation 2.10*).^{62, 13, 64}

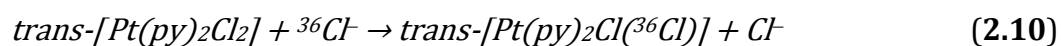


Table 2.5: Effect of solvent on the rate of chloride exchange from *trans*-[Pt(py)₂Cl₂] at 25 °C.^{2,6, 64}

Strongly Coordinating solvents		Weakly coordinating solvents	
	$k_2 / (10^{-5} \text{ s}^{-1})$		$k_{2(\text{Cl}^-)} / \text{M}^{-1} \text{ s}^{-1}$
DMSO	380	CCl ₄	10 ⁴
H ₂ O	3.5	C ₆ H ₆	10 ²
CH ₃ NO ₂	3.2	Me ₂ CO	10 ⁻²
C ₂ H ₅ OH	1.4	DMF	10 ⁻³

From **Table 2.5**, it is seen that reactivity rates of highly coordinating solvents such as DMSO show direct dependence on the nucleophilicity of the solvent ($k_s \gg k_{\text{Cl}^-}$) and independence to the entering nucleophile while the opposite is true for non/weakly coordinating solvents. The k_s values for coordinating solvents increase in the order:⁶



The larger exchange rate of DMSO compared to H₂O confirms that platinum(II) is a soft metal centre and prefers coordinating or interacting with the larger and more polarized S-atom of DMSO than it does with the O-atom of H₂O.⁶ Therefore, the platinum-solvent bond making is of great importance in the transition state compared to bond breaking.⁶

For non- or weakly coordinating solvents such as non-polar tetrachloromethane, benzene and the sterically hindered alcohols, larger reaction rates have been reported since the chloride act as a nucleophile hence $k_{\text{Cl}}[^{36}\text{Cl}^-] > k_{\text{s}}$.^{6, 13} Also, for such solvents, larger k_{s} values are expected because the solvent cannot coordinate to the metal.^{6, 13} Furthermore, the opposite is true for polar solvents such DMF where the chloride leaving group is not solvated.^{6, 13}

2.5 References

1. Tobe, M. L., *Inorganic Reaction Mechanisms Studies in Modern Chemistry*, Nelson, London, **1972**, p.17-23, 42-68.
2. Jordan, R. B., *Reaction Mechanisms of Inorganic and Organometallic Systems*, Oxford University Press, New York, **1991**, p. 29 - 40, 47-54, 58- 60.
3. Tobe, M. L. and Burgess, J., *Inorganic Reaction Mechanisms*, Addison Wesley Longman Limited, New York, **1999**, p. 30-43, 70-112.
4. Arnaut, L. F., S. and Burrows, H., *Chemical Kinetics From Molecular Structure to Chemical Reactivity*, Elsevier, New York, **2007**, p. 273 - 294.
5. Ingold, C. K., *Structure and Mechanism in Organic Chemistry, 2nd Edition*, Cornell University Press, Ithaca, New York, **1969**, p. 241.
6. Basolo, F. and Pearson, R. G., *Mechanisms of Inorganic Reactions: A Study of Metal Complexes in Solution, 2nd Edition*, John Wiley & Sons, New York, **1967**, p. 124 - 128, 351 -453.
7. Benson, D., *Mechanisms of Inorganic Reactions in Solution*, McGraw-Hill, London, **1968**, p. 1 - 31.
8. Langford, C. H. and Gray, H. B., *Ligand Substitution Processes*, W. A. Benjamin, New York, **1966**, p. 1 - 45.
- 9. Ašperger, S., *Chemical Kinetics and Inorganic Reaction Mechanisms, 2nd Edition*, Kluwer Academic/Plenum Publisher, New York, **2003**, p. 3, 7-23, 38 - 40, 105 - 106, 140-153.
10. Miessler, G. L. and Tarr, D. A., *Inorganic Chemistry*, Pearson Education International, Singapore, **2004**, p. 415- 426.
11. Henderson, R. A., *The Mechanisms of Reactions at Transition Metal Sites*, Oxford University Press, Oxford, **1993**, p. 1 - 4, 10 - 22.
12. Wilkins, R. G., *Kinetics and Mechanisms of Reactions of Transition Metal Complexes, 2nd Edition*, VCH, Weinheim, **1991**, p. 41 - 43, 199 - 201, 221, 232-242.
13. Atwood, J. D., *Inorganic and Organic Reaction Mechanisms, 2nd Edition*, Wiley-VCH Inc., New York, **1997**, p. 1 - 32 - 34, 43 - 61.

14. Atkins, P.; Overton, T.; Rourke, J.; Weller, M. and Armstrong, F., *Shriver & Atkins Inorganic Chemistry 4th Edition*, Oxford University Press, New York, **2006**, p. 63 - 65.
15. Langford, C. H. and Gray, H. B., *Ligand Substitution Processes*, Benjamin, New York, **1965**, p. 1 - 30.
16. Murmann, R. K.; Fraser, R. T. M. and Bauman, J., *Mechanisms of Inorganic Reactions*, American Chemical Society, Washington, D. C, **1965**, p. 20-23, 81-97.
17. Miessler, G. L. and Tarr, D. A., *Inorganic Chemistry*, Prentice Hall Internatioal Inc, New Jersey, **1991**, p. 372 - 375.
18. Banerjea, D.; Basolo, F.; Pearson, R. G., *Journal of the American Chemical Society*, **1957**, 79 (15), 4055-4062.
19. Cross, R. J., *Chemical Society Reviews*, **1985**, 14 (3), 197-223.
20. Cross, R. J., *Advances in Inorganic Chemistry and Radiochemistry*, **1989**, 34, 219-292.
21. Cattalini, L., *Progress in Inorganis Chemistry*, **1970**, 13, 263.
22. Peloso, A., *Coordination Chemistry Reviews*, **1973**, 10 (1-2), 123-181.
23. Belluco, U.; Cattalin, L; Basolo, F.; Pearson, R. G.; Turco, A., *Journal of the American Chemical Society*, **1965**, 87 (2), 241-&.
24. Haake, P.; Chan, S. C.; Jonas, V., *Inorganic Chemistry*, **1970**, 9 (8), 1925-&.
25. Beattie, J. K., *Inorg Chima-Lett.*, **1983**, 76 (2), L69-L69.
26. Hofmann, A.; Jaganyi, D.; Munro, O. Q.; Liehr, G.; van Eldik, R., *Inorganci Chemistry*, **2003**, 42 (5), 1688-1700.
27. Weber, C. F.; van Eldik, R., *European Journal of Inorganic Chemistry*, **2005**, (23), 4755-4761.
28. Chernayev, I. I., *Ann. Inst. Platine USSR.*, **1926**, 4 (1).
29. Pearson, R. G., *Journal of the American Chemical Society*, **1963**, 85 (22), 3533- 3567.
30. Page, J. D., *Journal of Chemical Education*, **1987**, 64, 561.
31. Wendt, O. F.; Elding, L. I., *Journal of the Chemical Society, Dalton Transaction*, **1997**, (24), 4725-4731.
32. Otto, S.; Elding, L. I., *Journal of the Chemical Society, Dalton Transaction*, **2002**, (11), 2354-2360.
33. Chval, Z.; Sip, M.; Burda, J. V., *Journal of Computational Chemistry*, **2008**, 29 (14), 2370-2381.

34. Belluco, U., *Organometallic Coordination Chemistry of Platinum*, Academic Press, London, **1974**, p. 40-53, 138-160, 220-221.
35. Chernyaev, I. I., *Ann. inst. platine USSR*, **1926**, 4, 261.
36. Chernyaev, I. I., *Ann. inst. platine. USSR*, **1926**, 4, 243.
37. Chernyaev, I. I., *Ann. inst. platine USSR*, **1928**, 6, 55.
38. Syrkin, Y. K., *Bull. Acad. Sci. U.S.S.R., Classe Sci. Chim.*, **1948**, 69.
39. Grinberg, A. A., *Acta Physicochim*, **1935**, (3), 573.
40. Meerwein, H. R., *Sitzber. Ges. Beforder ges. Naturwe. Marburg.*, **1930**, 64, 119.
41. Gill, D. S.; Hacker, M. P.; Duple, E. B.; Krakoff, I. H., *In Platinum Coordination Complexes in Cancer Chemotherapy*. M. P. Hacker, E. B. Duple, I. H. Krakoff Editions, Martinus Nijhoff Publishing, Boston MA, **1984**, p. 267.
42. Pidcock, A.; Richards, R. E.; Venanzi, L. M., *Journal of the Chemical Society A*, **1966**, (12), 1707- 1720.
43. Appleton, T. G.; Clark, H. C.; Manzer, L. E., *Coordination Chemistry Reviews*, **1973**, 10 (3-4), 335-422.
44. Shaira, A.; Reddy, D.; Jaganyi, D., *Dalton Transactions*, **2013**, 42 (23), 8426-36.
45. Pauling, L., *The Nature of the Chemical Bond*, Cornell University Press, Ithaca, New York, 3rd Edition, **1960**, p. 332.
46. Chatt, J.; Duncanson, L. A.; Venanzi, L. M., *Journal of the Chemical Society*, **1955**, 4456-4460.
47. Orgel, L. E., *Journal of Inorganic and Nuclear Chemistry*, **1956**, 2 (3), 137-140.
48. Schwietert, C. W.; McCue, J. P., *Coordination Chemistry Reviews*, **1999**, 184, 67-89.
49. Romeo, R., *Comments on Inorganic Chemistry*, **1990**, 11, 21.
50. Hofmann, A.; Dahlenburg, L.; van Eldik, R., *Inorganic Chemistry*, **2003**, 42 (20), 6528-6538.
51. Pitteri, B.; Bortoluzzi, M.; Marangoni, G., *Transition Metal Chemistry*, **2005**, 30 (8), 1008-1013.
52. Jaganyi, D.; Hofmann, A.; van Eldik, R., *Angewandte Chemie International Edition*, **2001**, 40 (9), 1680-1683.
53. Burdett, J. K., *Inorganic Chemistry*, **1977**, 16 (12), 3013-3024.

54. Basolo, F.; Pearson, R. G.; Chatt, J.; Gray, H. B.; Shaw, B. L., *Journal of the Chemical Society*, **1961**, 2207.
55. Bruice, P. Y., *Organic Chemistry*, 2nd Edition, *Prentice Hall*, **1998**, p. 363-366.
56. Faraone, G.; Ricevuto, V.; Romeo, R.; Trozzi, M., *Journal of the Chemical Society A*, **1971**, (11), 1877.
57. Gray, H. B., *Journal of the American Chemical Society*, **1962**, 84 (9), 1548.
58. Pearson, R. G., *Journal of Chemical Education*, **1968**, 45 (10), 643.
59. Swain, C. G.; Scott, C. B., *Journal of the American Chemical Society*, **1953**, 75 (1), 141-147.
60. Pearson, R. G.; Sobel, H.; Songstad, J., *Journal of the American Chemical Society*, **1968**, 90 (2), 319.
61. Cattallini, L., Orio, A. and Nicolini, M., *Journal of the American Chemical Society*, **1966**, 88, 5734.
62. Gray, H. B.; Olcott, R. J., *Inorganic Chemistry*, **1962**, 1 (3), 481.
63. Basolo, F.; Gray, H. B.; Pearson, R. G., *Journal of the American Chemical Society*, **1960**, 82 (16), 4200-4203.
64. Pearson, R. G.; Gray, H. B.; Basolo, F., *Journal of the American Chemical Society*, **1960**, 82 (4), 787-792.

Chapter 3 - Reaction Kinetics

3.1 Introduction

Chemical reactions are processes that convert reactants to products and a balanced or stoichiometric equation is written for that reaction.¹ These chemical reactions occur at different rates whereby some reactions occur at a very fast pace while others are slow such that in practical terms are considered unoccurring.²⁻³ Quantitative studies on chemical reactions usually fall into two groups:⁴

- i. The first group known as chemical thermodynamics involves the actual occurrence of the reaction.⁴⁻⁵ These reactions are performed on systems that are at a steady state with static concentrations and deals with the initial states of the reaction before the reaction occurs.⁶ They take into account the direction at which a reaction will proceed rather than how quickly or slowly a chemical reaction takes place.⁷⁻⁸ Chemical thermodynamics measure quantities such as the standard enthalpy and the standard Gibbs energy change of a reaction.^{4,7,9}
- ii. The second group known as chemical kinetics determines how fast or slow a chemical reaction is proceeding.^{3-4,10} The reaction measurements here are made under dynamic or hypothetical conditions leading to the determination of the reaction rate.⁷⁻⁸ Furthermore, the concentration of the reactants and products change as a function of time.^{4,10}

Chemical reaction kinetics was first studied by Ludwig Wilhelmy in 1850 followed by Marcillin Berthelot and Pean de St Gillies.⁶ The results obtained showed direct proportionality of the rate of the reaction to the concentration of the substrate under study.⁶ The study of chemical reactions is important because the data collected gives an indication of the rate at which the reactants or products are consumed or formed.¹¹ It also describes

the mechanisms and reaction pathways taking place in the chemical reaction and the factors that influence the formation of the products.¹¹ In addition, kinetic data helps to explain the relationship between the structure of a chemical complex and its reactivity as well as predicting the shelf-life¹⁰ or stability of chemical products such as drugs.

Chemical reactions are influenced by numerous factors.¹² Therefore, it is of great importance to know the influence that some key factors have on the rate of reaction in order to understand the kinetic behaviour of a chemical reaction.¹⁰ These include concentration, physical conditions, solvent and intensity of absorbed radiation.¹⁰

- An increase in the concentration of the reactants results in more effective collisions leading to enhanced reaction rates. Furthermore, the concentration of the reactants is most frequently to determine the rate of a chemical reaction therefore controlling and understanding the effect of concentration on the reaction is kinetically very important.
- Solvents may influence the rate of the reaction depending on their properties such as polarity, donor atoms, added electrolyte, viscosity and buffer components. Generally, the rate of the reaction is mainly influenced if the molecules interact with the reactant molecules such that the kinetics (rate) of the reaction are altered.
- Physical conditions include factors such as pressure and temperature which can affect the reaction rate. These factors are normally kept constant during kinetic measurements. However, for temperature-dependent studies, the entropy and enthalpy of a reaction can be determined. This gives an indication of the substitution mechanism for the reaction. Moreover, the volume of activation can be determined from pressure dependent studies leading to the assignment of a mechanism for the reaction.

- The intensity of the absorbed radiation depending on the source can be an influential factor on the rate of a reaction. Apart from photochemical effects, light from laboratory lights and sunlight can alter the rate of a chemical reaction.

It is important to control these factors to obtain meaningful kinetic data. However, as mentioned before, the concentration of the reactants is the underlying factor in chemical kinetics or quantitative analysis of the rapidity of the reaction.¹⁰

3.2 The Rate Law

The reaction rate can be defined as the amount of reactants converted to products in a period of time.^{2,13} It can be expressed as the change in the rate of the reactants or the products over time (*Equation 3.1*). The units of the rates are usually reflected as molarity per second ($M s^{-1}$ or $mol. dm^{-3} s^{-1}$).¹³⁻¹⁶ The negative sign signifies that the concentration of the reactants decreases with time during a chemical reaction.

$$\text{Rate} = -\frac{d[\text{reactants}]}{dt} = \frac{d[\text{products}]}{dt} \quad (3.1)$$

The rates of the reaction represented in this manner are independent of the sample size under consideration.^{2,13} Consider the chemical reaction given below (*Equation 3.2*):



The formulae of the chemical compounds are represented by the upper-case letters and the stoichiometry of the reaction is represented by the lower-case letters. The rate law in general describes the dependence of the reaction rate on the reagent concentrations therefore the rate for *Equation 3.2* can be written as:¹³⁻¹⁴

$$\text{Rate} = -\frac{1}{a} \cdot \frac{d[A]}{dt} = -\frac{1}{b} \cdot \frac{d[B]}{dt} = \frac{1}{c} \cdot \frac{d[C]}{dt} = \frac{1}{d} \cdot \frac{d[D]}{dt} \quad (3.3)$$

The rate law has the general form:

$$\text{Rate} = -k \prod_i [A_i]^{\alpha_i} [X_j]^{\beta_j} \quad (3.4)$$

Where A_i represent the chemical symbols for reactants i , k is the rate constant, and X_j are other species such as catalysts, that may affect the rate. α and β are reaction orders with respect to A_i and X_j respectively.

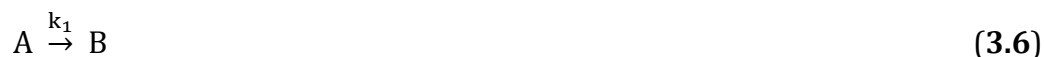
The units of the rate constant, k are dependent on the reaction order. The reaction order is defined as:

$$\text{Reaction order} = \sum_i \alpha_i \quad (3.5)$$

3.3 Integrated Rate Expressions

3.3.1 Irreversible First-Order Reactions

Most reactions are first-order or performed under conditions manipulated to approximate first-order reactions because these type of reactions are easier to interpret and understand.^{13-14, 17} The first-order reaction (*Equation 3.6*):



will give the following rate law,

$$\text{Rate} = -\frac{d[A]}{dt} = k_1 [A]_t \quad (3.7)$$

which rearranges to gives,

$$-\frac{d[A]}{[A]} = k_1 dt \quad (3.8)$$

and integrating between the limits $t = 0$ and $t = t$, where the concentration of the reactants changes from A_0 to A_t gives:

$$-\int_{[A]_0}^{[A]_t} \frac{1}{[A]} d[A] = \int_0^t k_1 dt \quad (3.9)$$

$$\ln \frac{[A]_t}{[A]_0} = -k_1 t \quad (3.10)$$

$$\ln[A]_t = -k_1 t + \ln[A]_0 \quad (3.11)$$

Where $[A]_0$ and $[A]_t$ are the concentrations of the reactant at $t = 0$ and $t = t$.

Thus from *Equation 3.11*, we see that it is in a linear form therefore a plot of $\ln[A]_t$ against time (t) will be linear with the slope equal to $-k_1$.¹³⁻¹⁴

Equation 3.11 can also be expressed as:

$$\frac{[A]_t}{[A]_0} = e^{-k_1 t} \quad (3.12)$$

or simplified to,

$$[A]_t = [A]_0 e^{-k_1 t} \quad (3.13)$$

Equation 3.13 also shows that the concentration of the reactants or products varies exponentially.

In a first-order rate law, any factor that is proportional to the concentration can be used to follow the kinetics of the reaction i.e. measure directly the first-order rate constant.^{10, 13-14, 17}

These factors include absorbance, pressure, conductivity or volume.

3.3.2 Reversible First-Order Reactions

Some chemical reactions do not necessarily go to completion but instead attain a dynamic equilibrium between the reactants and the products under certain reaction conditions.^{4, 10, 17}

They are then termed reversible reactions such that in principle, the rate of the forward and the reversible reaction are equal (Equation 3.14).⁴



The rate law for this equation can be written as:

$$\text{Rate} = \frac{d[B]}{dt} = -\frac{d[A]}{dt} = k_1 [A]_t - k_{-1} [B]_t \quad (3.15)$$

At $t = 0$, when no product have formed, $[B]_0 = 0$ and $[A]_t = [A]_0$, therefore at any time during the reaction ($t = t$),

$$[B]_t = [A]_0 - [A]_t \quad (3.16)$$

where $[B]_t = x$ and $[A]_t = [A]_0 - x$ and x is the amount of reactants used and products formed.

The substitution of Equation 3.16 into Equation 3.15 gives,

$$\frac{dx}{dt} = k_1 ([A]_0 - x) - k_{-1}(x) \quad (3.17)$$

At equilibrium no nett reaction occurs thus

$$\frac{dx}{dt} = k_1 ([A]_0 - x_{eq}) - k_{-1}(x_{eq}) = 0 \quad (3.18)$$

$x_{eq} = \text{equilibrium concentration}$

Rearranging Equation 3.18 gives:

$$k_{-1} = \frac{k_1([A]_0 - x_{eq})}{x_{eq}} \quad (3.19)$$

The substitution of Equation 3.19 into Equation 3.17 gives:

$$\frac{dx}{dt} = k_1 ([A]_0 - x) - \frac{k_1([A]_0 - x_{eq})x}{x_{eq}} = \frac{k_1[A]_0}{x_{eq}} (x_{eq} - x) \quad (3.20)$$

Separating the variables and integrating gives:

$$\ln(x_{eq} - x) = - \frac{k_1[A]_0}{x_{eq}} t + \ln(x_{eq}) \quad (3.21)$$

However, in order to obtain the individual rate constants, k_1 and k_{-1} , the equilibrium rate constant K_{eq} must be evaluated.

$$K_{eq} = \frac{[B]_{eq}}{[A]_{eq}} = \frac{k_1}{k_{-1}} \quad (3.22)$$

The observed rate constant, k_{obs} is sum of the two individual rate constants (k_1 and k_{-1}),

$$k_{obs} = k_1 + k_{-1} \quad (3.23)$$

However a problem often encountered with measuring of the reversible first-order rate constants is the inaccurate measurement of $[A]_{eq}$.^{13-14, 18}

3.3.3 Irreversible Second-Order Reactions

Second-order reactions are amongst the most encountered in reaction kinetics studies.^{10, 14,}

¹⁹ A reaction can be second order with respect to only one of the reactant or second order when the overall reaction is first order to two different reactants.

Consider the second order reaction:



The rate law is written as,

$$\text{Rate} = k[A][B] \quad (3.25)$$

$$\text{Rate} = \frac{d[C]}{dt} = -\frac{d[A]}{dt} = -\frac{d[B]}{dt} = k_2[A]_t[B]_t \quad (3.26)$$

At $t = 0$, $[A] = [A]_0$ and $[B] = [B]_0$ while the amount of the reactants that have reacted after time t to form the product C is represented by x thus the concentration of $[A]$ at time t is $[A]_t = ([A]_0 - x)$ and that of $[B]_0$ at time t is $[B]_t = [B]_0 - x$. Therefore, the rate at time t is:²⁰

$$-\frac{d[A]}{dt} = k_2([A]_0 - x)([B]_0 - x) \quad (3.27)$$

Knowing that $[A]_t = ([A]_0 - x)$ hence $\frac{dx}{dt} = -\frac{d[A]}{dt} = -\frac{d[B]}{dt}$, Equation 3.27 can also be expressed as follows:

$$\frac{dx}{dt} = k_2([A]_0 - x)([B]_0 - x) \quad (3.28)$$

or

$$\frac{dx}{([A]_0 - x)([B]_0 - x)} = k_2 dt \quad (3.29)$$

Integrating Equation 3.29 between the limits $x = 0$ to $x = x$ and $t = 0$ to $t = t$ affords,

$$\int_0^x \frac{dx}{([A]_0 - x)([B]_0 - x)} = k_2 \int_0^t dt \quad (3.30)$$

giving Equation E3.34 (provided $[A]_0 \neq [B]_0$),

$$\frac{1}{[A]_0 - [B]_0} \cdot \ln \frac{[B]_0([A]_0 - x)}{[A]_0([B]_0 - x)} = k_2 t \quad (3.31)$$

which further simplifies to give,

$$\frac{1}{[A]_0 - [B]_0} \cdot \ln \frac{[B]_0[A]_t}{[A]_0[B]_t} = k_2 t \quad (3.32)$$

From Equation 3.32, it can be seen that the second-order rate constant, k_2 can only be determined if the values of $[A]_0$, $[B]_0$, $[A]_t$ and $[B]_t$ are known. However, it is often time consuming and complicated to obtain these values.¹³⁻¹⁴

To overcome this, second-order reactions are optimized by using the first order rate law as it has lesser variables to work with and also leads to a more reliable rate constant. This is achieved by using *pseudo* first-order conditions where the concentration of one of the reactants is in large excess, i.e. $[B]_0 \gg [A]_0$ (at least 10-fold excess) such that its concentration remains constant during the reaction.^{10, 14, 19-20}

Assuming that the reaction order is one with respect to A , then the rate law in Equation E3.29 simplifies to,^{10, 14, 19-20}

$$-\frac{d[A]}{dt} = k_2[A]_t[B]_t = (k_2[B]_0)[A]_t = k_{\text{obs}}[A]_t \quad (3.33)$$

where k_{obs} is the observed rate constant in units of s^{-1} and equal to $k_2[B]_0$.

Integration of Equation 3.33 and plotting the graph of $\ln[A]_t$ versus time t gives a slope of k_{obs} (s^{-1}) (the observed rate constant). To further obtain the second order rate constant, k_2 , a series of k_{obs} values have to be determined by varying the concentration of B in excess

amounts.^{10, 14, 19-20} This generates a host of $[B]_0$ values such that k_{obs} in *Equation 3.33* can be expressed as,

$$k_{\text{obs}} = k_2[B]_0 \quad (3.34)$$

From *Equation 3.34*, a plot of k_{obs} versus $[B]_0$ will give a straight line with a slope of k_2 (the second-order rate constant) in $\text{M}^{-1} \text{s}^{-1}$.

3.3.4 Reversible Second-Order Reactions

Consider the following second-order reversible reaction,



Equation 3.35 demonstrates an example of a mixed order behaviour, i.e. the forward reaction is second-order while the reverse reaction is first-order. This behaviour is very complicated and should be avoided. This complexity is often avoided by selecting *pseudo* first-order conditions for the forward reaction such that $[B]_0 \gg [A]_0$. The system now becomes similar to reversible first-order and the rate can be represented as follows,

$$\text{Rate} = \frac{d[C]}{dt} = -\frac{d[A]}{dt} = -\frac{d[B]}{dt} = k_2[A]_t[B]_t - k_{-2}[C]_t \quad (3.36)$$

Assuming that the concentration of C is zero at the beginning and a stoichiometric ratio of 1:1:1 for the reaction, the mass balance at any time t are,

$$[A]_t = [A]_0 - [C]_t, \quad [B]_t = [B]_0 - [C]_t \quad (3.37)$$

At equilibrium, the mass balances are:

$$[A]_{\text{eq}} = [A]_0 - [C]_{\text{eq}}, \quad [B]_{\text{eq}} = [B]_0 - [C]_{\text{eq}} \quad (3.38)$$

At equilibrium, the forward and the reverse reactions are equal, therefore,

$$-\frac{d[B]}{dt} = k_2[A]_{\text{eq}}[B]_{\text{eq}} - k_{-2}[C]_{\text{eq}} = 0 \quad (3.39)$$

Hence,

$$k_2[A]_{\text{eq}}[B]_{\text{eq}} = k_{-2}[C]_{\text{eq}} \quad (3.40)$$

Rearranging and substituting *Equation 3.38* and *Equation 3.39* into *Equation 3.40* affords,

$$k_2[A]_{\text{eq}}[B]_{\text{eq}} = k_{-2}([A]_0 - [A]_{\text{eq}}) \quad (3.41)$$

Therefore,

$$k_{-2}[A]_0 = k_2[A]_{eq}[B]_{eq} + k_{-2}[A]_{eq} \quad (3.42)$$

Substitution for $[C]_t = [A]_0 - [A]_t$ in Equation 3.37 and substituting it into Equation 3.36 gives the rate as,

$$\begin{aligned} -\frac{d[B]}{dt} &= k_2[A]_t[B]_t - k_{-2}([A]_0 - [A]_t) \\ &= k_2[A]_t[B]_t - k_{-2}[A]_0 + k_{-2}[A]_t \end{aligned} \quad (3.43)$$

The combination of Equation 3.42 and Equation 3.43 yields,

$$-\frac{d[B]}{dt} = k_2[A]_t[B]_t - k_2[A]_{eq}[B]_{eq} - k_{-2}[A]_{eq} + k_{-2}[A]_t \quad (3.44)$$

By applying first-order conditions where $[B]_0 \gg [A]_0$, Equation 3.44 can be written as,

$$\begin{aligned} -\frac{d[B]}{dt} &= k_2[A]_t[B]_0 - k_2[A]_{eq}[B]_0 - k_{-2}[A]_{eq} - k_{-2}[A]_t \\ &= (k_2[B]_0 + k_{-2})([A]_t - [A]_{eq}) \end{aligned} \quad (3.45)$$

The separation of variables and integrating between the limits $t = 0$ to $t = t$ affords,

$$\begin{aligned} \int_{[A]_0}^{[A]_t} \frac{d[A]}{[A]_t - [A]_{eq}} &= -(k_2[B]_0 + k_{-2}) \int_0^t dt \\ \ln \left(\frac{[A]_t - [A]_{eq}}{[A]_0 - [A]_{eq}} \right) &= -(k_2[B]_0 + k_{-2})t \\ &= -k_{obs}t \end{aligned} \quad (3.46)$$

where $k_{obs} = k_2[B]_0 + k_{-2}$

Thus a plot of k_{obs} versus $[B]_0$ will give a straight line with a slope equal to k_2 and an intercept equal to k_{-2} . The equilibrium constant, K_{eq} can be given by the ratio of $\frac{k_2}{k_{-2}}$ or can be measured thermodynamically.²⁰

$$K_{eq} = \frac{k_2}{k_{-2}} \quad (3.47)$$

Pseudo first-order conditions are often applicable in the kinetic studies of square-planar complexes.^{10, 14, 19}

3.4 Activation Parameters and Temperature Dependence

Rate laws are important in assigning mechanisms for reactions. However, it is the dependence studies of rate constants that are undertaken to gain further insight about the energetics of a reaction allowing for the determination of the activation parameters of a given reaction.^{14, 19, 21-22} Once the experimental data for the rate constants have been collected, it can be analysed using the Arrhenius equation or transition-state theory (discussed below).^{13, 23-24}

3.4.1 The Arrhenius Equation

The quantitative relationship between the rate constant, k , and the temperature was first discovered by Arrhenius in 1856¹³, (*Equation E3.51 and E3.52*).^{13-14, 24}

$$k = Ae^{(-E_a/RT)} \quad (3.48)$$

Where A = Arrhenius pre-exponential factor measured in $M^{-1} s^{-1}$.

E_a = Arrhenius activation energy in $Jmol^{-1}$.

R = Gas constant ($8.314 J K^{-1} mol^{-1}$)

T = Temperature (K)

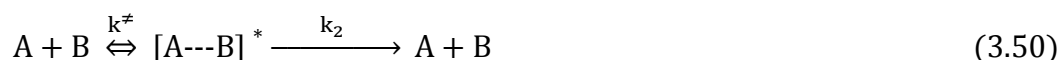
Equation 3.48 can be expressed in the logarithm form as follows,

$$\ln k = \ln A - \frac{E_a}{R} \left(\frac{1}{T} \right) \quad (3.49)$$

From *Equation 3.49*, it can be seen that a plot of $\ln k$ versus $\frac{1}{T}$ gives a straight line with a slope of $-\frac{E_a}{R}$ and an intercept of $\ln A$. The reaction rate, k , normally increases with an increase in temperature.¹³⁻¹⁴ The Arrhenius equation is often used in kinetic reactions and is of great importance in systems where the measured rate constant is thought to be a combination of rate constants.¹⁴

3.4.2 Transition-State Theory

The transition-state theory, which is also called the absolute reaction rate theory, was developed in 1935 by Henry Eyring²⁵ and Michael Polanyi²³ for a gas phase dissociation process.^{14, 17, 23, 25} The transition-state theory works on the assumption that there is a pre-equilibrium between the reactants and activated transition state complex of many reactants, (*Equation 3.50*).^{4-5, 14, 17}



The rate equation based on the transition state complex can be written as,

$$\frac{d[A]}{dt} = k_2[A\cdots B]^* = \frac{k_b T}{h} K^\ddagger [A][B] \quad (3.51)$$

Where k_b = Boltzmann's constant ($1.38 \times 10^{-23} \text{ J K}^{-1}$)

T = Temperature (Kelvin)

h = Planck's constant ($6.626 \times 10^{-34} \text{ J s}^{-1}$)

K^\ddagger = Equilibrium constant

The experimental second-order rate constant k_{exp} can be expressed as follows,

$$k_{\text{exp}} = \frac{k_b T}{h} K^\ddagger \quad (3.52)$$

The Gibbs free energy of activation, ΔG^\ddagger is expressed as follows,

$$\Delta G^\ddagger = -RT \ln K^\ddagger = \Delta H^\ddagger - T\Delta S^\ddagger \quad (3.53)$$

Where ΔH^\ddagger is the change in enthalpy of the activation and ΔS^\ddagger is the change in entropy of activation.

Upon substitution of *Equation E3.56* into *Equation E3.55* affords the following expression,

$$k_{\text{exp}} = \frac{k_b T}{h} \exp\left(-\frac{\Delta G^\ddagger}{RT}\right) = \frac{k_b T}{h} \exp\left(-\frac{\Delta H^\ddagger}{RT}\right) \exp\left(\frac{\Delta S^\ddagger}{R}\right) \quad (3.54)$$

Taking the logarithms gives the following expression,

$$\ln\left(\frac{k_{\text{exp}}}{T}\right) = -\frac{\Delta H^\ddagger}{RT} + \ln\left(\frac{k_b}{h}\right) + \frac{\Delta S^\ddagger}{R} \quad (3.55)$$

Rearranging *Equation 3.55* and simplifying affords,

$$\ln\left(\frac{k_{\text{exp}}}{T}\right) = -\frac{\Delta H^\ddagger}{R} \cdot \frac{1}{T} + \left[23.8 + \frac{\Delta S^\ddagger}{R}\right] \quad (3.56)$$

From *Equation E3.59* above, the activation parameters, enthalpy of activation (ΔH^\ddagger) and entropy of activation (ΔS^\ddagger) can be obtained from a plot of $\ln\left(\frac{k_{\text{exp}}}{T}\right)$ versus $\frac{1}{T}$. ΔH^\ddagger is determined from the slope whereas ΔS^\ddagger is determined from the y -intercept of the graph.^{7, 14,}

¹⁷ This plot is commonly known as the Eyring plot.^{13, 17, 25-26} In addition, due to the determination of ΔS^\ddagger by extrapolation, the errors associated with it are in general three times higher than that of ΔH^\ddagger .¹⁰

3.4.3 Effect of Pressure on the Rate Constant

In rare cases, the enthalpy and entropy of activation may be insufficient to deduce a reaction mechanism. In such cases, a more reliable parameter for mechanistic assignment is the volume of activation because it is less sensitive to temperature, (*Equation 3.57*).^{13-14, 27}

$$\left(\frac{d(\ln k_2)}{dP}\right) = -\frac{\Delta V^\ddagger}{RT} \quad (3.57)$$

Where, ΔV^\ddagger is the volume of activation for the forward process of the reaction. It is also the difference in partial molar volume between the activated complex and the reactants.²⁸

Equation 3.57 shows that the volume of activation, ΔV^\ddagger for a reaction can be determined only after the effect of pressure on the reaction rate is determined.^{13-14, 27}

Therefore, a plot of $\ln(k_2)$ versus P gives a linear fit with a slope equal to $-\frac{\Delta V^\ddagger}{RT}$. A positive volume of activation is associated with a dissociative mechanism whereas a negative value is indicative of an associative substitution reaction.¹⁵

3.5 Instrumental Techniques Associated with the Study of Chemical Kinetics

There are various experimental techniques and methods by which the rates of the reactions can be measured. Each of these techniques or methods involves measuring or controlling of certain physical properties (such as temperature, concentration, pressure etc.) of a reaction mixture.^{5, 22, 29} The most commonly used method involves measurements of the concentration of either the reactants or products with time. The data collected can then be used to determine the rate law of the reaction. However, the choice of method and/or equipment often depends on the time scale of the reaction of interest.⁸ Rapid reactions are

those that proceed to 50% completion in 10 seconds or less.⁸ Such reactions demand specialized equipment that empowers both the rapid mixing and rapid data recording.^{8, 10} Furthermore, quenching is often employed for reactions that are too rapid or an instrumental technique that continuously collects concentration data as the reaction proceeds is used.^{1, 7-8} Adequate reactions are often monitored by standard methods of analysis to determine the concentration of either the reactants or products as a function of time.

Techniques such as pulse methods, infrared spectroscopy (IR) and nuclear resonance spectroscopy (NMR) are suitable and available for kinetic studies but the two methods to be used in this study are ultraviolet/Visible (UV/Vis) spectrophotometry and stopped-flow analysis (**Figure 3.1**).²⁶ These methods are based on the absorption of ultraviolet-visible light.

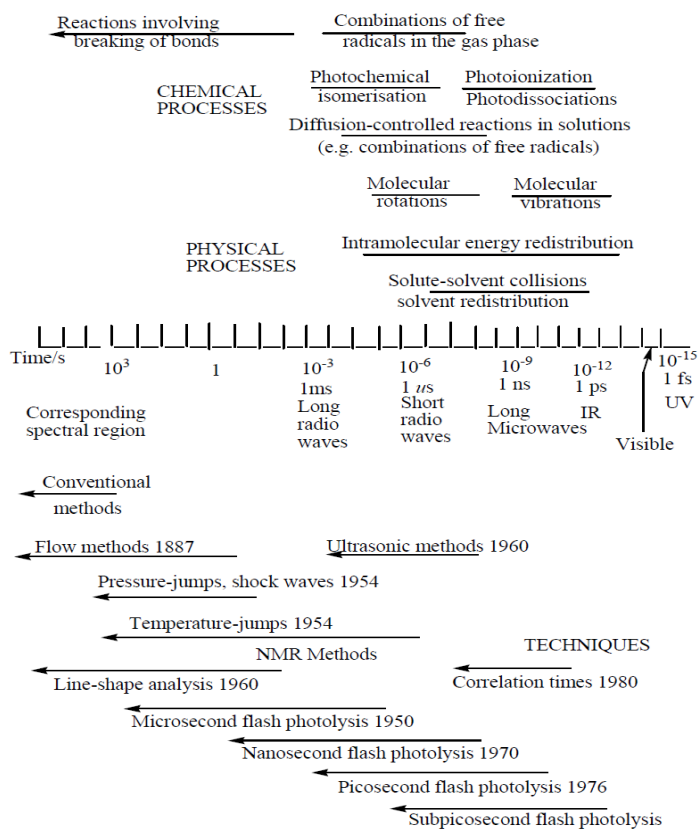


Figure 3.1: A summary of reaction techniques and their associated time scales available for the monitoring chemical kinetics.²⁶

3.5.1 UV/Visible Spectrophotometry

UV/Visible spectrophotometry is one of the most frequently used and powerful techniques²² in chemical kinetic studies.^{13, 30} It is a slow and sensitive technique which has the ability to detect sample concentration ranging from 10^{-4} – 10^{-6} M.³¹⁻³² It is most useful in the detection of the electronic transitions originating from the highest occupied molecular orbitals (HOMO) to the lowest unoccupied molecular orbitals (LUMO) in compounds having π -electrons/non-bonding electrons-pair upon absorption of light in the ultraviolet and visible regions.^{30, 33-34} The key components of a spectrophotometer include the radiation source, monochromatic light, sample compartment, detector and the data processor, (**Figure 3.2**).

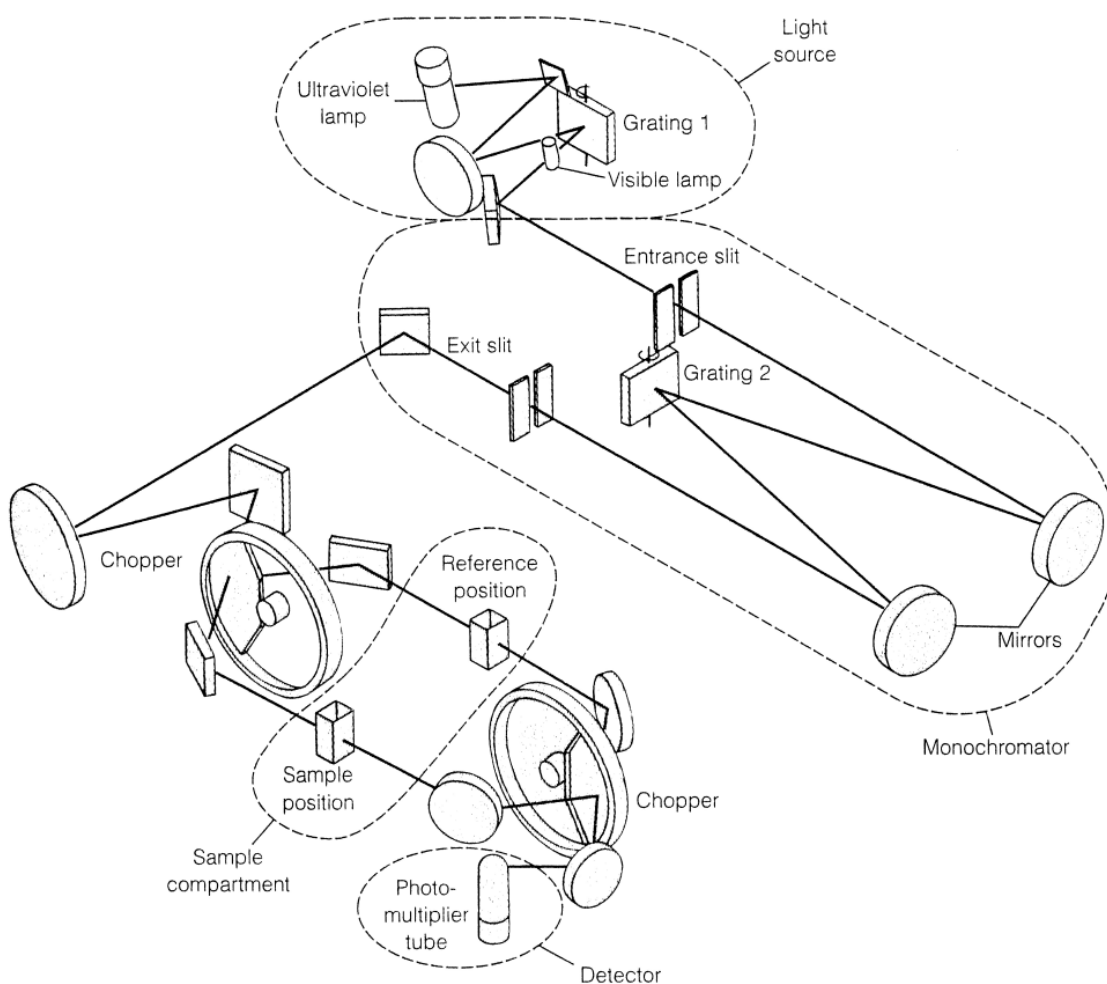


Figure 3.2: A schematic diagram of a UV/Visible spectrophotometer set-up.³³

A UV/Vis spectrophotometer can measure the fraction of the incident light passing through the sample, this is known as the Transmittance, T , and is represented as,^{22, 35-38}

$$T = \frac{I}{I_0} \quad (3.58)$$

where I_0 = the intensity of the incident light, I = the intensity of the transmitted light.

The absorbance, A , is a more useful quantity and can be determined from the intensities.^{22, 35-38}

$$A = \log\left(\frac{I_0}{I}\right) = -\log T \quad (3.59)$$

Absorbance is important because by the application of the Beer's law (*Equation E3.60*),^{22, 35-38} there is a direct proportionality of the absorbance with the concentration of the sample.^{1, 8, 22, 39}

$$A = \epsilon cl \quad (3.60)$$

where A = absorbance (it is dimensionless), ϵ = molar absorptivity or the extinction coefficient ($L \text{ mol}^{-1} \text{ cm}^{-1}$), c = concentration (mol dm^{-3}) and l = path length (cm)³⁹

The broad absorptions observed from the UV/Visible absorption spectra often overlap with other species in solution making the analysis of the product complicated and difficult. However, kinetic analysis can be done on the overlapping absorption spectra.¹⁷

For a first-order reaction, (*Equation 3.61*)



At any time t , the absorption is,⁸

$$A_t = \epsilon_A[A]_t + \epsilon_B[B]_t \quad (3.62)$$

where A_t = the absorbance at any time, t , ϵ_A , ϵ_B = molar absorptivity of A and B respectively.

When the reaction has reached completion, the absorbance will be,⁸

$$A_\infty = \epsilon_A[A]_0 + \epsilon_B[B]_0 \quad (3.63)$$

where A_∞ = the absorbance at infinity, $[A]_0$ and $[B]_0$ = initial concentration of A and B respectively.

For the kinetic analysis, the absorbance of the sample can be expressed as,

$$\ln \frac{[A]_0}{[A]_t} = \ln \left(\frac{[A]_0 - [A]_\infty}{[A]_t - [A]_\infty} \right) = k_1 t \quad (3.64)$$

where A_t is said to be the absorbance of the reactant at any time, t .

The absorbance-time resolved data is often used to directly determine or evaluate the observed rate constants using *Equation 3.64*.

Figure 3.3 below shows the reaction profile obtained for the substitution of [Pt{4'-(*o*-tolyl)-2,2':6',2''-terpyridine}Cl]CF₃SO₃ with 1-methylimidazole). The kinetics for the reaction were studied at 333 nm and the trace obtained for the reaction at 298.15 K is shown as an insert in *Figure 3.3*. The rate constant for the reaction was obtained by fitting first-order exponential decay function using Origin 9.0®.⁴⁰⁻⁴¹

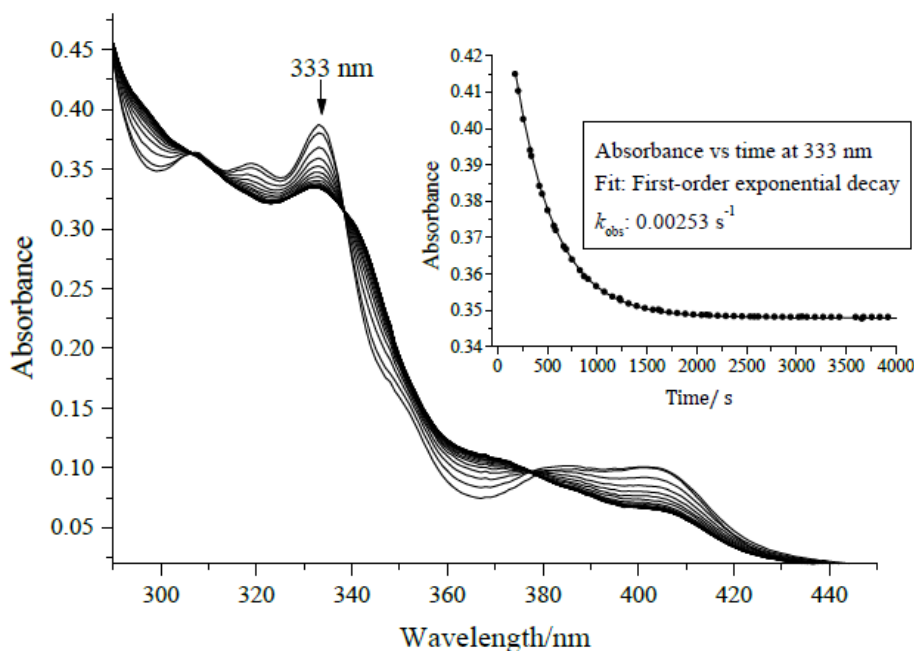


Figure 3.3: The spectrum obtained from Cary UV/Visible spectrophotometer for the substitution of Cl⁻ from [Pt{4'-(*o*-tolyl)-2,2':6',2''-terpyridine}Cl]CF₃SO₃ ($2.50 \times 10^{-5} \text{ mol dm}^{-3}$) with 1-methylimidazole ($5.00 \times 10^{-4} \text{ mol dm}^{-3}$) in methanol solution ($I = 0.10 \text{ M}$ (0.09 M LiCF₃SO₃ + 0.01 M NaCl)) at 333 nm and 298.15K.⁴¹

3.5.2 Flow Methods

Many chemical reactions happen too quickly such that it is impossible to monitor them by conventional absorption spectroscopy, i.e. in the time taken to mix the samples and collecting data, the reaction would have already occurred.^{8, 10, 26} These reactions therefore require

shorter sampling and mixing time.⁸ The most reliable and popular method used to monitor such fast reactions in solution is the stopped-flow mixing.^{5, 8, 10, 26, 42} This method involves rapid mixing (with 1 millisecond) of the reagents by the pistons and suddenly stopping the flow of the mixed solutions. The progress of the reaction is observed/analyzed near the mixer.^{8, 13, 22, 26} A schematic diagram of this apparatus is shown in **Figure 3.4**.⁸

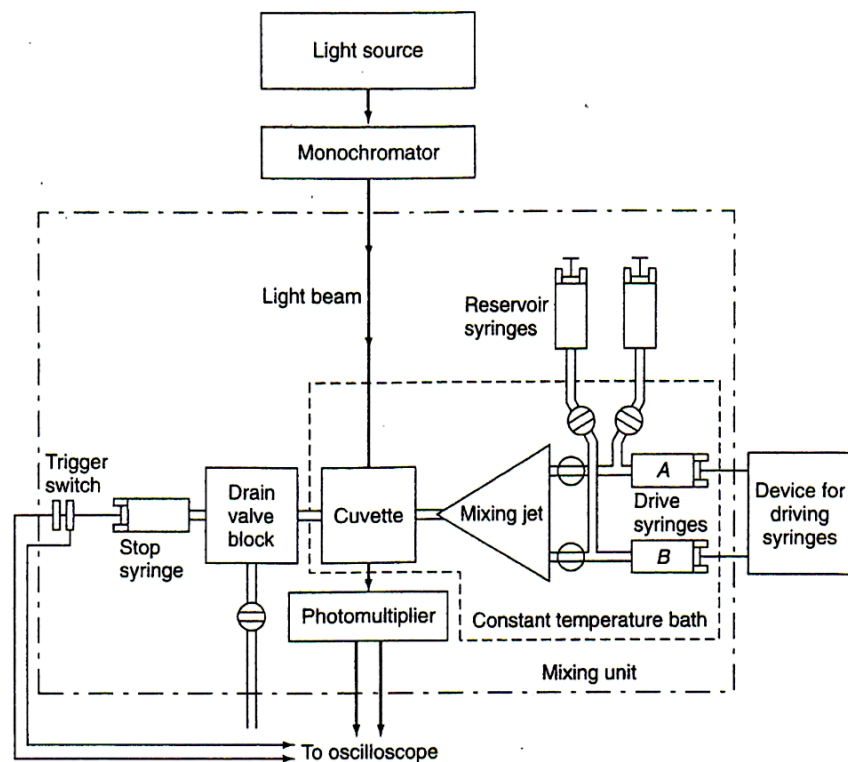


Figure 3.4: A schematic diagram of a *stopped-flow* spectrophotometer apparatus.^{8, 42}

This technique is designed to monitor the reaction of the two substances where equal amount of reactants are filled in Syringes A and B respectively, (**Figure 3.4**).

The two reactants are rapidly forced into the mixing chamber (**Figure 3.4**) by pressure applied on the plungers at constant temperature. The mixing in the stopped-flow takes about 0.001s.³⁹ The solution is then driven into the reaction cuvette where the reaction solution gets mixed and allowed to rest at a fixed time interval (rest period) when the stopping syringe comes against its seating (**Figure 3.4**).^{1,8} The reaction is then followed spectrophotometrically.

3.6 References

1. Logan, S. R., *Fundamentals of Chemical Kinetics*. Longman, Essex, **1996**, p. 24 - 37.
2. King, E. L., *How Chemical Reactions Occur: An Introduction to Chemical Kinetics and Reaction Mechanisms*. W. A. Benjamin, Inc, New York, **1964**, p. 1.
3. Ball, D. W., *Physical Chemistry, Brooks/Cole*, Pacific Grove, **2003**, p. 680-703.
4. Logan, S. R., *Fundamentals of Chemical Kinetics*. Addison Wesley Longman, Harlow, **1996**, p. 1 - 9, 17, 20, 33 - 34, 55, 70 - 71.
5. Cox, B. G., *Modern Liquid Phase Kinetics*. Oxford University Press, New York, **1994**, p. 6 - 12, 23 - 30, 44, 59.
6. Mortimer, M. and Taylor, P., *Chemical Kinetics and Mechanism*. The Open University. Walton Hall, Milton Keynes, London, **2002**, p. 11.
7. Logan, S. R., *Fundamentals of Chemical Kinetics*. Longman, Essex, **1996**, 1-30.
8. Skoog, D. A.; West, D. M.; Holler, F. J.; Crouch, S. R., *Fundamentals of Analytical Chemistry, 8th edition*. Brooks/Cole - Thomson Learning, Inc., United States, **2004**, p. 718 - 734, 771 - 775, 878 - 894.
9. Silberberg, M. S., *Chemistry: The Molecular Nature of Matter and Change, 2nd Edition*. McGraw-Hill, United States, **2000**, 664-684.
10. Espenson, J. H., *Chemical Kinetic and Reaction Mechanisms, 2nd Edition*, McGraw-Hill, New York, **1995**, p. 1 - 80, 155 - 159, 161 - 162, 253 - 256.
11. Denisov, E. T.; Sarkisov, O. M. and Likhtenshtein, G. I., *Chemical Kinetics: Fundamentals and New Development*. Elsevier Science & Technology Books, **2003**, p. 1-6.
12. Ladd, M. F. C. and Lee, W. H., *Introduction to Physical Chemistry*. Cambridge University Press, New York, **1986**, p. 273-301.
13. Atwood, J. D., *Inorganic and Organic Reaction Mechanisms, 2nd Edition*. Wiley-VCH Inc., New York, **1997**, p. 1- 32 - 34, 43 - 61.
14. Jordan, R. B., *Reaction Mechanisms of Inorganic and Organometallic Systems*. Oxford University Press, New York, **1991**, p. 1-29 - 40, 47-54, 58- 60.
15. Tobe, M. L. and Burgess, J., *Inorganic Reaction Mechanisms*. Addison Wesley Longman Limited, New York, **1999**, p. 30-43, 70-112.

16. Moore, J. W. and Pearson, R. G. , *Kinetics and Mechanism, 3rd Edition*. John Wiley and Sons, New York, **1981**, p. 12-19.
17. Ašperger, S., *Chemical Kinetics and Inorganic Reaction Mechanisms, 2nd Edition*. Kluwer Academic/Plenum Publisher, New York, **2003**, p. 3, 7-23, 38 - 40, 105 - 106, 140-153.
18. Connors, K. A., *Chemical Kinetics: The Study of Reaction Rates in Solution*. Wiley-VCH, New York, **1990**, p. 1-22, 176-180.
19. Atwood, J. D., *Inorganic and Organic Reaction Mechanisms, 2nd Edition*. Wiley-VCH Inc., New York, **1997**, p. 32 - 34, 43 - 61.
20. Atkins, P.; de Paula, J., *Atkins' Physical Chemistry, 8th Edition*. Oxford University Press, Oxford, **2006**, p. 791-829.
21. Benson, D., *Mechanisms of inorganic reactions in solution*. McGraw-Hill, London, **1968**, p. 1 - 31.
22. Wilkins, R. G., *Kinetics and Mechanisms of Reactions of Transition Metal Complexes, 2nd Edition*. VCH, Weinheim, **1991**, p. 41 - 43, 130 - 140, 199 - 201, 221, 232-242.
23. Evans, M. G.; Polanyi, M., *Trans. Faraday Soc.* **1935**, *31*, 875.
24. Laidler, J. H., Meiser, *Physical Chemistry, 4th Edition*. Houghton Mifflin, New York, **2003**, p. 363 - 371, 373 - 393.
25. Eyring, H., *J. Chem. Phys.* **1935**, *3*, 107.
26. Laidler, K. J.; Meiser, J. H. and Sanctuary, B. C., *Physical Chemistry, 4th Edition*. Houghton Mifflin Company, New York, **2003**, p. 374-379, 390-393.
27. Helm, L.; Merbach, A. E., *Applications of advanced experimental techniques: high pressure NMR and computer simulations*. J Chem Soc Dalton, **2002**, 633-641.
28. Katakis, D. and Gordan, G., *Mechanisms of Inorganic Reactions*. Wiley-Interscience, New York, **1987**, p. 58 - 66.
29. Wilkinson, F., *Chemical Kinetics and Reaction Mechanisms*. Van Nostrand Reinhold Company, New York, **1980**, p. 1-11, 66-99.
30. Christian, G. D.; O'Reilly, J. E., *Instrumental Analysis, 2nd Edition*. Allyn and Bacon, Boston, **1986**, p. 184, 192 - 198.
31. Reddy, D., PhD Thesis, *Tuning the Reactivity of Platinum(II) Complexes*. University of KwaZulu-Natal, Pietermaritzburg, South Africa, **2009**, p. 88, 90.

32. Mambanda, A., PhD Thesis, *Influence of Bridging Groups on the Reactivity of Dinuclear Platinum(II) Complexes with bis(2-pyridylmethyl)amine Chelate Headgroups*. University of KwaZulu-Natal, Pietermaritzburg, South Africa, **2009**, p. 82 - 88.
33. Harris, D. C., *Quantitative Chemical Analysis, 4th Edition*. W. H. Freeman and Company, New York, **1995**, p. 480.
34. Owen, T., *Fundamentals of UV-Visible Spectroscopy*. Hewlett-Packard, **1996**, p. 24 - 50.
35. Bauer, H. H.; Christian, G. D.; O'Reilly, J. E., *Instrumental Analysis*. Allyn and Bacon, Inc., Boston, **1978**, p. 167-188.
36. Skoog, D. A.; West, D. M., *Principles of Instrumental Analysis, 2nd Edition*. Saunders College, **1980**, p. 180-186.
37. Harris, D. C., *Quantitative Chemical Analysis*. W.H Freeman and Company, San Francisco, **1982**, p. 468-485.
38. Willard, H. H.; Merritt, L. L.; Dean Jr., J. A.; Settle Jr., F. A., *Instrumental Methods of Analysis, 7th Edition*. Wadsworth Publishing Company, California, **1988**, p. 118-156, 159-162.
39. Skoog, D. A.; West, A. M.; Holler, F. J. and Crouch, S. R., *Fundamentals of Analytical Chemistry, 8th Edition*. Thomson Brooks/Cole, Canada, **2002**, p. 374-379, 720, 769-775.
40. Microcal™ Origin™ Version 9.0. Microcal Software, Inc., One Roundhouse Plaza, Northampton, MA, 01060, USA, **1991-1997**.
41. Shaira, A., *MSc Thesis, A Kinetic and Mechanistic Study into the Substitution Behaviour of Platinum(II) Polypyridyl Complexes with a Series of Azole Ligands*. University of Natal, Pietermaritzburg, South Africa, **2010**, p. 82.
42. Hague, D. N., *Fast Reactions*. Wiley, London, **1971**, 16 - 17.

Chapter 4: Experimental

4.1 Materials and Procedures

All synthetic reactions were carried out in air unless otherwise stated. Potassium tetrachloroplatinate (K_2PtCl_4 , 99.99%), 1-(2-chloroethyl)piperidine hydrochloride (98%), 4-(2-chloroethyl)morpholine hydrochloride (99%), 1-(2-chloroethyl)pyrrolidine hydrochloride (98%), 4'-chloro-2,2':6',2''-terpyridine (99%), anhydrous pyridine (99.8%), acetonitrile (CH_3CN , $\geq 99.9\%$), potassium carbonate (K_2CO_3 , $\geq 99.0\%$), sodium tetrafluoroborate (NaBF_4 , 98%), sodium hexafluorophosphate (NaPF_6 , 98%), 1.5-cyclooctadiene (**COD**), and chloroform-*d* (CDCl_3 , 99.8%) were purchased from Sigma-Aldrich and used without further purification. Sodium chloride (NaCl , 99.0%), sodium hydroxide (NaOH , 98%), potassium hydroxide (KOH , 98%), methanol-*d*₄ (CD_3OD , 98.8%), *N,N'*-dimethyl-formamide (**DMF**, $\geq 99\%$), Dimethyl sulfoxide (**DMSO**, min 99%) and all the other solvents used for synthesis were purchased from Merck and used without further purification. Anhydrous sodium sulphate (Na_2SO_4) and anhydrous magnesium sulfate (MgSO_4) were obtained from Associated Chemical Enterprises (ACE). All other chemicals were of analytical reagent quality.

The four (4) ligands reported here, namely **L1S1**, **L2S1**, **L3S1** and **L4S1** were synthesized by adaptations of established literature procedures.¹⁻³ The platination of all the ligands to form **C1S1**, **C2S1**, **C3S1** and **C4S1** respectively, was achieved by using the method described by Annibale *et al.*⁴ and Liu *et al.*⁵ All ligands and complexes were obtained at satisfactory yields and high purity which was confirmed through ¹H-NMR, ¹³C-NMR, FT-IR, LC-MS and elemental analysis.

4.2 Instrumentation and Physical Measurements

4.2.1 Characterization

Characterization of the precursors, ligands and complexes was achieved through the use of nuclear magnetic resonance (NMR) spectroscopy, infrared (IR) spectroscopy, mass spectrometry and elemental analysis.

^1H -, ^{13}C - and ^{195}Pt -NMR spectra were recorded on a Bruker Avance III 500 or Bruker Avance III 400 at frequencies of 500 MHz or 400 MHz (^1H) and 125 MHz/100 MHz (^{13}C) using either a 5 mm BBOZ probe or a 5 mm TBIZ probe. All proton and carbon chemical shifts are reported relative to the relevant solvent signals at 25 °C unless stated otherwise. The chemical shifts are referenced to $\text{Si}(\text{CH}_3)_4$. ^{195}Pt NMR were done on a 500 MHz spectrometer (^{195}Pt , 107.5 MHz) chemical shifts externally referenced to $\text{K}_2[\text{PtCl}_6]$. Analysis was completed using the software packages, either Spinworks or Topspin

Elemental compositions of the ligands and complexes were performed on a Thermo Scientific Flash 2000. The mass spectral data of the ligands and complexes were acquired on a Waters Micromass LCT Premier spectrometer i.e. LCT Premia LC-MS with a ESI source and time of flight (ToF) analyser. Melting points of the ligands **L1S1**; **L2S1**; **L3S1** and **L4S1** were recorded on a Stuart SMP3 machine.

4.2.2 Computational Modelling

The computational modelling for the complexes **C1S1**; **C2S1**; **C3S1** and **C4S1** were carried out in the gaseous phase at the density functional theory (DFT) level.⁷ The B3LYP functionals and a basis set of LANL2DZ was used.⁸⁻¹⁰ B3LYP relates to the hybrid functional Becke's three parameter formulation⁹ which has been proven to be better to model traditional metal

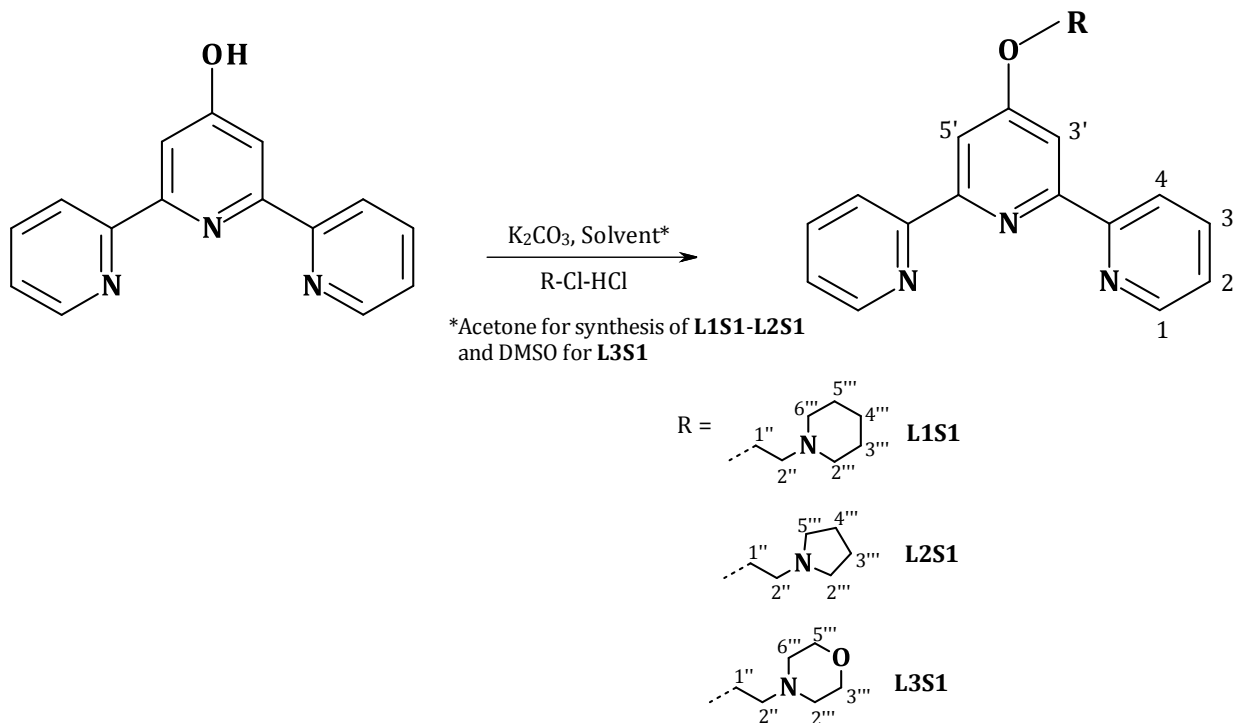
functionals. All the computational calculations were done by the Gaussian 09 software suite.¹¹ All the platinum(II) complexes were optimized at a +1 charge.

4.2.3 Kinetic Analyses

All kinetic measurements were performed under *pseudo* first-order conditions using at least 10-fold excess of the incoming nucleophile. The wavelengths for kinetic investigations were pre-determined using the Agilent Cary 100 Bio UV/Visible spectrophotometer with an attached Varian Peltier temperature control unit. Ligand substitution reactions which took less than sixteen minutes to go to completion (**C2S1** with 40x, 50x **Histidine**, **C2S1** with **Histidine** at 30°C and 35°C and **C4S1** reactions with **Im**, **1-MIm** and **Histidine**), an Applied Photophysics SX.20MV (v4.33) stopped-flow system coupled with an online data acquisition system was used to follow these reactions, otherwise the UV/Visible spectrophotometer was used to study all the reactions that reached completion in a time greater than or equal to sixteen minutes. All measurements (UV/Visible and stopped-flow) were carried out in a thermostated environment to within $ca \pm 0.1$ °C. All data were graphically analysed using the software package, Origin 9.0®.¹²

4.3 Synthesis of the Ligand Systems (L1 – L4)

4.3.1 Synthesis of ligands (4'-[2-(1-Piperidinyloxy)]-2,2':6',2''-terpyridine (L1S1), (4'-[2-(1-Pyrrolidino)ethoxy]-2,2':6',2''-terpyridine (L2S1) and (4'-[2-(1-Morpholino)ethoxy]-2,2':6',2''-terpyridine (L3S1)).¹⁻³



The synthesis of **L1S1**, **L2S1** and **L3S1** followed a common method described by Suntharalingam *et al.*²⁻³

2,6-bis(2-pyridyl)-4-(1H)pyridone (0.25 g, 1.00 mmol) and K_2CO_3 (3.3 eq.) were placed in a suitable solvent* (30 ml) and heated to reflux, after which 1-(2-chloroethyl)piperidine hydrochloride, 1-(2-chloroethyl)pyrrolidine hydrochloride or 1-(2-chloroethyl)morpholine hydrochloride (1 eq.) was then added to the refluxing mixture to form **L1S1**, **L2S1** or **L3S1** respectively. The resulting mixture was heated at reflux for a further 12 hours. The resulting product was cooled and allowed to settle after which the unreacted solid material were filtered off and the filtrate evaporated to dryness under reduced pressure. **L1S1**, **L2S1** and

L3S1 were isolated as a light yellow solid, an off-white solid and a yellow solid respectively. The crude products were purified by recrystallization with diethyl ether.

*Acetone was used for the synthesis of **L1S1** and **L2S1** respectively while *N,N*-dimethylformamide was used in the synthesis of **L3S1**.

L1S1

Yield: 0.63 g, 1.75 mmol (87.4%)

Melting point: 94.2 – 95.8 °C, **¹H-NMR:** [400 MHz, DMSO-*d*₆, RT, δ(ppm)]: δ_H **8.73** (d, py 2-H), **8.63** (d, 2H, py 5-H), **8.02** (dt, 2H, py 4-H), **7.99** (s, 2H, py', 3'-H and 5'-H), **7.51** (ddd, 2H, py 3-H), **4.35** (t, 2H, ethyl 1''-H), **2.76** (t, 2H, ethyl 2''-H), **2.53** (br m, 4H, piperidine 2'''-H), **1.52** (m, piperidine 3'''-H), **1.40** (m, 2H, piperidine 4'''-H), **¹³C-NMR:** [400 MHz, DMSO-*d*₆, RT, δ(ppm)]: δ_C **167.1, 157.2, 155.4, 149.7, 137.8, 125.0, 121.4, 107.3, 66.7, 57.5, 54.9, 26.1, 24.4**, Mass spectrum **LC/MS(HR)/TOF-MS-ESI⁺:** C₂₂H₂₄N₄ONa [M + Na]: = 383.1837 *m/z*
Anal. **Calc.** for: C = 73.31, H = 6.71, N = 15.54 %, **Found:** C = 73.00, H = 6.62, N = 15.69 %.

L2S1

Yield: 0.59 g, 1.70 mmol (85%),

Melting point: 82.2 – 84 °C, **¹H-NMR:** [400 MHz, DMSO-*d*₆, RT, δ(ppm)]: δ_H **8.73** (d, py 2-H), **8.63** (d, py 5-H), **8.03** (dt, 2H, py 4-H), **7.99** (s, 2H, py' 3'-H and 5'-H), **7.52** (ddd, py 3-H), **4.32** (t, 2H, ethyl 1''-H), **2.90** (t, ethyl 2''-H), **2.58** (br m, 4H, pyrrolidine 2'''-H), **1.71** (m, pyrrolidine 3'''-H), **¹³C-NMR:** [400 MHz, DMSO-*d*₆, RT, δ(ppm)]: δ_C **167.1, 157.2, 155.4, 149.7, 137.8, 125.0, 121.4, 107.3, 67.8, 54.5, 54.5, 23.7**, Mass spectrum **LC/MS(HR)/TOF-MS-ESI⁺:** C₂₁H₂₃N₄O [M + H] = 347.1864 *m/z*
Anal. **Calc.** for: C = 72.81, H = 6.40, N = 16.17 %, **Found:** C = 72.86, H = 6.48, N = 15.98 %.

L3S1

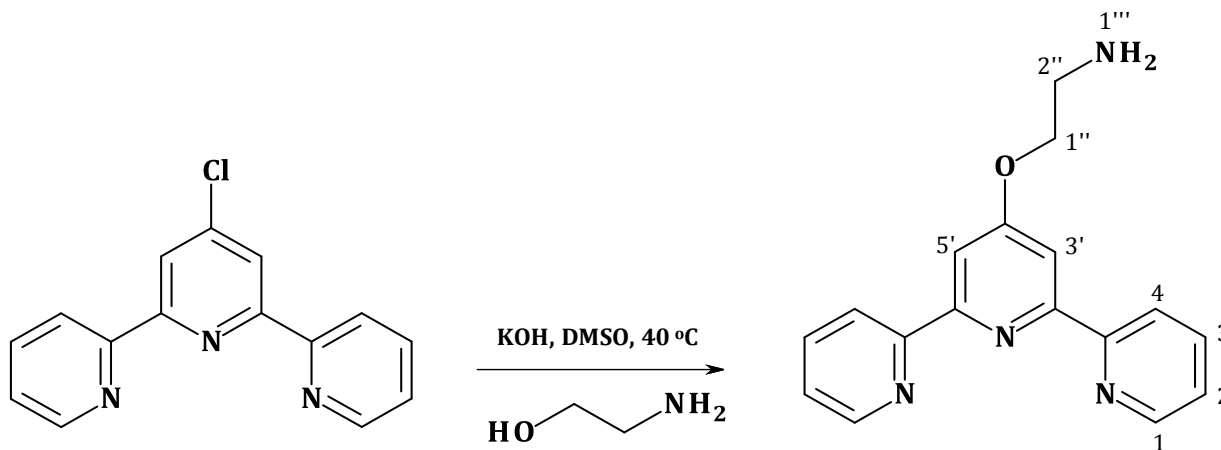
Yield: 0.61 g, 1.69 mmol (84%),

Melting point: 81 – 82.7 °C, **¹H-NMR:** [400 MHz, DMSO-*d*₆, RT, δ(ppm)]: δ_H **8.73** (d, 2H, py 2-H), **8.63** (d, 2H, py 5-H), **8.03** (dt, 2H, py 4-H), **8.00** (s, 2H, py' 3'-H and 5'-H), **7.51** (ddd, 2H, py 3-H), **4.37** (t, 2H, ethyl 1''-H), **3.61** (m, 4H, morpholine 2'''-H), **2.80** (t, 2H, ethyl 2''-H),

2.50 (m, 4H, morpholine 3'''-H), ¹³C-NMR: [400 MHz, DMSO-*d*₆, RT, δ(ppm)]: δ_c **166.6, 156.7, 154.9, 149.2, 137.3, 124.5, 120.9, 106.8, 66.2, 66.0, 56.7, 53.6**, Mass spectrum LC/MS(HR)/TOF-MS-ESI⁺: C₂₁H₂₂N₄O₂Na [M + Na] = 385.1635 *m/z*

Anal. Calc. for: C = 69.59, H = 6.12, N = 15.46 %, **Found**: C = 69.65, H = 6.29, N = 15.61 %.

4.3.2 Synthesis of 2,6-Di(2-pyridyl)-β-(aminoethoxy)pyridine (L4S1).¹



Ethanolamine (99 μl, 1.1 mmol) was added dropwise to a suspension of powdered potassium hydroxide (286 mg, 5.2 mmol) in dimethyl sulfoxide (**DMSO**) (50 ml) at 40 °C and stirred for twenty minutes. Thereafter, 4'-chloro-2,2':6'2''-terpyridine (286 mg, 1.0 mmol) was added and the resultant mixture was further stirred for 2.5 hours at 40 °C. The reaction mixture was then added to dichloromethane (40 ml) and washed with water, 25 ml (3 ×). The organic extract was dried over anhydrous magnesium sulfate and the resulting filtrate was evaporated to dryness under reduced pressure to yield a pale yellow solid. The crude product was purified by recrystallization from dichloromethane.

Yield: 0.23 g, 0.79 mmol (79%)

Melting Point: 82 – 83.7 °C, ¹H-NMR: [400 MHz, Chloroform-*d*, RT, δ(ppm)]: δ_H **8.72** (d, 2H, py 2-H), **8.64** (d, 2H, py 5-H), **8.06** (s 2H, py' 3'-H and 5'-H), **7.87** (t, 2H, py 4-H), **7.36** (t, 2H, py 3-H), **4.29** (t, 2H, ethyl 2''-H), **3.19** (t, 2H, 1''-H), **1.69** (s, 2H, NH₂, 1'''-H), ¹³C-NMR: [400 MHz, Chloroform-*d*, RT, δ(ppm)]: δ_c **167.2, 157.2, 156.1, 149.1, 136.8, 123.8, 121.4, 107.4, 70.5, 41.4**, Mass spectrum LC/MS/TOF-MS-ESI⁺: C₁₇H₁₇N₄O [M+H]: 293.1399 *m/z*

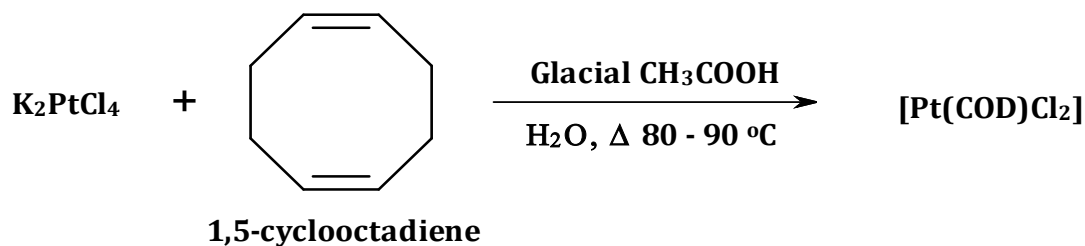
Anal. Calc. for: C = 69.85, H = 5.52, N = 19.17 %, **Found**: C = 69.79, H = 5.25, N = 19.19 %

¹³C-NMR: [400 MHz, DMSO-*d*₆, RT, δ(ppm)]: δ_c **166.6, 156.7, 154.9, 149.2, 137.3, 124.5, 120.9, 106.8, 66.2, 66.0, 56.7, 53.6**

Mass spectrum LC/MS(HR)/TOF-MS- ESI⁺: C₂₁H₂₂N₄O¹⁹⁴Pt³⁵ClBF₄ [M⁺] = 589.1265 *m/z*

4.4.2 Synthesis of [Pt(COD)Cl₂]⁶

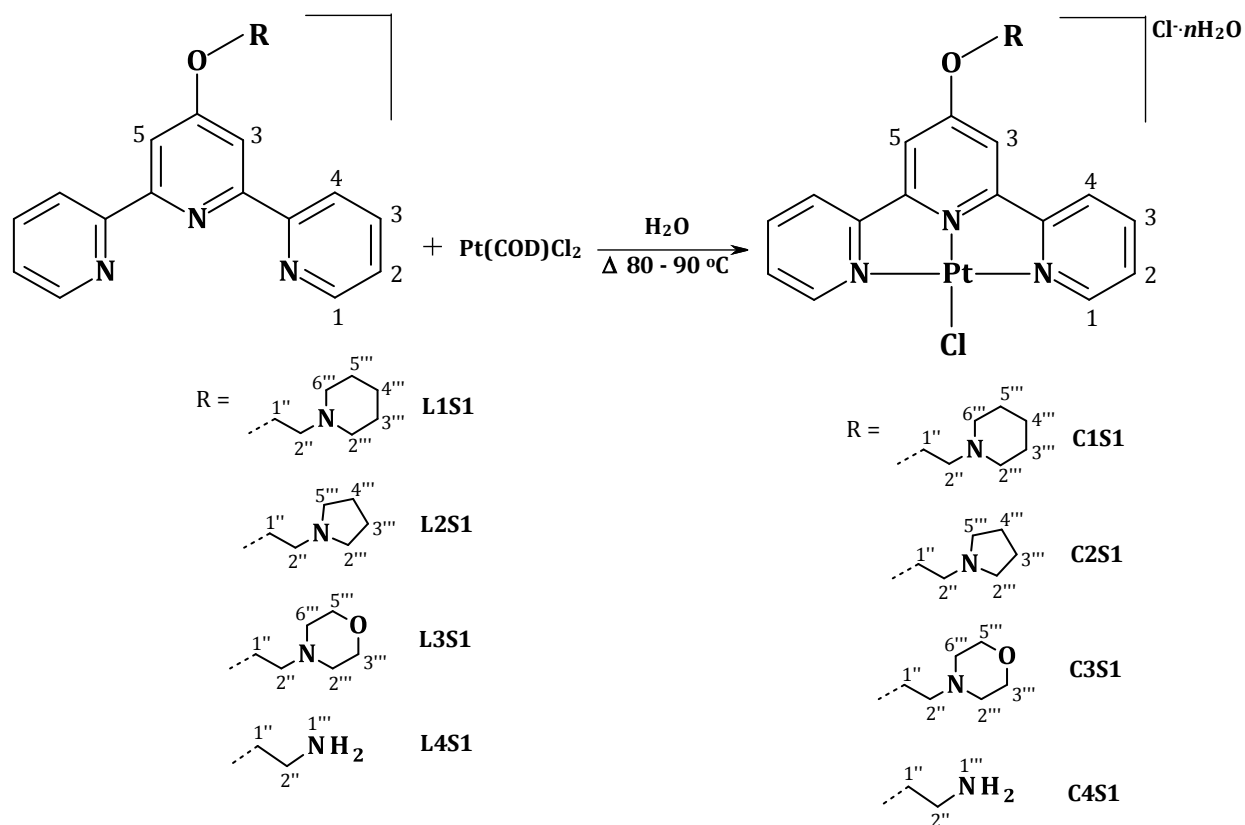
The synthesis of Pt(COD)Cl₂ was achieved by following the method of McDermott *et al.*⁶ as shown in the reaction scheme below.



To a filtered aqueous solution (20.0 mL) of K₂PtCl₄ (1.1 g, 2.6 mmol) was added to a solution of 1,5-cyclooctadiene (1.0 g, 8.0 mmol) in glacial acetic acid (37.0 ml). The resulting mixture was stirred vigorously whilst heating at 80-90 °C for two hours. The colour of the solution changed from orange to pale yellow within 30 minutes after which a pale-yellow precipitate of dichloro(1,5-cyclooctadiene)platinum(II) began to form. After two hours, the mixture was cooled to room temperature and the solvent removed under reduced pressure to approximately 10.0 mL. The precipitate was filtered off using 0.45 μm nylon filter membrane on Millipore filtration unit, washed with copious amount of water, ethanol, and diethyl ether and dried in the oven at 100 °C for 30 minutes.

Yield: 0.86 g, 2.30 mmol (87%)

4.4.3 Platination of L1S1, L2S1, L3S1 and L4S1.⁶



To a stirred suspension of [Pt(COD)Cl₂] (100 mg, 0.27 mmol) in ultrapure water (20 ml), a suspension of the respective ligand **L1S1**, **L2S1**, **L3S1** and **L4S1** (0.27 mmol) in ultrapure water was added dropwise with stirring. The reaction mixture turned yellow and was further heated with stirring at 80-90 °C for 12 hours. After being cooled to room temperature, the mixture was filtered to remove unreacted material. The filtrate was evaporated to dryness under reduced pressure to yield a deep orange solid for **C1S1**, **C2S1** and **C4S1** respectively. **C3S1** was isolated a reddish solid. The crude platinum(II) complexes (**C1S1**, **C2S1**, **C3S1** and **C4S1**) were washed thoroughly with diethyl ether and dried under vacuum.

C1S1

Yield: 94.5 mg, 0.13 mmol (49%)

¹H-NMR: [400 MHz, DMSO-*d*₆, RT, δ(ppm)]: δ_H **8.63** (d, 2H, py 2-H), **8.52** (d, 2H, py 5-H), **8.42** (dt, 2H, py 4-H), **8.26** (s, 2H, py' 3'-H and 5'-H), **7.87** (ddd, 2H, py 3-H), **4.80** (t, 2H, ethyl 1''-H), **¹³C-NMR:** [400 MHz, DMSO-*d*₆, RT, δ(ppm)]: δ_C **168.8, 157.8, 154.9, 150.7, 142.3, 129.2, 125.8, 111.1, 68.0, 66.0, 56.3, 53.4**, Mass spectrum **LC/MS(HR)/TOF-MS-ESI⁺:** C₂₂H₂₄N₄O³⁷Cl¹⁹⁴Pt [M⁺] = 591.1250 *m/z*

Anal. **Calc.** for: C = 36.88, H = 4.78, N = 7.82 %, **Found:** C = 36.49, H = 4.65, N = 8.14 %

C2S1 [Pt(L2S1)Cl]Cl·5H₂O

Yield: 99.2 mg, 0.142mmol (53%)

¹H-NMR: [400 MHz, DMSO-*d*₆, RT, δ(ppm)]: δ_H **8.77** (d, 2H, py 2-H), **8.68** (d, 2H, py 5-H), **8.50** (dt, 2H, py 4-H), **8.35** (s, 2H, py' 3'-H and 5'-H), **7.93** (ddd, 2H, py 3-H), **4.75** (t, 2H, ethyl 1''-H), **¹³C-NMR:** [400 MHz, DMSO-*d*₆, RT, δ(ppm)]: δ_C **168.7, 158.4, 155.8, 151.6, 142.9, 129.8, 126.3, 111.6, 54.4, 52.6, 23.3**, Mass spectrum **LC/MS(HR)/TOF-MS-ESI⁺:** C₂₁H₂₂N₄OCl¹⁹⁴Pt [M⁺] = 575.1116 *m/z*

Anal. **Calc.** for: C = 35.90, H = 4.59, N = 7.98%, **Found:** C = 35.59, H = 4.24, N = 7.66%

C3S1 [Pt(L3S1)Cl]Cl·5H₂O

Yield: 98.6 mg, 0.137 mmol (52%)

¹H-NMR: [400 MHz, DMSO-*d*₆, RT, δ(ppm)]: δ_H **8.57** (d, 2H, py 2-H), **8.49** (d, 2H, py 5-H), **8.39** (dt, 2H, py 4-H), **8.18** (s, 2H, py' 3'-H and 5'-H), **7.81** (ddd, 2H, py 3-H), **4.50** (t, 2H, ethyl 1''-H), **¹³C-NMR:** [400 MHz, DMSO-*d*₆, RT, δ(ppm)]: δ_C **168.8, 157.8, 154.9, 150.7, 142.3, 129.2, 125.8, 111.1, 68.0, 66.0, 56.3, 53.4**, Mass spectrum **LC/MS(HR)/TOF-MS-ESI⁺:** C₂₁H₂₂N₄O₂Cl¹⁹⁶Pt [M⁺] = 593.1077 *m/z*

Anal. **Calc.** for: C = 35.10, H = 4.49, N = 7.80 %, **Found:** C = 34.91, H = 4.38, N = 7.61%.

C4S1 [Pt(L4S1)Cl]Cl·5H₂O

Yield: 66.2 g, 0.102 mmol (45.3%)

¹H-NMR: [400 MHz, DMSO-*d*₆, RT, δ(ppm)]: δ_H **8.54** (d, 2H, py 2-H), **8.37** (d, 2H, py 3-H), **8.25** (s 2H, py' 3'-H and 5'-H), **7.77** (t, 2H, py 4-H), **5.15** (t, 2H, py 5-H), **3.67** (t, 2H, ethyl 2''-H), **3.40** (t, 2H, ethyl 1''-H), **2.49** (s, 2H, NH₂, 1'''-H), Mass spectrum **LC/MS(HR)/TOF-MS-ESI⁺:** C₁₇H₁₆N₄OClPt [M⁺] = 522.0659 *m/z*

Anal. **Calc.** for: C = 35.43, H = 3.15, N = 9.72%, **Found:** C = 35.77, H = 3.36, N = 9.42%.

4.5 Kinetic Measurements

The electrolyte (ionic strength solution, *I*) for the platinum complexes and the nucleophiles were prepared by dissolving a known amount of lithium trifluoromethanesulfonate (LiCF₃SO₃) and lithium chloride (LiCl) in ultrapure water to afford a solution of the concentration 0.010 M (0.009 M LiCF₃SO₃ and 0.001 M LiCl). Lithium trifluoromethanesulfonate was used as the anion since the triflate anion does not coordinate to platinum complexes while lithium chloride was used to prevent spontaneous solvolysis.¹³

4.5.1 Preparation of Platinum Complexes for Kinetic Analyses

Metal complex solutions were prepared by dissolving the required quantities of the platinum(II) complex in 100 mL of the constant ionic strength solution to afford solutions with the concentration of 5 × 10⁻⁴ M before mixing.

4.5.2 Preparation of Nucleophile Solutions for Kinetic Analysis

The nucleophile stock solutions, *viz.* **Im**, **1-MIm**, **Pyz** and **Histidine** of *ca.* 50 times greater than the metal complex solutions were prepared by dissolving a known amount of the nucleophile in 250.0 mL of the constant ionic strength (*I* = 0.01 M, (0.009 M LiCF₃SO₃ + 0.001 M LiCl)). The dilute nucleophile solution were prepared by subsequent dilutions of the 50

times nucleophile stock solutions to afford a series of standards of 10, 20, 30 and 40 greater than that of the platinum(II) complex.

As mentioned above, all reactions were done under *pseudo* first-order conditions with at least 10-fold excess of the nucleophiles. The UV/Visible lamps were warmed up and allowed to equilibrate at the required temperature prior to kinetic measurements. The instrument was zeroed at the wavelength chosen for measurements using the ultrapure water ionic strength solution ($I = 0.01$ M (LiCF₃SO₃ + LiCl)). The tandem cuvettes were then filled with equal amounts of the respective complex and nucleophile solutions and equilibrated for 10 minutes at the required temperature.

An initial absorbance reading of the solutions before mixing was recorded after which the solutions were quickly mixed and the substitution reaction was analysed by measuring the change in absorbance over time. The reaction was observed to reach completion when no further change in the absorbance was visible. All the kinetic ligand substitutions were carried out in duplicate on the UV/Visible spectrophotometry and stopped-flow spectrophotometer. All the kinetic traces obtained at the suitable wavelengths (see *Table B1*) were fitted to the first-order exponential decay function (*Equation E4.1*)¹⁴ to determine the observed *pseudo* first-order rate constants (k_{obs}) at the different nucleophilic concentrations and temperatures.

$$A_t = A_0 + (A_0 - A_\infty)e^{(-k_{obs}t)} \quad (4.1)$$

These k_{obs} values are represented in *Tables B2 – B9* of the Appendix B supporting information and were determined in the same way. The second-order rate constants, k_2 and k_{-2} for the platinum (II) complex reactions with the nucleophiles were determined from the slopes and intercepts of the plotted graphs of k_{obs} versus effective nucleophile concentrations (*Equation 3.34*)¹⁴ drawn using the software package, Origin 9.0®.¹¹

$$k_{obs} = k_2[Nu]_0 \quad (3.34)$$

The temperature dependence of the rate of reaction were studied at five different temperatures within the range of 10 – 35 °C in 5 °C intervals. All temperature dependence

studies were conducted using the 30X concentration for each nucleophile since the concentration dependence studies gave linear fits with no meaningful y-intercepts for the plots of k_{obs} versus effective nucleophile concentration ($[\text{Nu}]_{\text{eff}}$) at 298.15 K.

$\ln(k_2/T)$ versus $1/T$ (Eyring plot)¹⁵ from the Eyring equation (*Equation E3.59*) were fitted using the software package, Origin 9.0[®]. The activation parameters, enthalpy of activation (ΔH^\ddagger) and entropy of activation (ΔS^\ddagger) were calculated from the slopes and y-intercepts of the Eyring Equation (*Equation 3.56*)¹⁵, respectively.

$$\ln\left(\frac{k_2}{T}\right) = -\frac{\Delta H^\ddagger}{R} \cdot \frac{1}{T} + \left[23.8 + \frac{\Delta S^\ddagger}{R}\right] \quad (3.56)$$

4.6 References

1. Maayan, G.; Yoo, B.; Kirshenbaum, K., *Tetrahedron Lett.*, **2008**, *49* (2), 335-338.
2. Suntharalingam, K.; White, A. J.; Vilar, R., *Inorg Chem.*, **2009**, *48* (19), 9427-35.
3. Suntharalingam, K.; White, A. J.; Vilar, R., *Inorg Chem.*, **2010**, *49* (18), 8371-80.
4. Annibale, G.; Brandolisio, M.; Pitteri, B., *Polyhedron*, **1995**, *14* (3), 451-453.
5. Liu, X. M.; McInnes, E. J. L.; Kilner, C. A.; Thornton-Pett, M.; Halcrow, M. A., *Polyhedron*, **2001**, *20* (22-23), 2889-2900.
6. Mcdermott, J. X.; White, J. F.; Whitesides, G. M., *J Am Chem Soc.*, **1976**, *98* (21), 6521-6528.
7. Friesner, R. A., *Chem. Phys. Lett.*, **1985**, *116*, 39 - 43.
8. Hay, P. J.; Wadt, W. R., *Chem. Phys.*, **1985**, *82*, 270 - 282.
9. Becke, A. D., *J. Chem. Phys.*, **1993**, *98*, 5648 - 5652.
10. Becke, A. D., *J. Chem. Phys.*, **1993**, *99*, 3898 - 3905.
11. Frisch, M. J.; Trucks, G. W.; Schlegel, H. B.; Scuseria, G. E.; Robb, M. A.; Cheeseman, J. R.; Montgomery, J., J. A. ; Vreven, T.; Kudin, K. N.; Burant, J. C.; Millam, J. M.; Iyengar, S. S.; Tomasi, J.; Barone, V.; Mennucci, B.; Cossi, M.; Scalmani, G.; Rega, N.; Petersson, G. A.; Nakatsuji, H.; Hada, M.; Ehara, M.; Toyota, K.; Fukuda, R.; Hasegawa, J.; Ishida, M.; Nakajima, T.; Honda, Y.; Kitao, O.; Nakai, H.; Klene, M.; Li, X.; Knox, J. E.; Hratchian, H. P.; Cross, J. B.; Adamo, C.; Jaramillo, J.; Gomperts, R.; Stratmann, R. E.; Yazyev, O.; Austin, A. J.; Cammi, R.; Pomelli, C.; Ochterski, J. W.; Ayala, P. Y.; Morokuma, K.; Voth, G. A.; Salvador, P.; Dannenberg, J. J.; Zakrzewski, V. G.; Dapprich, S.; Daniels, A. D.; Strain, M. C.; Farkas, O.; Malick, D. K.; Rabuck, A. D.; Raghavachari, K.; Foresman, J. B.; Ortiz, J. V.; Cui, Q.; Baboul, A. G.; Clifford, S.; Cioslowski, J.; Stefanov, B. B.; Liu, G.; Liashenko, A.; Piskorz, P.; Komaromi, I.; Martin, R. L.; Fox, D. J.; Keith, T.; Al-Laham, M.; Peng, C. Y.; Nanayakkara, A.; Challacombe, M.; Gill, P. M. W.; Johnson, B.; Chen, W.; Wong, M. W.; Gonzalez, C.; Pople, J. A., *Gaussian, Inc., Pittsburgh PA*, **2010**, Gaussian 09, Revision C.01.
12. Microcal™ Origin™ Version 9.0, M. S., Inc., *One Roundhouse Plaza, Northampton, MA, 01060, USA*, **1991-2014**.

13. Appleton, T. G.; Hall, J. R.; Ralph, S. F.; Thompson, C. S. M., *Inorg. Chem.*, **1984**, *23*, 3521 - 3525.
14. Atwood, J. D., *Inorganic and Organic Reaction Mechanisms, 2nd Edition*, Wiley- VCH Inc., New York, **1997**, p. 43-46.
15. Eyring, H., *J. Chem. Phys.* **1935**, *3*, 107.

Chapter 5: Results and Discussion

5.1 Synthesis and Characterization of the Terpyridyl Ligands

The ligands, **L1S1** and **L2S1**, were synthesized according to literature procedure.¹⁻² The 2,6-bis(2-pyridyl)-4-(1H) pyridone was reacted with the corresponding hydrochloride salt of the 1-(2-chloroethyl) cyclic amines, namely 1-(2-chloroethyl)piperidine hydrochloride (**L1S1**) and 1-(2-chloroethyl)pyrrolidine hydrochloride (**L2S1**) in refluxing acetone with K_2CO_3 as a base. **L1S1** and **L2S1** were obtained as white to yellow solids in satisfactory yields of 87 and 85%, respectively. The ligands were characterized by 1H NMR and ^{13}C NMR spectroscopy, mass spectrometry and elemental analysis. The 1H NMR and ^{13}C NMR spectra were recorded in deuterated dimethyl sulphoxide and the characteristic data was in good agreement with both the structural formula of the molecule as well as the data reported in literature.¹⁻² High resolution liquid chromatography-mass spectrometry (LC-MS) gave an accurate mass of 383.1837 *amu* for **L1S1** which corresponds to the $[M + Na]^+$ ion. **L2S1** had an accurate mass of 347.1864 *amu* which corresponds to its protonated ion, $[M + H]^+$.

The syntheses of ligand **L3S1** was achieved in high yields averaging 84% in *N,N'*-dimethylformamide. The 1H NMR and ^{13}C NMR spectra of this ligand were recorded in deuterated dimethyl sulphoxide and the chemical shifts were in good agreement with that reported in literature.¹ High resolution LC-MS analysis of **L3S1** gave an accurate mass of 385.1635 *amu* due to its $[M + Na]^+$ adduct ion.

The ligand **L4S1** was synthesized according to the method described by Maayan *et al.*³ The 1H NMR and ^{13}C NMR spectra of this ligand were recorded in deuterated chloroform and the chemical shifts were in agreement with that reported in literature.³ High resolution LC-MS for **L4S1** gave an accurate mass, with an experimental mass of 293.1399 *amu* which corresponds to the adduct ion, $[M + H]^+$.

5.2 Synthesis and Characterization of the Platinum Complexes

The platinum(II) complexes; **C1S1**, **C2S1**, **C3S1** and **C4S1** were synthesized using slightly modified method reported by Annibale *et al.*⁴ for [Pt(terpy)Cl]Cl·2H₂O (where terpy = 2,2':6',2''-terpyridine) and involves the use of metal precursor, Pt(COD)Cl₂. The COD ligand is weakly coordinated to platinum and has a good *trans*-labilizing effect allowing its facile replacement as well as the *trans* chloride by the incoming terpyridyl moiety.⁵

One equivalent of the pure ligands (**L1S1**, **L2S1**, **L3S1** and **L4S1**) were reacted with 1 equivalent of the Pt(COD)Cl₂ in ultrapure water to yield crude complex materials of **C1S1**, **C2S1**, **C3S1** and **C4S1**, respectively. The resulting red to brick red solid pentahydrate salts were washed thoroughly with copious amounts of cold diethyl ether to remove any unreacted ligand material. These complexes were dried *in vacuo* overnight. All the complexes were characterized spectropically (¹H-NMR, ¹³C-NMR), LC-MS and by elemental analysis. All the characterization data obtained were in good agreement with the structural formula and the literature data available.¹

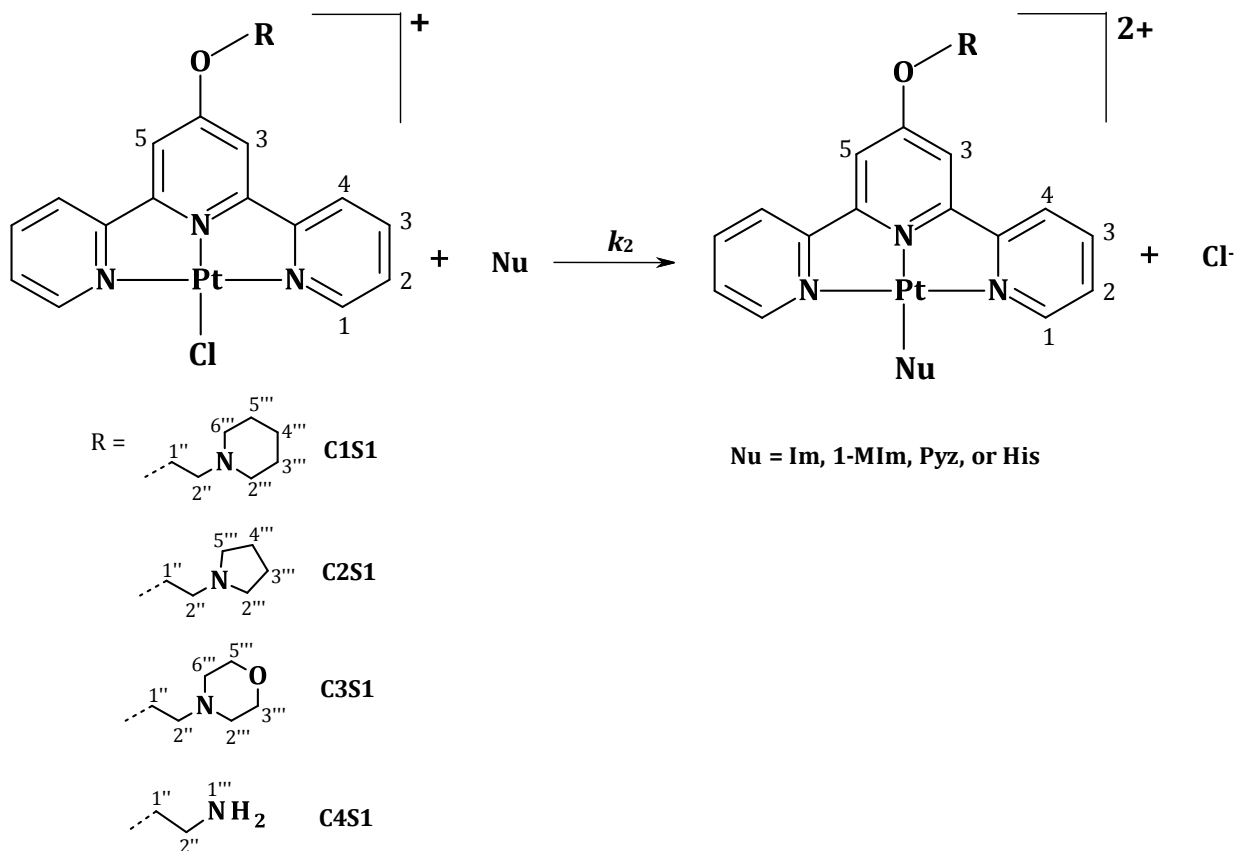
The four platinum(II) complexes were obtained in satisfactory yields of 70-85%. The ¹H-NMR and ¹³C-NMR were recorded in deuterated dimethyl sulphoxide (DMSO-*d*₆). The chemical shifts obtained were in good agreement with the structural formula of the complexes. However, all ¹H-NMR resonance peaks of the platinum(II) complexes showed a shielding effect in which the chemical shifts of the coordinated ligands were shifted upfield relative to that of free ligand instead of the normally observed deshielding effect experienced by most platinum(II) complexes. This shift has been previously reported by Yam *et al.*⁶ and was associated with the presence of molecular interactions or self-assembly processes, probably intramolecular in nature.⁶ Stang *et al.*⁷ also witnessed this upfield shift due to the shielding of the bipyridyl units by the dppp phenyl rings.⁷ These reports support the observed upfield shift since elemental analysis of each complex indicated the presence of five water molecules.

For **C1S1**, a molecular ion peak was found at 591.1250 *amu* on the mass spectrum which corresponds to cationic molecular formula of $C_{22}H_{24}N_4O^{37}Cl^{194}Pt$, (Figure A13, **Appendix A**). **C2S1** and **C3S1** had a molecular ion peaks at 575.1116 and 593.1077 *amu* respectively, which corresponds well to the cationic molecular formula of $C_{21}H_{22}N_4OCl^{194}Pt$ and $C_{21}H_{22}N_4O_2Cl^{196}Pt$ respectively, (Figure A16 and A19, **Appendix A**).

For the novel platinum(II) complex, **C4S1**, high-resolution mass analysis showed the accurate molecular mass of the compound ($C_{17}H_{16}N_4OCl^{194}Pt$), with the experimental mass of 521.0645 and the calculated mass of 521.0639 [M⁺].

5.3 Kinetic Measurements

The substitution of the coordinated chloride from the square-planar platinum(II) complexes (**Scheme 5.1**) with nitrogen donor nucleophiles was investigated under *pseudo* first-order conditions and constant ionic strength (0.01 M (0.009 M LiCF₃SO₃ and 0.001 M LiCl)) as a function of concentration and temperature using four (4) different biorelevant nitrogen donor nucleophiles (Nu), *viz.* Imidazole (**Im**), 1-methylimidazole (**1-MIm**), pyrazole (**Pyz**) and *L*-Histidine (**His**). The substitution process was monitored using UV/Visible and conventional stopped-flow spectrophotometry. Initially, conventional UV/Visible spectrophotometry was used to follow the reaction in order to determine the time-scale for complete ligand substitution and to find a suitable wavelength for the kinetic studies. For each kinetic investigation, the wavelength showing the greatest change in absorbance was selected for kinetic analysis.



Scheme 5.1: Proposed mechanism of chloride substitution from the 4'-substituted terpy platinum(II) complexes by azole ligands.

Figure 5.1 shows the typical absorption spectra obtained during the course of the reaction. The presence of a clear isosbestic point is an indication that reactants are converted to a single product at constant mole ratio⁸ in accordance with **Scheme 5.1**.⁹⁻¹⁰

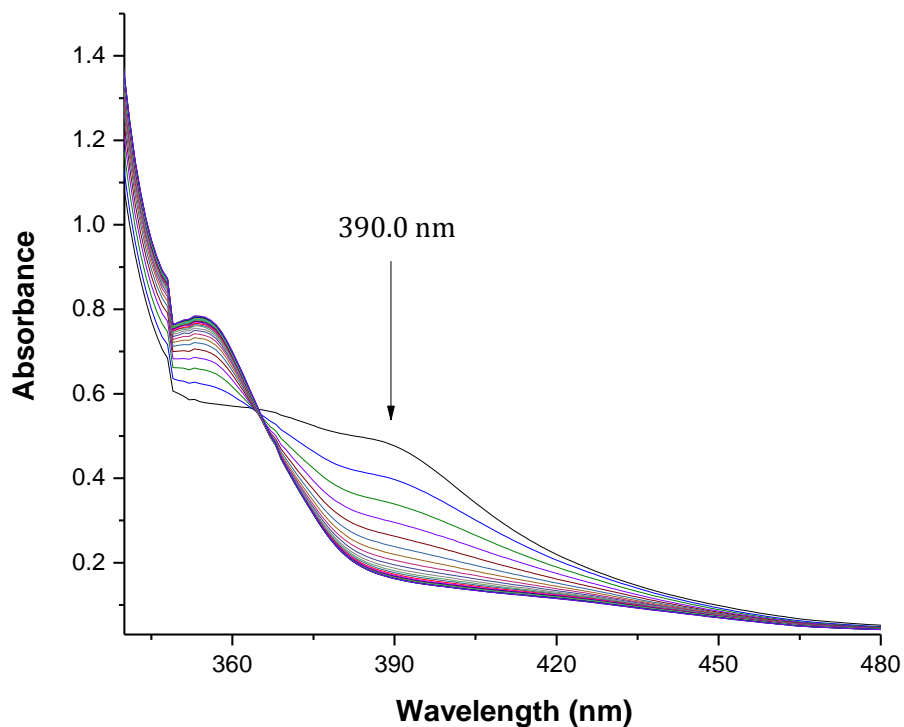


Figure 5.1: Absorbance spectra of **C2S1** (2.50×10^{-4} M) and **His** (2.50×10^{-3} M) at an ionic strength of 0.01 M (0.009 M LiCF_3SO_3 and 0.001 M LiCl) at 298.15 K.

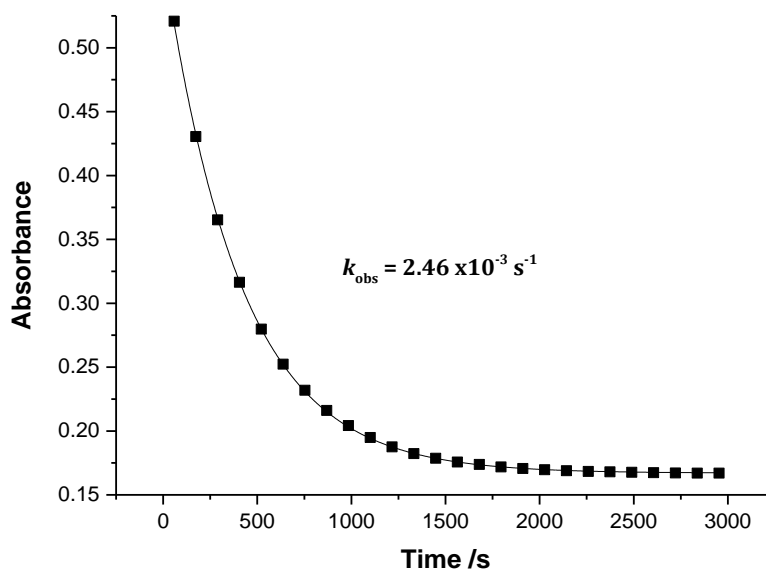


Figure 5.2: Corresponding kinetic trace and the corresponding single-exponential fit for **C2S1** (2.50×10^{-4} M) and **His** (2.50×10^{-3} M) at 390 nm at an ionic strength of 0.01 M (0.009 M LiCF_3SO_3 and 0.001 M LiCl) at 298.15 K.

The spectra of other complexes and nucleophiles are included in the *Appendix B* of the supporting information.

Chloride substitution that reached completion in sixteen minutes or less were studied using conventional stopped-flow spectrophotometry. A typical stopped-flow kinetic trace recorded for the substitution reaction of **C4S1** with **His** is shown in **Figure 5.3**.

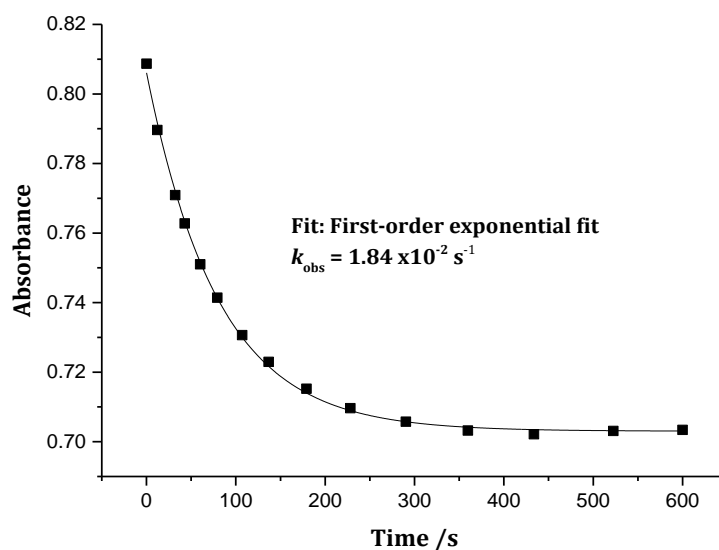


Figure 5.3: Kinetic trace for the reaction of **C4S1** ($2.5 \times 10^{-4} \text{ M}$) and **His** ($5.0 \times 10^{-3} \text{ M}$) obtained from stopped-flow spectrophotometry at an ionic strength of 0.01 M ($0.009 \text{ M LiCF}_3\text{SO}_3 + 0.001 \text{ M LiCl}$) at 380.0 nm and 298.15 K.

The *pseudo* first-order rate constants were plotted against the concentration of the incoming nucleophiles (**Im**, **1-MIm**, **Pyz** and **His**) to obtain the second-order rate constant for the forward reaction from the slopes as described by *Equation 5.1*.

$$k_{\text{obs}} = k_2[\text{Nu}]_0 \quad (5.1)$$

Figure 5.4 shows a typical concentration dependence plots for **C1S1** against the concentration of each of the four nucleophiles at 298.15 K with the calculated values for the second-order rate constants summarized in **Table 5.1**.

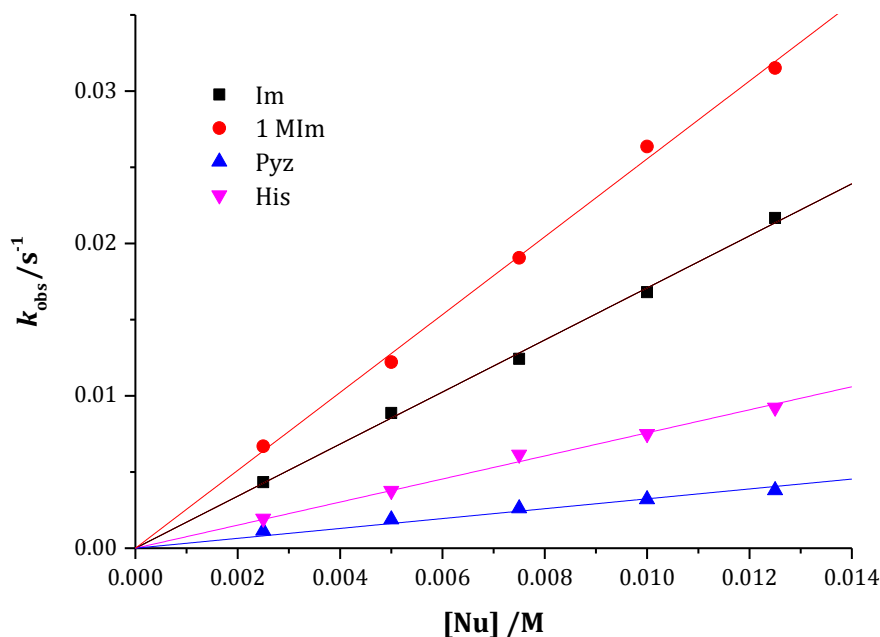


Figure 5.4: Dependence of the *pseudo* first-order rate constant (k_{obs}) on the concentrations of the azole nucleophiles for the chloride substitution from **C1S1** in an aqueous solution of constant ionic strength ($I = 0.01 \text{ M}$ (0.009 M $\text{LiCF}_3\text{SO}_3 + 0.001 \text{ M LiCl}$)) at 298.15 K.

The temperature dependence studies of the rate constants were investigated within the range 10-30 °C or 15-35 °C at 5 °C intervals, depending on the observed reactivity with the nucleophiles. A typical Eyring plot is shown in **Figure 5.5** for chloride substitution from **C1S1**. The enthalpies of activation (ΔH^\ddagger) and entropies of activation (ΔS^\ddagger) were calculated from the Eyring equation (*Equation 3.56*) and are summarized in **Table 5.1**.

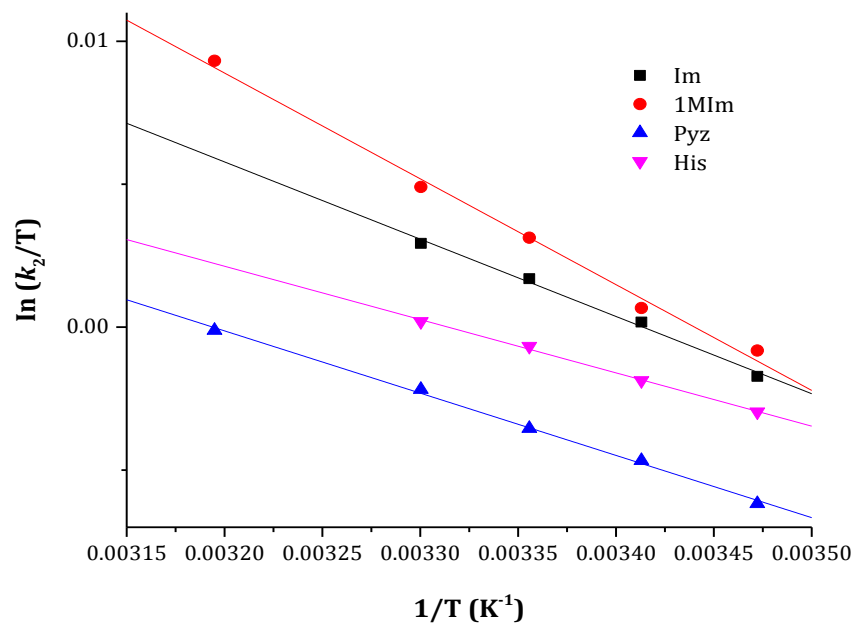


Figure 5.5: Eyring plots used to calculate the activation parameters for the direct nucleophilic substitution reaction for **C1S1** with the four azole nucleophiles at various temperatures (ranging between 15 – 35 °C).

5.4 Kinetic results

Table 5.1: Summary of second-order rate constants (k_2) (\pm standard deviations) and activation parameters for the chloride displacement from the investigated platinum(II) complexes by **Im**, **1-MIm**, **Pyz** and **His** in an aqueous solution of constant ionic strength, ($I = 0.010 \text{ M}$ ($0.009 \text{ M LiCF}_3\text{SO}_3 + 0.001 \text{ M LiCl}$) at $25.0 \text{ }^\circ\text{C}$.

	Parameter	Im	1-MIm	Pyz	His
C1S1	$k_2 \text{ (M}^{-1}\text{s}^{-1}\text{)}$	1.51 ± 0.08	2.46 ± 0.13	0.265 ± 0.008	0.732 ± 0.03
	$\Delta H^\ddagger \text{ (kJ mol}^{-1}\text{)}$	225.0 ± 0.013	307.8 ± 0.014	181.1 ± 0.005	155.0 ± 0.006
	$\Delta S^\ddagger \text{ (J K}^{-1} \text{ mol}^{-1}\text{)}$	-197.1 ± 0.04	-196.8 ± 0.050	-197.3 ± 0.017	-197.4 ± 0.02
C2S1	$k_2 \text{ (M}^{-1}\text{s}^{-1}\text{)}$	1.66 ± 0.038	2.69 ± 0.045	0.271 ± 0.0051	0.880 ± 0.017
	$\Delta H^\ddagger \text{ (kJ mol}^{-1}\text{)}$	249.2 ± 0.0013	244.5 ± 0.006	190.2 ± 0.006	128.7 ± 0.002
	$\Delta S^\ddagger \text{ (J K}^{-1} \text{ mol}^{-1}\text{)}$	-197.0 ± 0.005	-197.1 ± 0.022	-197.3 ± 0.019	-197.4 ± 0.007
C3S1	$k_2 \text{ (M}^{-1}\text{s}^{-1}\text{)}$	1.04 ± 0.0121	1.25 ± 0.0402	0.259 ± 0.002	0.501 ± 0.016
	$\Delta H^\ddagger \text{ (kJ mol}^{-1}\text{)}$	249.1 ± 0.003	246.3 ± 0.01	252.8 ± 0.005	215.1 ± 0.003
	$\Delta S^\ddagger \text{ (J K}^{-1} \text{ mol}^{-1}\text{)}$	-197.1 ± 0.012	-197.1 ± 0.003	-197.1 ± 0.016	-197.2 ± 0.009
C4S1	$k_2 \text{ (M}^{-1}\text{s}^{-1}\text{)}$	3.24 ± 0.07	3.74 ± 0.09	0.512 ± 0.002	2.65 ± 0.09
	$\Delta H^\ddagger \text{ (kJ mol}^{-1}\text{)}$	207.3 ± 0.004	195.1 ± 0.002	286.6 ± 0.007	185.1 ± 0.007
	$\Delta S^\ddagger \text{ (J K}^{-1} \text{ mol}^{-1}\text{)}$	-197.2 ± 0.014	-197.2 ± 0.008	-197.0 ± 0.002	-197.3 ± 0.03

5.5 Computational Analysis

In order to gain an in-depth understanding of how the observed reactivity might be influenced by the structural and electronic properties of the complexes under study, computational analysis of each complex was undertaken. Computational modelling for the complexes **C1S1**; **C2S1**; **C3S1** and **C4S1** were carried out in the gaseous phase at the density functional theory (DFT) level. The B3LYP functionals and a basis set of LANL2DZ was followed.¹¹⁻¹³ B3LYP relates to the hybrid functional Becke's three parameter formulation which has been proven better to traditional functional.¹¹⁻¹⁴ All the platinum(II) complexes were optimized at a +1 charge. The minimum energy optimized structures of the complexes are represented in **Table 5.4**. Since the frontier orbital energy is an important tool to understand the substitution mechanism of inorganic reactions, the energy for the Highest Occupied Molecular Orbital (HOMO) and the Lowest Unoccupied Molecular Orbital (LUMO) were also obtained from the computational modelling and are shown in **Table 5.4**.

The Pt–Cl bond lengths, bond angles, NBO charges, energies of the frontier molecular orbitals with the chemical reactivity indices of the calculated structures are tabulated.

Table 5.2: Selected bond lengths (Å) and bond angles(°) for the platinum complexes **C1S1**, **C2S1**, **C3S1** and **C4S1** obtained from the computational studies.

Bond Lengths				
Properties	C1S1	C2S1	C3S1	C4S1
Pt – N1 (Cis)	2.0407	2.0408	2.0407	2.0407
Pt – N2 (Trans)	1.9640	1.9639	1.9640	1.9639
Pt – N3 (Cis)	2.0399	2.0399	2.0398	2.0402
Pt - Cl	2.3980	2.3980	2.3973	2.3981
Bond Angles				
Cl-Pt-N1	99.09	99.07	99.08	99.07
Cl-Pt-N2	179.95	179.94	179.94	179.95
Cl-Pt-N3	98.95	98.96	98.94	98.96
N1-Pt-N2	80.86	80.87	80.87	80.88
N1-Pt-N3	161.97	161.97	161.98	161.97
N2-Pt-N3	81.11	81.10	81.11	81.09

Table 5.3: DFT-calculated (B3LYP/LANL2DZ) molecular orbitals diagrams showing the HOMO's and LUMO's and the planarity of the tridentate Pt(II) complexes.

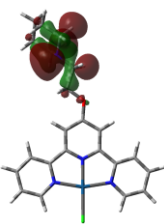
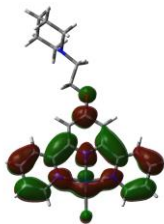
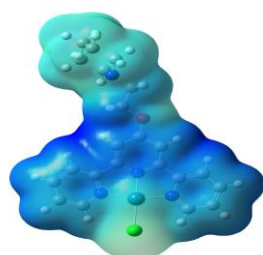
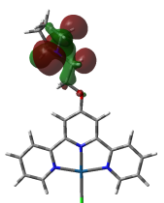
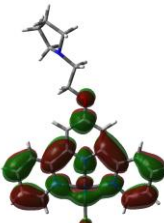
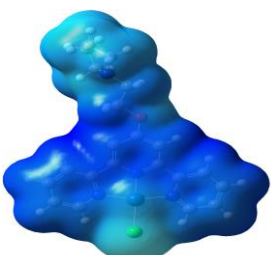
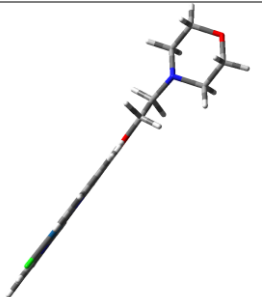
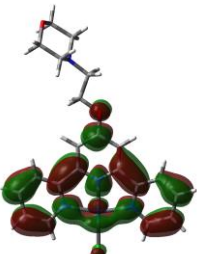
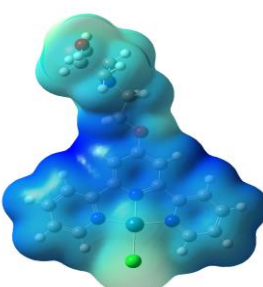
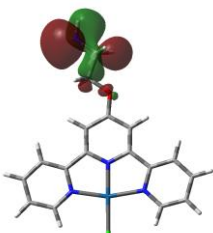
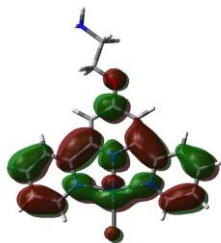
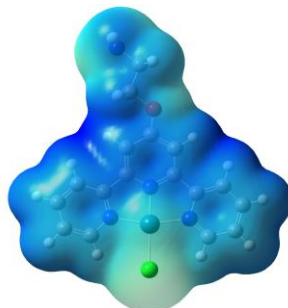
Geometry Optimized Structure	HOMO	LUMO	ESP Map Electronegativity
 <p data-bbox="308 735 389 766">C1S1</p>			
 <p data-bbox="308 1123 389 1155">C2S1</p>			
 <p data-bbox="308 1501 389 1533">C3S1</p>			
 <p data-bbox="308 1848 389 1879">C4S1</p>			

Table 5.4: Energies of HOMO-LUMO gap, the DFT-calculated Dipole moment (D), the calculated parameter and electronic chemical potential, μ obtained for the platinum(II) complexes studied.

Energy gaps				
Properties	C1S1	C2S1	C3S1	C4S1
HOMO/eV	-7.83	-7.68	-8.12	-8.72
LUMO/eV	-6.00	-6.00	-6.07	-6.01
$\Delta E/eV$	1.83	1.68	2.05	2.71
μ/eV	6.915	6.815	7.095	2.71
Dipole moment (Debye)				
	4.2487	5.3878	2.3603	9.6816

Table 5.5: The DFT-calculated NBO charges on the central Pt, the donor nitrogen atoms and the leaving group, Cl.

Complex	Pt	N1	N2	N3	Cl⁻
C1S1	0.543	-0.490	-0.482	-0.491	-0.408
C2S1	0.543	-0.490	-0.482	-0.491	-0.408
C3S1	0.543	-0.490	-0.482	-0.491	-0.406
C4S1	0.559	-0.490	-0.483	-0.491	-0.408

5.6 Discussion

5.6.1 Reactivity of the Platinum(II) Complexes

The slightest modification on the terpyridyl framework has been reported to influence the rate of chloride substitution and this was examined in this study.

The four complexes investigated in this study were chosen based on their structural motifs in the 4'-position and to investigate whether the trends in their substitutional reactivity correlate to their trends in the binding capacity to quadruplex DNA as reported by Suntharalingam *et al.*¹⁻² These complexes have a terpyridyl framework functionalized with an aliphatic cyclic amine (**C1S1**, **C2S1** and **C3S1**) on the 4'-positions. These functional groups were meant to provide steric bulk in an effort to prevent the terpyridyl complex from intercalating between base-pairs of duplex DNA and render the complex more selective towards quadruplex DNA structures as well as to improve their water solubility.

In comparing the reactivity of chloride substitution for the investigated complexes, the data provided in **Table 5.1** shows a general reactivity trend where **C4S1** > **C2S1** > **C1S1** > **C3S1**. In the case of chloride substitution by **Im**, we found that the relative reactivity for **C4S1**, **C2S1**, **C1S1** and **C3S1** is 3: 2: 2: 1 respectively with similar trends shown for substitution by **1-MIm**, **Pyz** and **His**. In addition, the rate of substitution followed the rate law: $k_{\text{obs}} = k_2[\text{Nu}]$, with any solvolysis or reverse reaction contributing negligible to the rate law.

When considering the geometry about the platinum atoms, the structural formulae of the complexes **C1S1**, **C2S1**, **C3S1** and **C4S1** show a similar distorted square-planar geometry with *cis*-N-Pt-Cl and *trans*-N-Pt-Cl with angles of 80 – 81° and bite angles 161 – 162°, deviating from 90 °C and linearity (**Table 5.2**), respectively. These are also similar in terms of planarity, bond angles and lengths. In **C1S1**, **C2S1** and **C3S1**, the attached cyclic amine lies out-of-plane with respect to the terpy moiety. This expression is assumed to reduce the repulsions between the electron density of the cyclic amines and the terpy chelate ligand (**Table 5.3**). The distance of the appended cyclic amine substituents from the metal centre

is not expected to pose any steric hindrance on the path of the incoming nucleophile. However, the presence of a flexible chain on the ancillary amine groups ensures that these groups indeed make the steric influence significant. Therefore, the trend in reactivity of the four complexes can be explained in terms of both electronic and steric effects (electron density) imposed by the presence of the cyclic amines at the ancillary position of the terpyridyl framework. The cyclic amine rings attached to terpy moiety making **C1S1**, **C2S1** and **C3S1** are strong σ -donors and electron-donating groups of different magnitude. The increase in the σ -donor ability of the attached cyclic amine from pyrrolidine to piperidine to morpholine is expected to decrease the reactivity of the complexes, from **C1S1**, **C2S1** to **C3S1** respectively while **C4S1** is expected to be most reactive since it has the weakest σ -donor ability.^{15-20, 19, 20} The basis is that, a strong σ -donor would inductively donate electrons towards the platinum centre which reduces the π -acceptor ability of the terpyridine ligand and subsequently decreases the reactivity of the metal centre.

From **Table 5.2**, **5.4** and **5.5**, it can be seen that, due to structural similarities of **C1S1** and **C2S1**, the *cis* and Pt – N1(*trans*) bonds, NBO charges and Pt–Cl bonds remain fairly constant, hence we would expect a small difference in their reactivity or a negligible influence upon moving from the piperidine ancillary group to pyrrolidine. This is supported by the observed reactivity of **C1S1**, $1.66 \text{ M}^{-1}\text{s}^{-1}$ and **C2S1**, $1.51 \text{ M}^{-1}\text{s}^{-1}$ with **Im** (**Table 5.1**) which show a marginal difference. For this reason the reactivity's of **C2S1** and **C4S1** are compared.

In comparing the reactivity of **C2S1** and **C4S1**, we find that by adding a strong σ -electron-donating cyclic amine towards the terpy ligand, the reactivity of **C2S1** is decreased by a factor of 2.20 compared to **C4S1**. The strong σ -donating pyrrolidine cyclic amine inductively donates electrons towards terpyridyl chelate ligand thereby reducing its π -backbonding ability. This renders the reactivity of the metal centre towards the incoming nucleophiles. This reactivity trend has been previously reported by Jaganyi *et al.*^{17, 21}, Gullam *et al.*²⁵ and Lowe *et al.*²²⁻²³

In addition, the data in **Table 5.5** shows that, the inductive σ -electron donation from the pendant pyrrolidine cyclic amine marginally increases the negative NBO charge on the *trans* N-atom (N2) on **C2S1** (0.483) compared to **C4S1** (0.481). The positive NBO charge on the

platinum(II) centre decreases from 0.559 (**C4S1**) to 0.543 (**C2S1**) pointing out to the well-known *trans*-effect. Consequently, the difference in the **Pt-Cl** bond length despite being so small, is shortened marginally from 2.3981 (**C4S1**) to 2.3980 (**C2S1**) indicating that the σ -donation of electrons is towards the metal centre and reflects the *trans* effect of the appended pyrrolidine cyclic amine, (**Table 5.2**). A similar trend has been previously reported by Shaira *et al.*²⁰

The DFT-calculated dipole moments (**Table 5.4**) also support this observed trend given that a higher dipole moment favours π -backbonding, therefore the smaller dipole moment of **C2S1** (5.388) compared to that of **C4S1** (9.682) further supports its lower reactivity compared to that of **C4S1**.¹⁵⁻²⁰ This also confirms the decreased ability of complexes appended with cyclic amines at the 4'-ancillary position to accept electron density from the incoming nucleophiles when compared to the parent **C4S1**. This retardation effect observed between **C4S1** and **C2S1** upon addition of electron-donating groups has been noted previously by Shaira *et al.*^{20, 24} and Schmulling *et al.*²⁵ The effect due to electron-donating groups attached in the ancillary 4'-position of a terpyridine chelate ligand has also been reported by Jaganyi *et al.*^{17, 21} In addition, the decrease in the reactivity of **C2S1** can also be attributed to the steric contribution imposed on the platinum(II) coordination site by the combined electron density of the pendant pyrrolidine amine and the terpy chelate ligand which reduces the effectiveness of the axially incoming nucleophile thereby lowering the reactivity of **C2S1**. The increased steric influence exists in **C2S1** given the appended cyclic amine which is absent in **C4S1**. From these observations, we can therefore conclude the difference in reactivity between **C4S1** and **C2S1** is due to both the electronic (σ -donation) and steric effects.

In analysing the reactivity of the complexes appended with the cyclic amines (**C1S1**, **C2S1** and **C3S1**), the expectation is that the reactivity would follow the trend **C3S1** > **C2S1** > **C1S1** due to an increasing σ -inductive effect since an increase in σ -inductive effect lowers the π -acceptor ability of the terpy ligand leading to a weaker *trans* labialization effect.^{20, 24, 26}

The morpholine pendant on **C3S1** has an oxygen atom that is electronegative and is expected to withdraw electron density away from the terpy backbone making it more weakly σ -donating than the piperidine moiety in **C1S1**. We would therefore expect an increased reactivity for **C3S1** compared to **C1S1** and **C2S1**. This effect is also expected to elongate the **Pt–Cl** bond thereby making **C3S1** the more reactive metal centre through an enhanced *trans* labialization effect of the metal-to-leaving group bond hence the expected reactivity is **C3S1** > **C2S1** > **C1S1**.²⁷ However, this trend is not what is observed in the magnitude of the rate constants nor the DFT-calculations.

Clearly, the reactivity of **C3S1** (**Table 5.1**) shows that the σ -donating ability of the ancillary ligand is not the only controlling factor hence **C3S1** stands as an anomaly given that DFT calculations and the observed reactivity show it as the slowest. In addition, the DFT-calculated NBO charges for the platinum(II) centre and *trans* N-atom (N2) remain constant from **C1S1** to **C3S1** (**Table 5.6**) reflecting that there is no significant change experienced by the platinum(II) centres upon changing the σ -donor ability of the appended cyclic amine. This indicates that the platinum(II) centres of the complexes appended with cyclic amines are in the same electronic environment. Therefore, the remaining factor accounting for the observed reactivity from **C1S1** to **C3S1** is the steric influence due to the electron density around the cyclic amine group appended to the plane containing the platinum(II) (**Table 5.3, ESP map**). As mentioned above, this steric influence becomes a factor due to the presence of a flexible linker in appended cyclic amines.

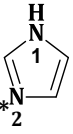
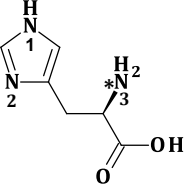
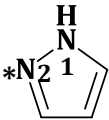
The analysis on these complexes show a moderate increase in the rate of substitution as the pendant cyclic amine gets smaller in electron density. The experimental data reveals a higher reactivity for **C2S1** followed by **C1S1** and **C3S1** respectively (**Table 5.1**). The DFT calculated dipole moments, a parameter that correlates to the inductive negative charge of the metal complex¹⁴ are synchronized with observed experimental reactivity trend, (**Table 5.4**). **Table 5.4** shows a sharp decrease in molecules polarity (dipole moment) as you increase the electron density of the appended cyclic amine, therefore reducing the π -backbonding ability of the terpyridine chelate. This observation reiterates that the remaining factor controlling the reactivity of these complexes is fundamentally related to the steric properties of the

complexes. Therefore, an increase in electron density of the complex retards the reaction by repelling the incoming nucleophile. Furthermore, a direct relationship is noticed between the observed reactivity trend and the HOMO-LUMO energy gaps. As explained above, the increase in electron density around the complexes from **C2S1**, **C1S1** to **C3S1** substantiates with the electronic chemical potential as a function of HOMO-LUMO gap (**Table 5.4**). The minimal electronic effects of the cyclic amines as reflected in the observed reactivity trends confirms the dominance of steric properties over the σ -donor abilities.

When comparing the reactivity of all the investigated complexes, the DFT-calculated **Pt-Cl** bond lengths despite being small and negligible support the observed overall reactivity trend. There is a slight increase in the **Pt-Cl** bond from **C4S1** > **C2S1** \geq **C1S1** > **C3S1** which concurs with the observed reactivity trend. This trend can be associated with a ground state destabilization of the complexes since the LUMO frontier molecular orbital mappings are concentrated on the terpyridyl moiety with the DFT-calculated LUMO energies remaining relatively constant (**Table 5.4**).²⁷ A similar effect due to the electron-donating substituents attached at the 4'-position of the terpyridine ligand has been previously reported by Reddy *et al.*²⁷ Therefore, we can conclude that, ground state destabilization of the complexes due to increased steric effect is a common and superior factor controlling the rate of chloride substitution. Furthermore, evidence affirming this conclusion is the changing the dipole moment (**Table 5.4**) and HOMO energy which further confirms that although the electronic effect is the difference in the reactivity of **C4S1** and the complexes appended with cyclic amines, the steric effects are the major contributors towards the overall reactivity hence **C4S1** > **C2S1** > **C1S1** > **C3S1**.

5.6.2 Reactivity of the Nucleophiles

Table 5.6: The p*K*_a values and the DFT-calculated NBO charges for the donor atoms of the nucleophiles (**1-MIm**, **Im**, **His** and **Pyz**) used in this study.

				
	1-MIm	Im	His	Pyz
N1	-0.437	-0.607	-0.600	-0.392
N2	-0.533	-0.529	-0.571	-0.307
N3	-	-	-0.957	-
p<i>K</i>_a	7.30	7.00	6.00	2.49

The reactivity of the metal complexes in **Table 5.1** clearly demonstrate the dependence of the chloride substitution on the nature of the nucleophile. The substitution of the chloride leaving group by the incoming nucleophile follow the trend: **1-MIm** > **Im** > **His** > **Pyz**. It has been previously reported in kinetic studies usingazole nucleophiles that the second-order rate constants for forward substitution reactions usually depends on a combination of both the electronic and steric factors of the incoming nucleophiles.^{24, 28-30} This phenomenon is typical for square-planar platinum(II) complexes. However, in this study the steric difference in features of the incoming nucleophiles did not show correlation with their reactivity towards the complexes. In fact, the most sterically hindered **His** showed a much faster reactivity compared to the less sterically hindered **Pyz** for all the platinum(II) complexes. The rate of chloride substitution showed a dependence on the electronic properties of the incoming nucleophiles with the observed reactivity trend of the nucleophiles explained in terms of the nucleophilicities associated with the pyridinic nitrogens (*) obtained from the respective p*K*_a values (**Table 5.6**). Previous studies^{24, 29-30} have also shown that the reactivity of these nucleophiles depend upon the basicity of the nitrogen-atom which

coordinates to the platinum(II) centre during the substitution process. In comparing the reactivity of theazole nucleophiles, it was found that **1-MIm** reacts faster than **Im**, **His** and **Pyz**. This trend has been previously reported^{24, 29-30} and is in line with the basicity of the nucleophiles whose pK_a values are **1-MIm** = 7.30, **Im** = 7.00, **His** = 6.00 and **Pyz** = 2.49, (**Table 5.8**).

Therefore one can conclude that the overall reactivity of all theazole nucleophiles follow the trend, **1-MIm** > **Im** > **His** > **Pyz** and is solely controlled by the basicity of the incoming nucleophile and not the steric hindrance carried by the nucleophile. In addition, the higher reactivity of **1-MIm** is associated to the inductive σ -donation of electrons by the methyl substituent present in the β -position to the reactive nitrogen(*) thereby making the nucleophilic nitrogen more reactive. Also, the side chain on the **His** has a reduced σ -inductive electron donation due to the carbonyl and amine substituents attached to the side chain therefore it is less reactive compared to the **Im** as well as **1-MIm**. The observed nucleophile reactivity is in line with the results previously found^{24, 30-31}, where the reactivity of these 5-membered nitrogen donors have been found to depend linearly on their basicity according to a linear energy relationship (LFER) of the type, $k_2 = \alpha (\text{pK}_a) + b$, where α accounts for the electronic effects and b the steric effects.

5.7 Conclusion

In this study, the effect of increasing the inductive σ -donation of the group attached at the 4'-position of the terpyridine chelate ligand on the rate of chloride substitution was investigated. The reactivity trend for the complexes under study followed the order **C4S1** > **C2S1** > **C1S1** > **C3S1**. This trend in reactivity was attributed to the inherent electronic effects (*trans*-effect) and steric effects imposed by the presence of cyclic amines. The results indicated that the introduction of a strong inductive σ -donor (cyclic amine) *trans* to the leaving group in **C1S1**, **C2S1** and **C3S1** decreases the rate of chloride substitution compared to the parent complex, **C4S1**. The σ -donor ability of the cyclic amine reduces the positive charge on the platinum(II) centre by inductively donating electrons to the terpyridine

chelate ligand. However, the σ -donor ability of the cyclic amine is only effective up to one unit regardless of the size. Beyond this point, there is no significant electronic contribution to the platinum(II) centre. Therefore, the reactivity retardation of **C2S1**, **C1S1** and **C3S1** is sterically controlled. The increase in electron density from **C2S1**, **C1S1** to **C3S1** blocks the metal centre from the incoming azole nucleophile thereby lowering the reactivity of the platinum(II) centre. The reactivity trends for the chloride substitution from complexes **C1S1**, **C2S1**, **C3S1** and **C4S1** are further supported by the DFT calculations.

The reactivity of the entering N-donor heterocyclic nucleophiles is dependent upon the basicity of the reactive pyridinic nitrogen. The substitution of the chloride leaving group by the incoming azole nucleophile follow the trend: **1-MIm** > **Im** > **His** > **Pyz**. In addition, the temperature dependent studies afforded large negative values for the entropy of activation (ΔS^\ddagger) supporting an associative type mechanism of substitution.

5.8 References

1. Suntharalingam, K.; White, A. J.; Vilar, R., *Inorganic Chemistry*, **2009**, *48* (19), 9427-9435.
2. Suntharalingam, K.; White, A. J.; Vilar, R., *Inorganic Chemistry*, **2010**, *49* (18), 8371-8380.
3. Maayan, G.; Yoo, B.; Kirshenbaum, K., *Tetrahedron Letters*, **2008**, *49* (2), 335-338.
4. Annibale, G.; Brandolisio, M.; Pitteri, B., *Polyhedron*, **1995**, *14* (3), 451-453.
5. McDermott, J. X.; White, J. F.; Whitesides, G. M., *Journal of the American Chemical Society*, **1976**, *98* (21), 6521-6528.
6. Yam, V. W. W.; Chan, K. H. Y.; Wong, K. M. C.; Chu, B. W. K., *Angewandte Chemie*, **2006**, *118* (37), 6315-6319.
7. Stang, P. J.; Cao, D. H., *Journal of the American Chemical Society*, **1994**, *116* (11), 4981-4982.
8. Ray, M.; Bhattacharya, S.; Banerjee, P., *Polyhedron*, **1999**, *18*, 1569.
9. Pitteri, B.; Bortoluzzi, M., *Polyhedron*, **2006**, *25*, 2698.
10. Pitteri, B.; Marangoni, G.; Viseutin, F. V.; Cattalini, L.; Bobbo, T., *Polyhedron*, **1997**, *17*, 475.
11. Hay, P. J.; Wadt, W. R., *Journal of Chemical Physics*, **1985**, *82* (1), 270-283.
12. Becke, A. D., *Journal of Chemical Physics*, **1986**, *84* (8), 4524-4529.
13. Becke, A. D., *Physical Review A*, **1988**, *38* (6), 3098.
14. Frisch, M. J.; Trucks, G.; Schlegel, H. B.; Scuseria, G.; Robb, M.; Cheeseman, J.; Scalmani, G.; Barone, V.; Mennucci, B.; Petersson, G., *Gaussian 09, revision A. 1. Gaussian Inc. Wallingford CT*, **2009**, *27*, 34.
15. Hofmann, A.; Jaganyi, D.; Munro, O. Q.; Liehr, G.; van Eldik, R., *Inorganic Chemistry*, **2003**, *42* (5), 1688-700.
16. Jaganyi, D.; Tiba, F.; Munro, O. Q.; Petrovic, B.; Bugarcic, Z. D., *Dalton Transactions*, **2006**, (24), 2943-9.
17. Jaganyi, D.; De Boer, K. L.; Gertenbach, J.; Perils, J., *International Journal of Chemical Kinetics*, **2008**, *40* (12), 808-818.
18. Mambanda, A.; Jaganyi, D., *Dalton Transactions*, **2011**, *40* (1), 79-91.

19. Reddy, D.; Akerman, K. J.; Akerman, M. P.; Jaganyi, D., *Transition Metal Chemistry*, **2011**, 36 (6), 593-602.
20. Shaira, A.; Jaganyi, D., *Journal of Coordination Chemistry*, **2014**, 67 (17), 2843-2857.
21. Jaganyi, D.; Reddy, D.; Gertenbach, J. A.; Hofmann, A.; van Eldik, R., *Dalton Transactions*, **2004**, (2), 299-304.
22. Lowe, G.; Droz, A. S.; Vilaivan, T.; Weaver, G. W.; Tweedale, L.; Pratt, J. M.; Rock, P.; Yardley, V.; Croft, S. L., *Journal of Medicinal Chemistry*, **1999**, 42 (6), 999-1006.
23. Lowe, G.; Droz, A. S.; Vilaivan, T.; Weaver, G. W.; Park, J. J.; Pratt, J. M.; Tweedale, L.; Kelland, L. R., *Journal of Medicinal Chemistry*, **1999**, 42 (16), 3167-3174.
24. Shaira, A.; Reddy, D.; Jaganyi, D., *Dalton Transactions*, **2013**, 42 (23), 8426-36.
25. Schmülling, M.; Ryabov, A.; van Eldik, R., *Journal of the Chemical Society, Dalton Transactions*, **1994**.
26. Papo, T. R.; Jaganyi, D., *Journal of Coordination Chemistry*, **2015**, 68 (5), 794-807.
27. Reddy, D.; Jaganyi, D., *Dalton Transactions*, **2008**, (47), 6724-31.
28. Gillham, K. J., *MSc Thesis. A Detailed Kinetic and Mechanistic Investigation into the Rate of Chloride Substitution from Chloro Terpyridine Platinum(II) and Analogous Complexes by a Series of Azole Nucleophiles, University of Natal, Pietermaritzburg, RSA*, **2010**, p. 130 - 143.
29. Papo, T. R.; Jaganyi, D., *Transition Metal Chemistry*, **2015**, 40 (1), 53-60.
30. Nkabinde, S. V.; Kinunda, G.; Jaganyi, D., *Inorganic Chim Acta.*, **2017**, 466, 298-307.

Appendix A – Synthesis Supporting Information

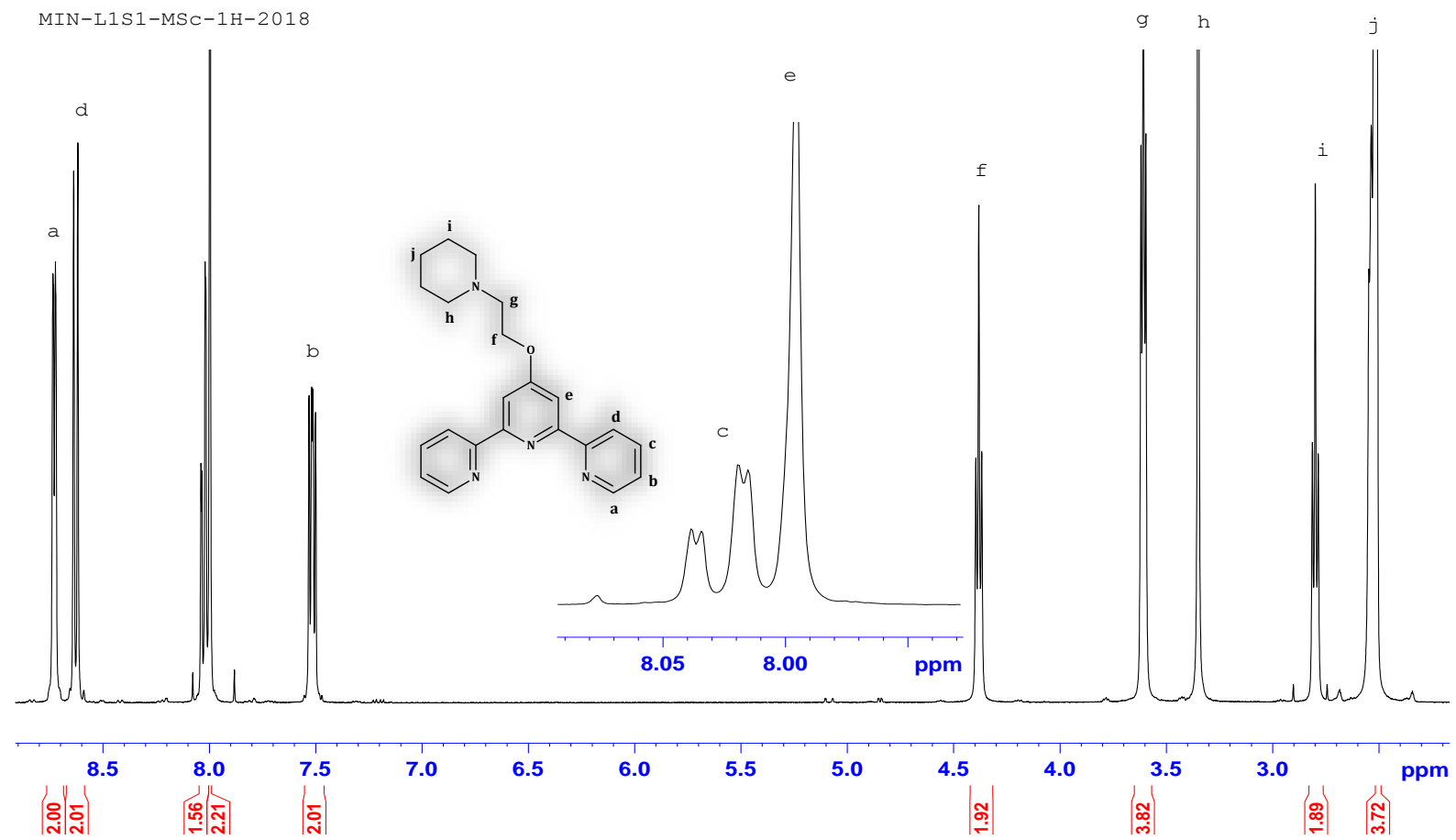


Figure A1: ^1H NMR spectrum of L1S1 recorded in deuterated dimethyl sulfoxide ($\text{DMSO-}d_6$).

MIN-L1S1-MSc-13C-2018

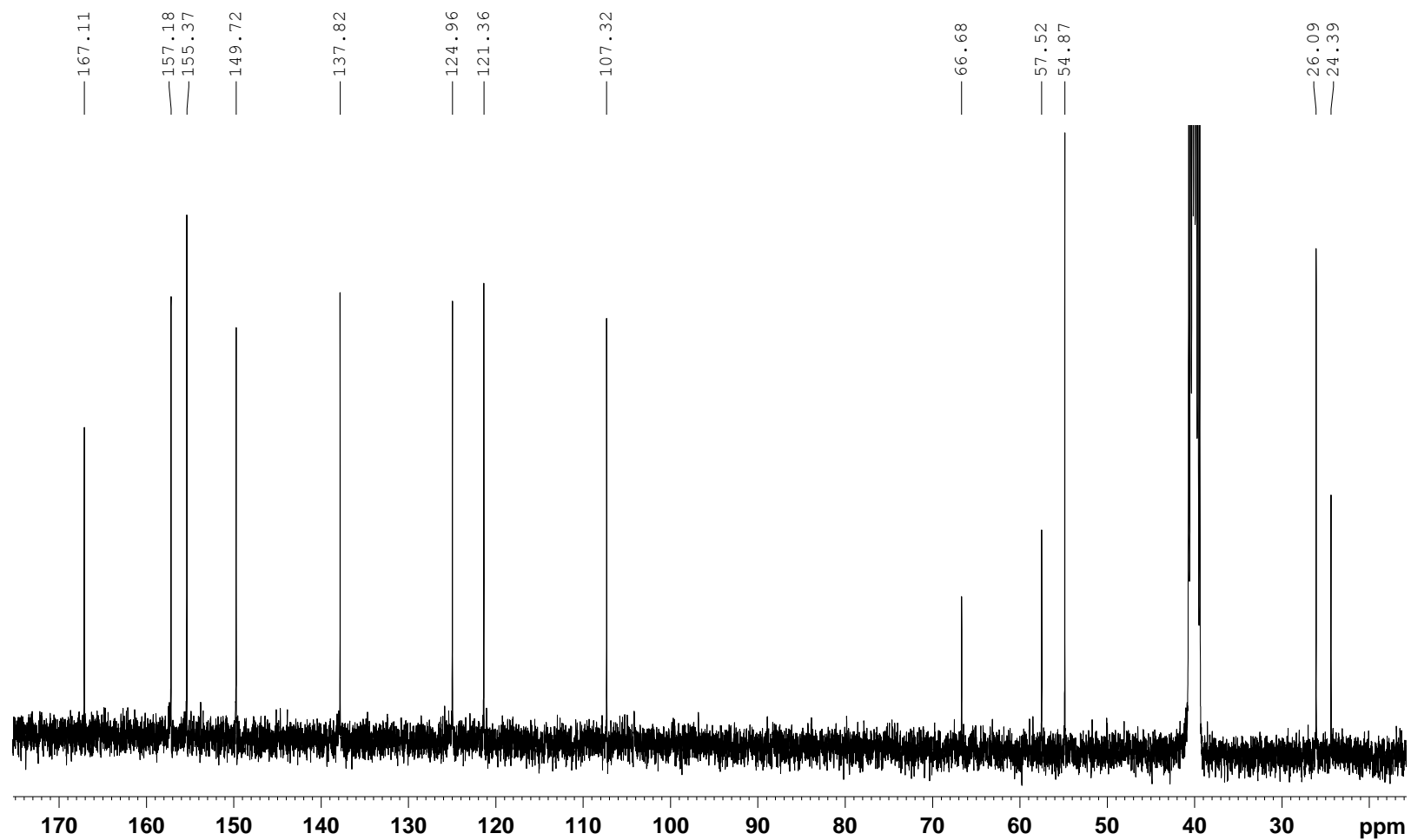


Figure A2: ^{13}C NMR spectrum of L1S1 recorded in deuterated dimethyl sulphoxide ($\text{DMSO-}d_6$).

Elemental Composition Report

Page 1

Single Mass Analysis

Tolerance = 5.0 PPM / DBE: min = -1.5, max = 100.0

Element prediction: Off

Number of isotope peaks used for i-FIT = 2

Monoisotopic Mass, Even Electron Ions

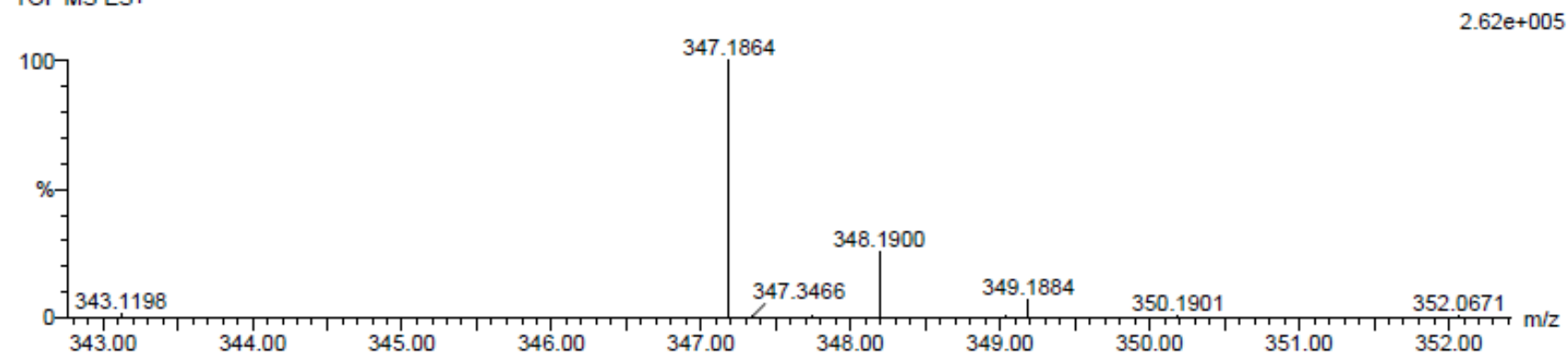
15 formula(e) evaluated with 1 results within limits (up to 20 best isotopic matches for each mass)

Elements Used:

C: 20-25 H: 20-25 N: 0-5 O: 0-5

MIN-DRCS-L1S1 34 (1.147) Cm (1:60)

TOF MS ES+



Minimum:				-1.5					
Maximum:		5.0	5.0	100.0					
Mass	Calc. Mass	mDa	PPM	DBE	i-FIT	i-FIT (Norm)	Formula		
347.1864	347.1872	-0.8	-2.3	12.5	38.4	0.0	C21	H23	N4 O

Figure A3: Mass spectrum of L1S1.

MIN-L2S1-MSc-1H-2018

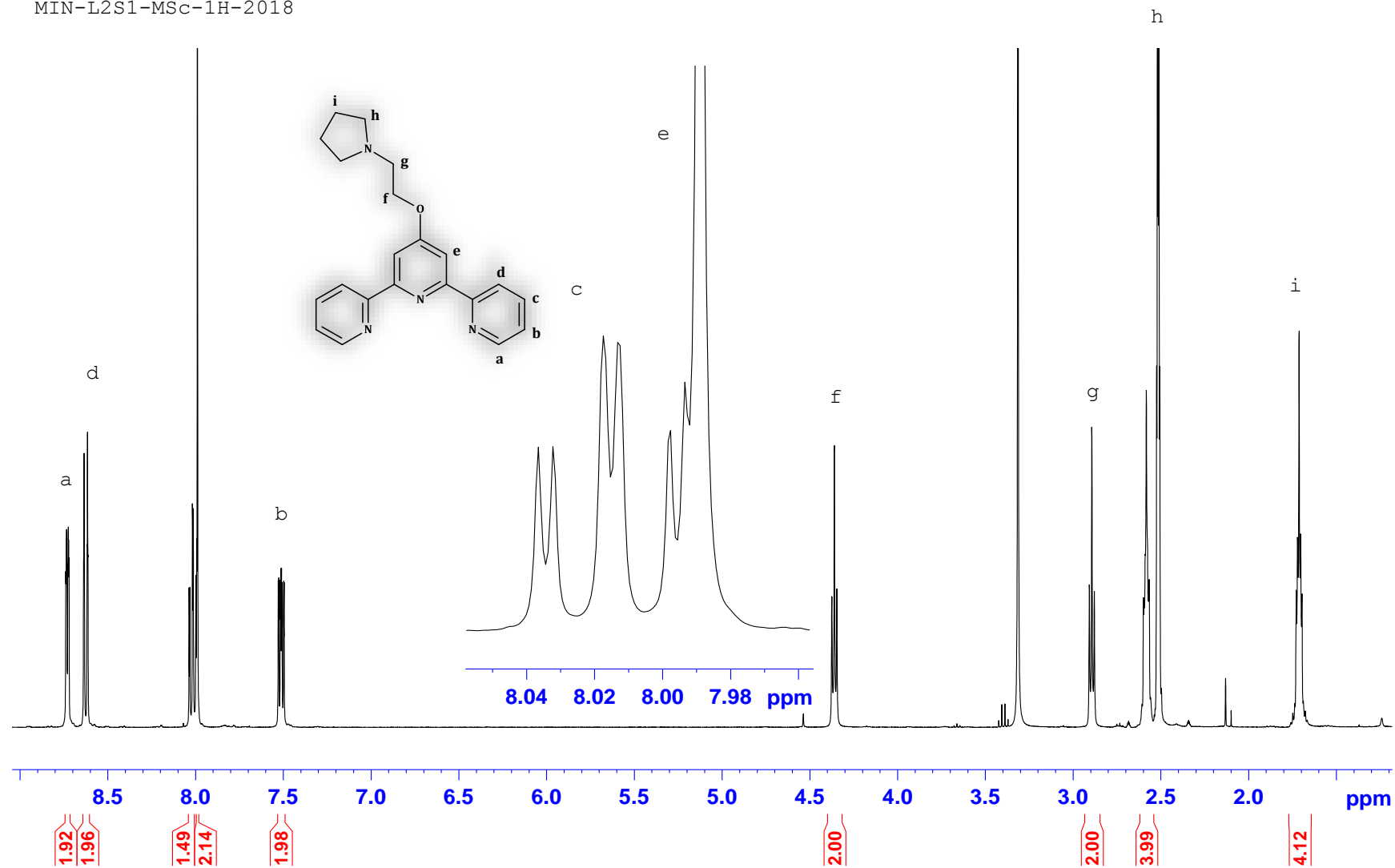


Figure A4: ¹H NMR spectrum of L2S1 recorded in deuterated dimethyl sulphoxide (DMSO-*d*₆).

MIN-L2S1-MSc-13C-2018

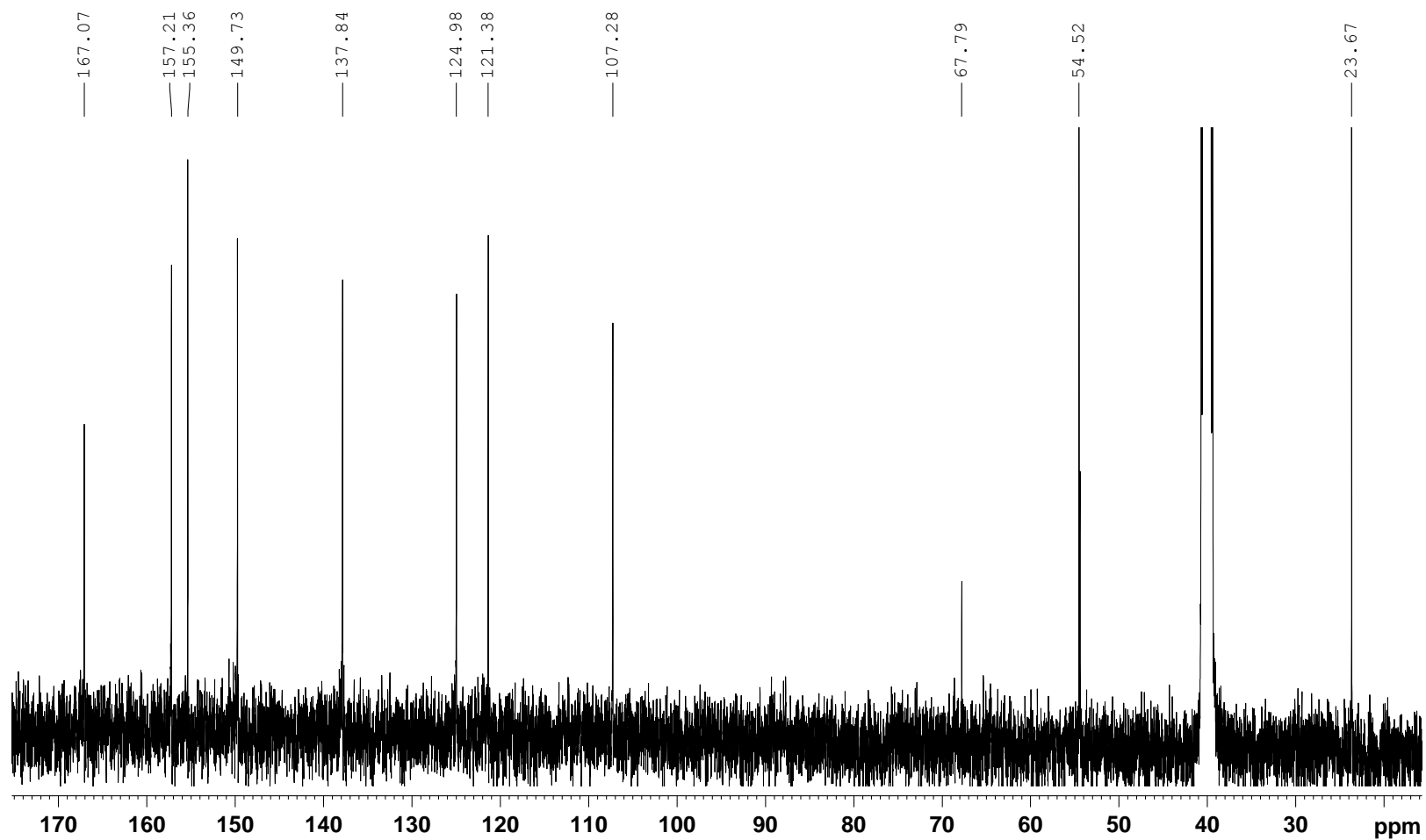


Figure A5: ^{13}C NMR spectrum of **L2S1** recorded in deuterated dimethyl sulfoxide ($\text{DMSO-}d_6$).

Elemental Composition Report

Single Mass Analysis

Tolerance = 5.0 PPM / DBE: min = -1.5, max = 100.0

Element prediction: Off

Number of isotope peaks used for i-FIT = 2

Monoisotopic Mass, Even Electron Ions

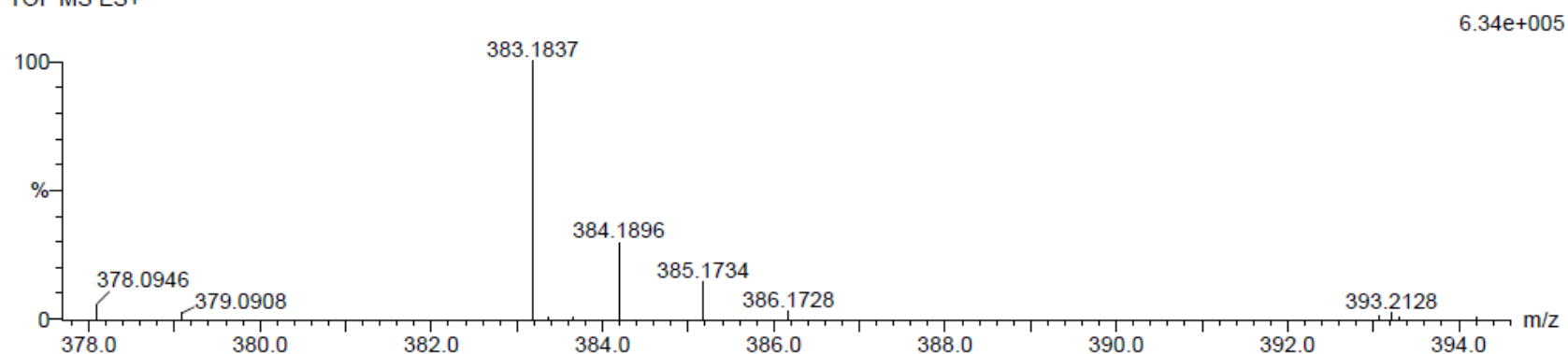
27 formula(e) evaluated with 1 results within limits (up to 20 best isotopic matches for each mass)

Elements Used:

C: 20-25 H: 20-25 N: 0-5 O: 0-5 Na: 0-1

MIN-DRCS-L2S1 13 (0.404) Cm (1:61)

TOF MS ES+



Minimum:

Maximum:

5.0 5.0 -1.5 100.0

Mass	Calc. Mass	mDa	PPM	DBE	i-FIT	i-FIT (Norm)	Formula
383.1837	383.1848	-1.1	-2.9	12.5	54.9	0.0	C22 H24 N4 O Na

Figure A6: Mass spectrum of L2S1.

MIN-L3S1-MSc-1H-2018

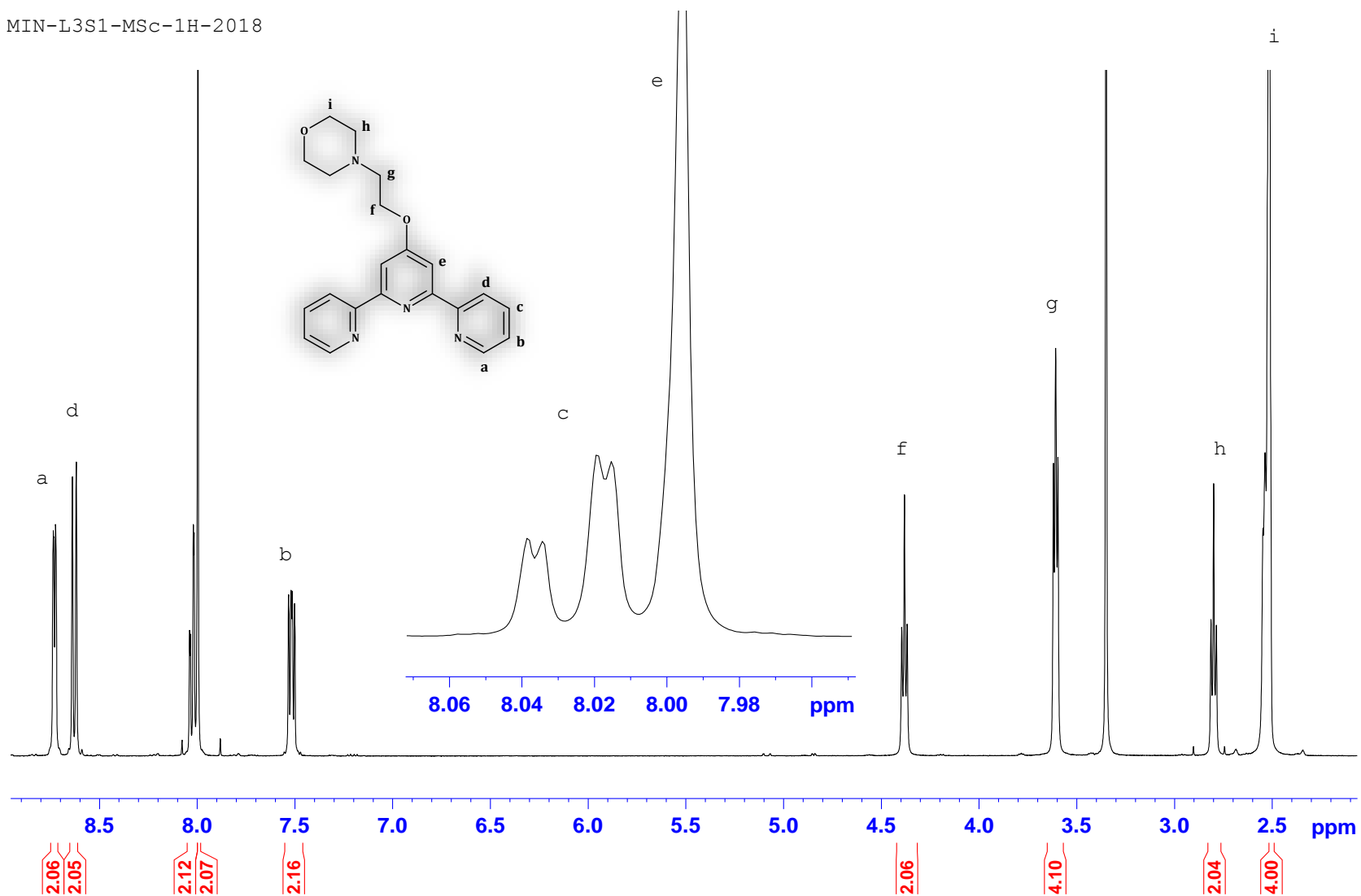


Figure A7: ^1H NMR spectrum of **L3S1** recorded in deuterated dimethyl sulphoxide ($\text{DMSO-}d_6$).

MIN-L3S1-MSc-13C-2018

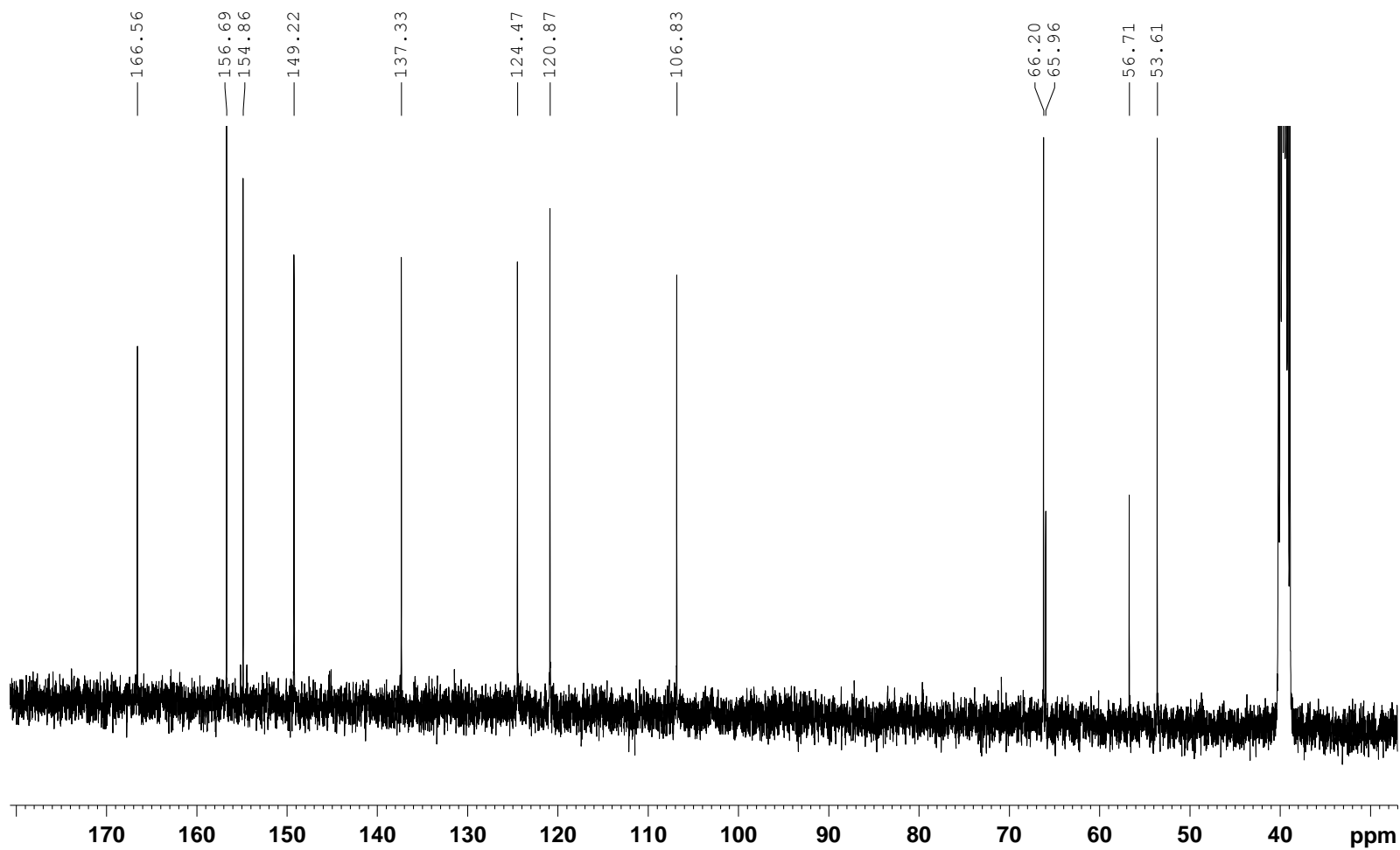


Figure A8: ^{13}C NMR spectrum of **L3S1** recorded in deuterated dimethyl sulfoxide ($\text{DMSO-}d_6$).

Elemental Composition Report

Page 1

Single Mass Analysis

Tolerance = 5.0 PPM / DBE: min = -1.5, max = 100.0

Element prediction: Off

Number of isotope peaks used for i-FIT = 2

Monoisotopic Mass, Even Electron Ions

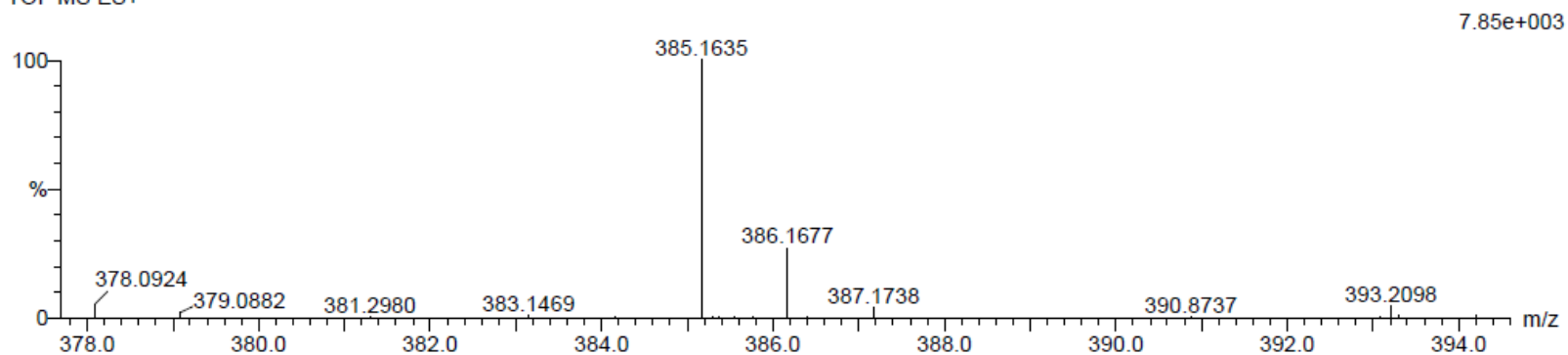
25 formula(e) evaluated with 1 results within limits (up to 20 best isotopic matches for each mass)

Elements Used:

C: 20-25 H: 20-25 N: 0-5 O: 0-5 Na: 0-1

MIN-DRCS-L3S1 4 (0.135)

TOF MS ES+



Minimum:				-1.5						
Maximum:		5.0	5.0	100.0						
Mass	Calc. Mass	mDa	PPM	DBE	i-FIT	i-FIT (Norm)	Formula			
385.1635	385.1640	-0.5	-1.3	12.5	44.4	0.0	C21	H22	N4	O2 Na

Figure A9: Mass spectrum of L2S1.

MIN-L4S1-MS_C-1H-2018

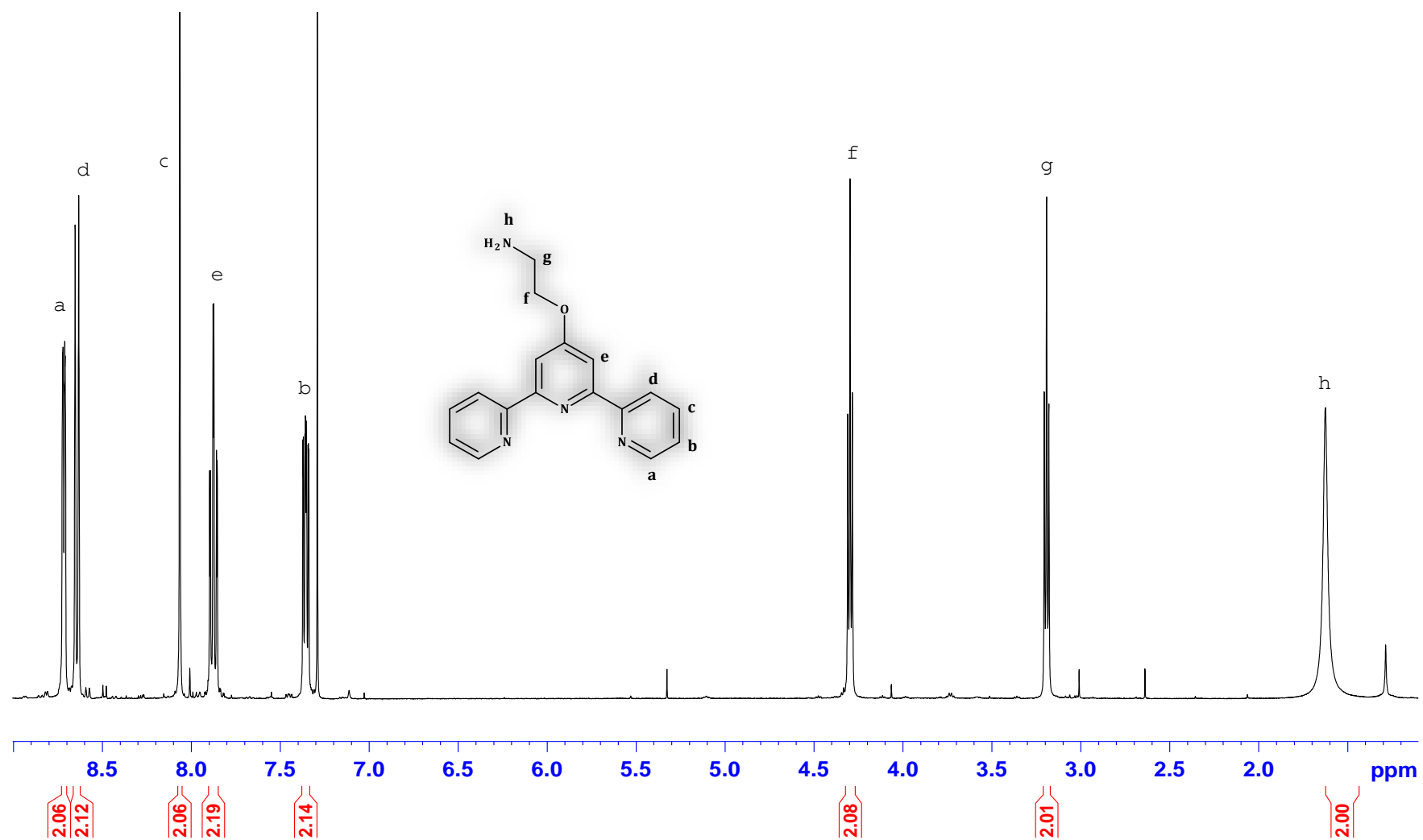


Figure A10: ¹H NMR spectrum of L4S1 recorded in deuterated chloroform (CDCl₃)

MIN-L4S1-MSc-13C-2018

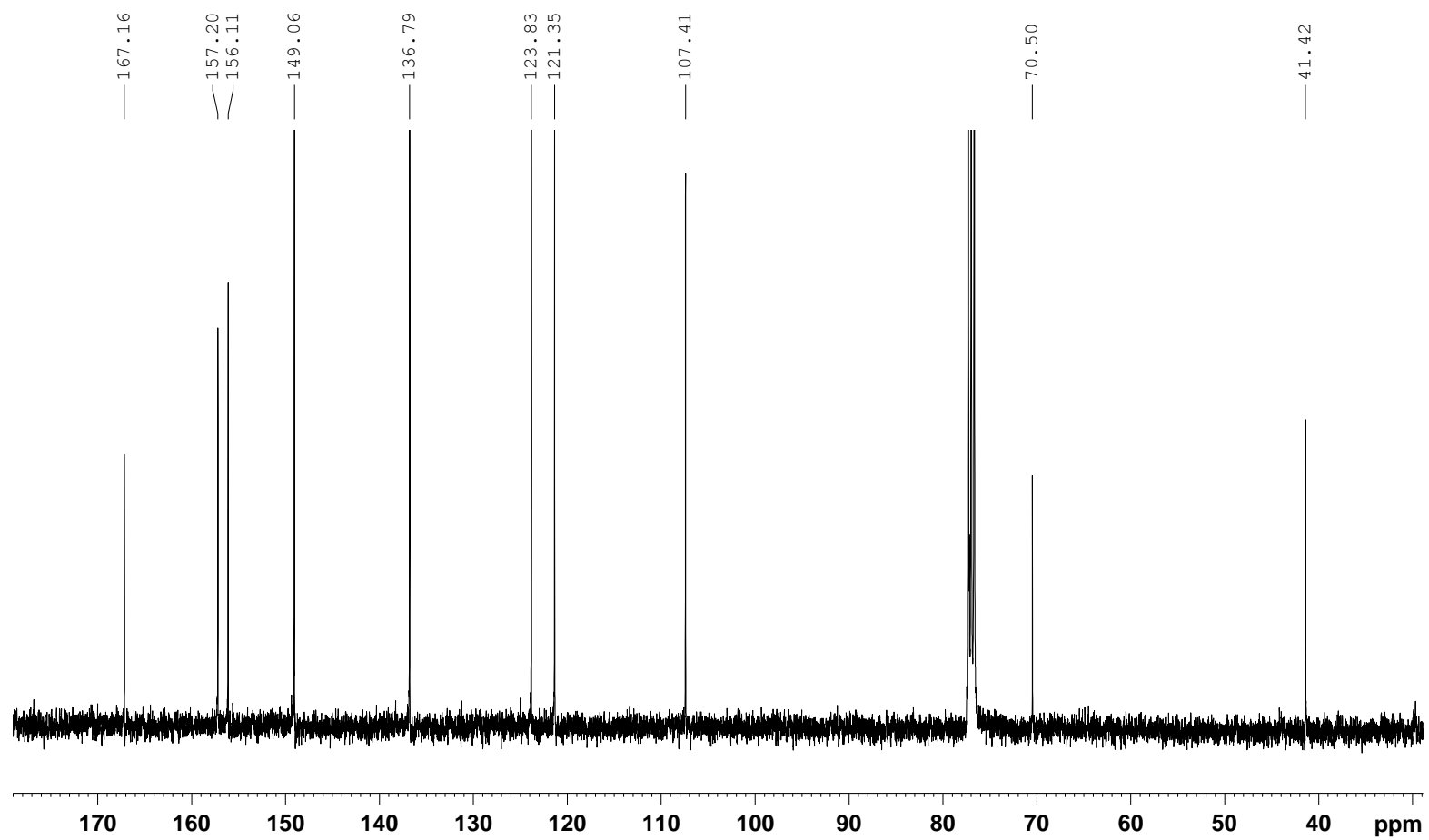


Figure A11: ^{13}C NMR spectrum of **L4S1** recorded in deuterated chloroform (CDCl_3).

Elemental Composition Report

Single Mass Analysis

Tolerance = 5.0 PPM / DBE: min = -1.5, max = 100.0

Element prediction: Off

Number of isotope peaks used for i-FIT = 2

Monoisotopic Mass, Even Electron Ions

15 formula(e) evaluated with 1 results within limits (up to 20 best isotopic matches for each mass)

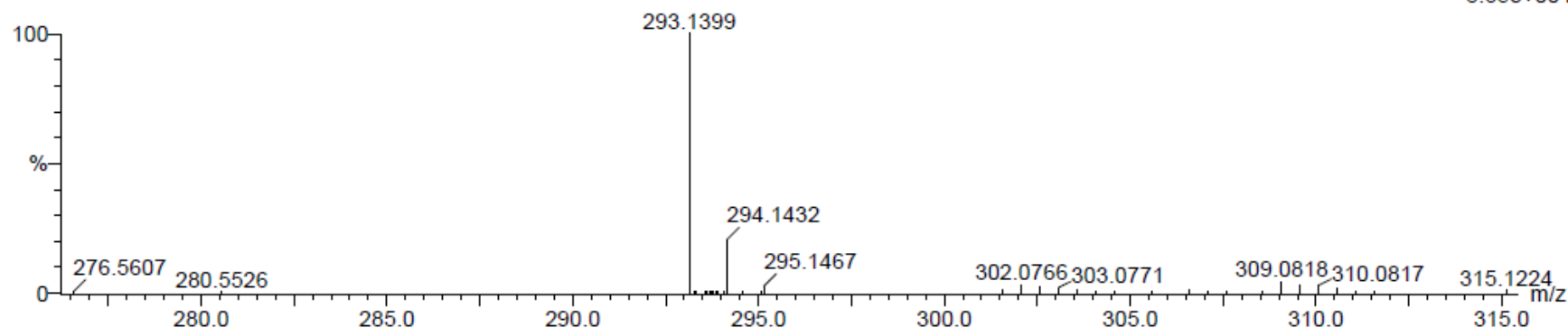
Elements Used:

C: 15-20 H: 15-20 N: 0-5 O: 0-5

MIN-L4S1-MSc2017 17 (0.540) Cm (1:61)

TOF MS ES+

8.65e+004



Minimum: -1.5
Maximum: 5.0 5.0 100.0

Mass	Calc. Mass	mDa	PPM	DBE	i-FIT	i-FIT (Norm)	Formula
293.1399	293.1402	-0.3	-1.0	11.5	138.2	0.0	C17 H17 N4 O

Figure A12: Mass spectrum of L4S1.

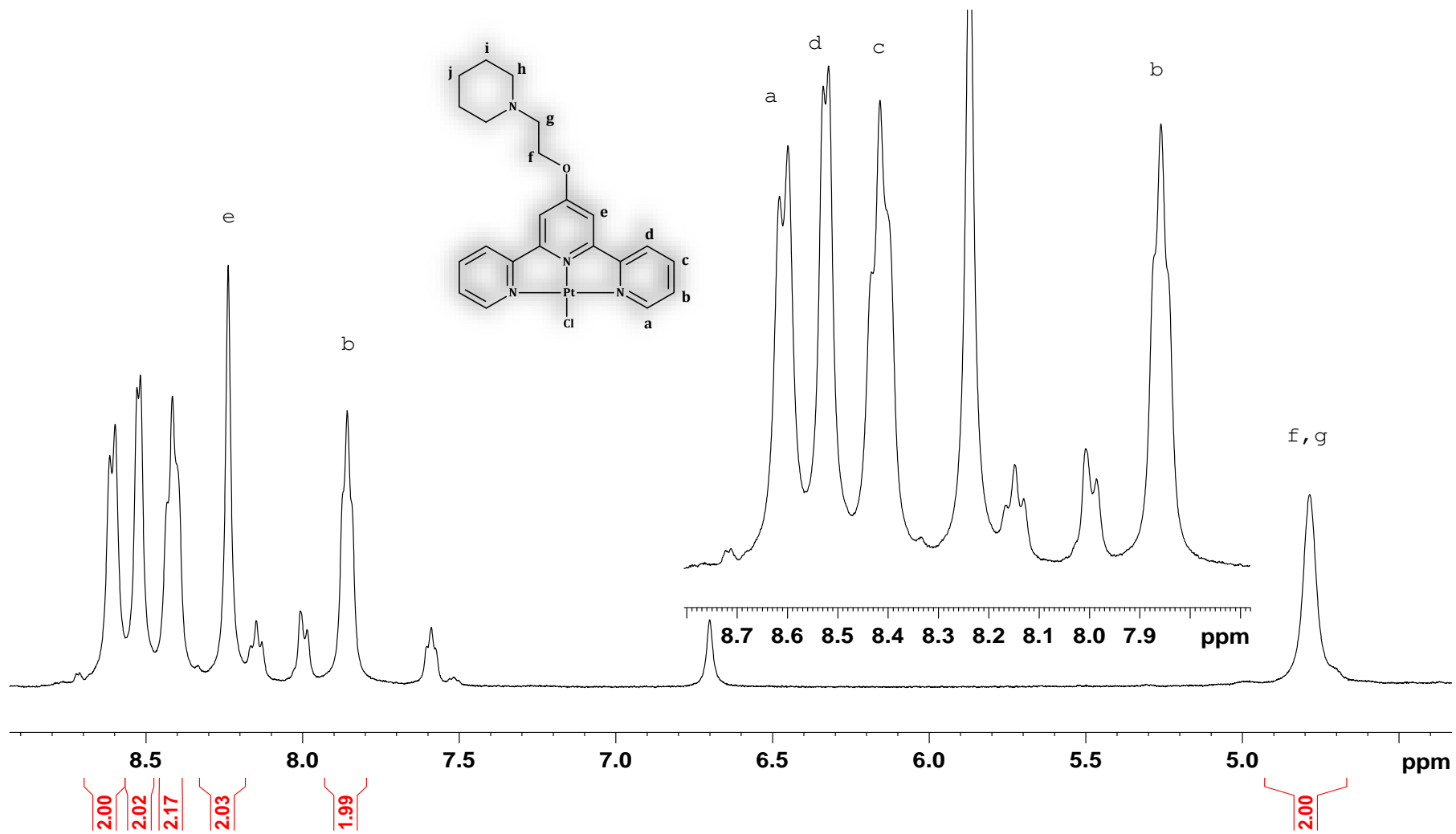


Figure A13: ¹H NMR spectrum of **C1S1** recorded in deuterated dimethyl sulfoxide (DMSO-*d*₆).

Elemental Composition Report

Single Mass Analysis

Tolerance = 5.0 PPM / DBE: min = -1.5, max = 500.0

Element prediction: Off

Number of isotope peaks used for i-FIT = 2

Monoisotopic Mass, Even Electron Ions

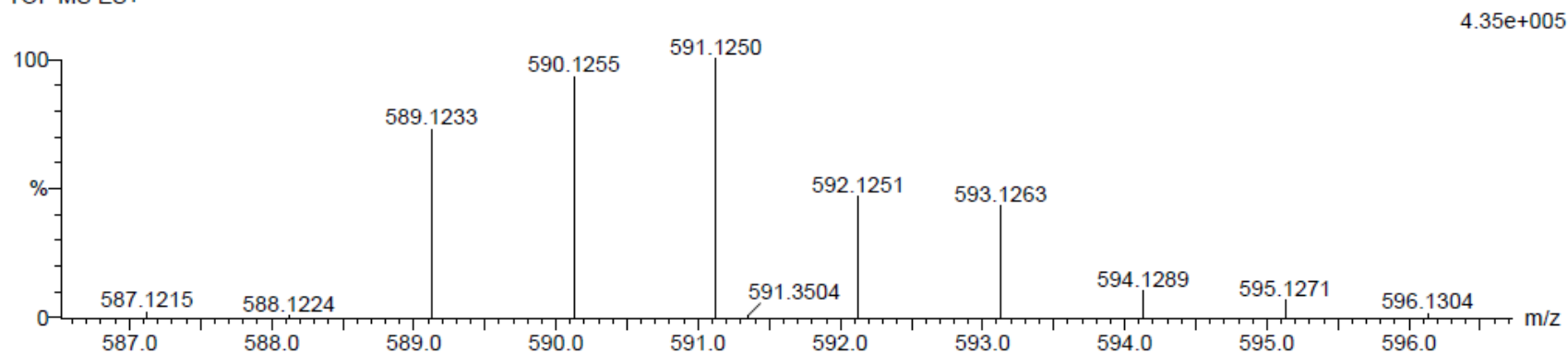
48 formula(e) evaluated with 1 results within limits (up to 20 closest results for each mass)

Elements Used:

C: 20-25 H: 20-25 N: 0-5 O: 0-5 37Cl: 1-1 194Pt: 0-1

MIN-C1S1-COD-DMSO 37 (1.215) Cm (1:61)

TOF MS ES+



Minimum:

Maximum: 5.0 5.0 -1.5 500.0

Mass	Calc. Mass	mDa	PPM	DBE	i-FIT	i-FIT (Norm)	Formula
591.1250	591.1236	1.4	2.4	13.5	42.2	0.0	C22 H24 N4 O 37Cl 194Pt

Figure A14: Mass spectrum of C1S1.

MIN-C2S1-MSc-1H-2018

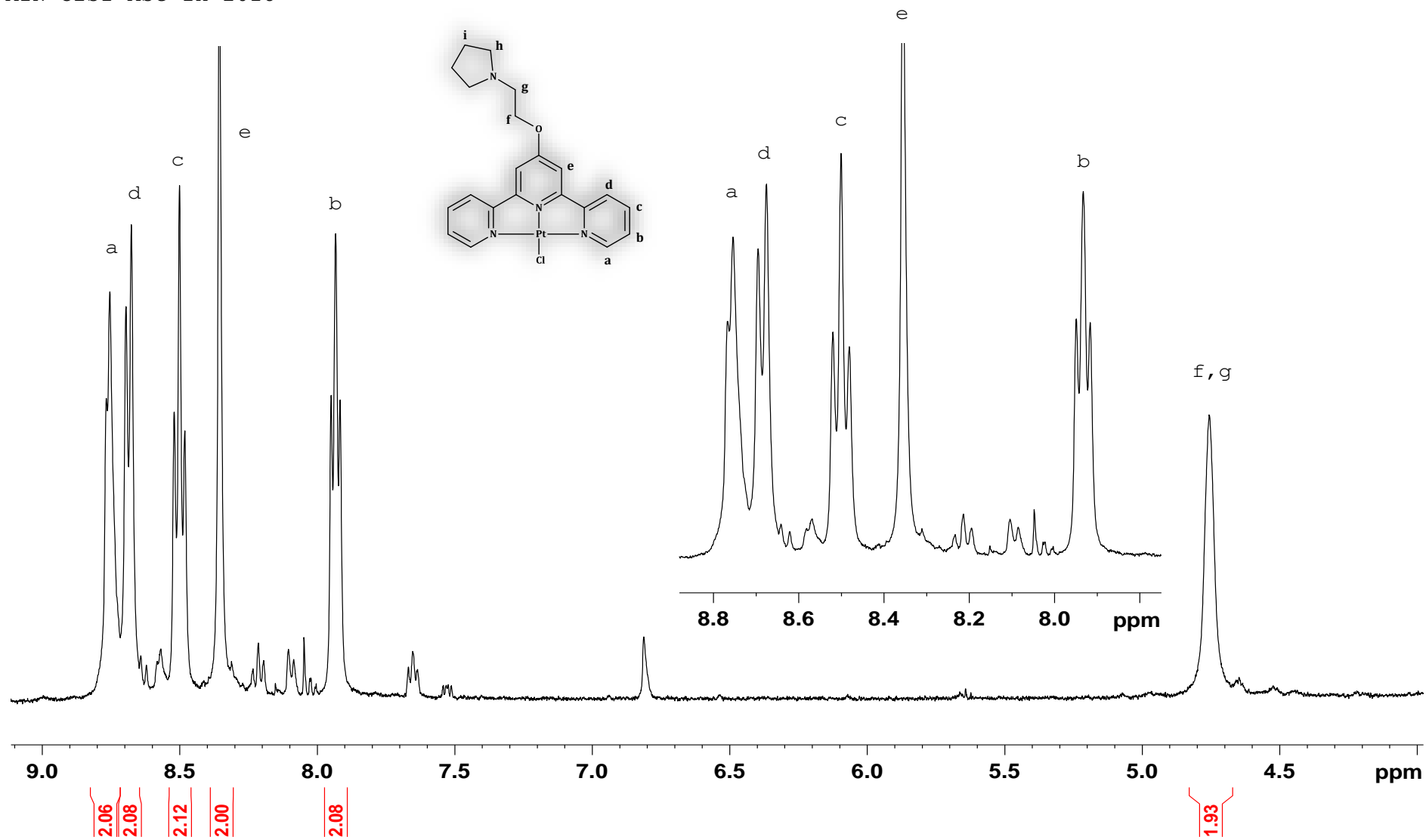


Figure A15: ¹H NMR spectrum of C2S1 recorded in deuterated dimethyl sulphoxide (DMSO-d₆).

Elemental Composition Report

Single Mass Analysis

Tolerance = 5.0 PPM / DBE: min = -1.5, max = 500.0

Element prediction: Off

Number of isotope peaks used for i-FIT = 2

Monoisotopic Mass, Even Electron Ions

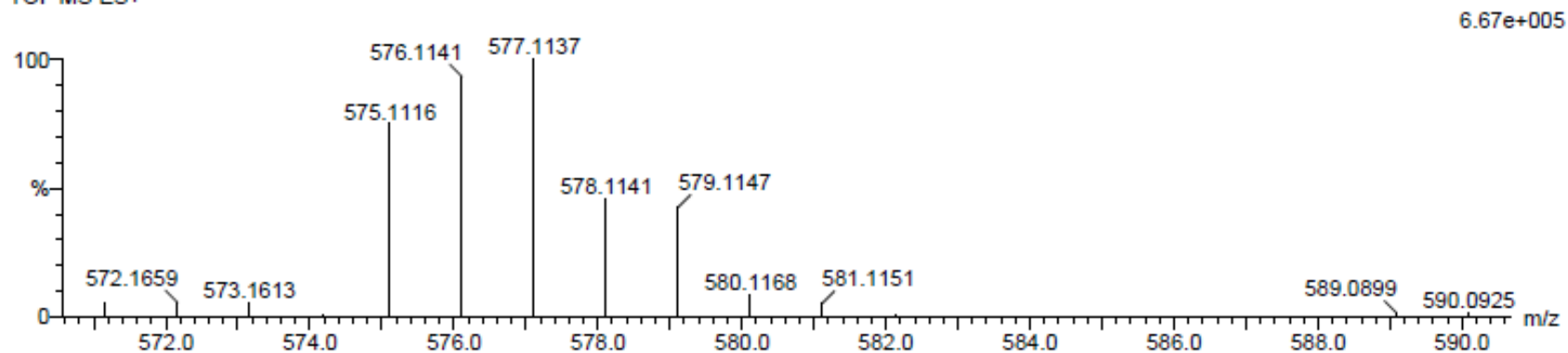
102 formula(e) evaluated with 1 results within limits (up to 20 closest results for each mass)

Elements Used:

C: 20-25 H: 20-25 N: 0-5 O: 0-5 Cl: 0-1 194Pt: 0-1

MIN-C2S1-COD 27 (0.877) Cm (1:61)

TOF MS ES+



Minimum:				-1.5					
Maximum:		5.0	5.0	500.0					
Mass	Calc. Mass	mDa	PPM	DBE	i-FIT	i-FIT (Norm)	Formula		
575.1116	575.1109	0.7	1.2	13.5	28.1	0.0	C21	H22	N4 O Cl 194Pt

Figure A16: Mass spectrum of C2S1.

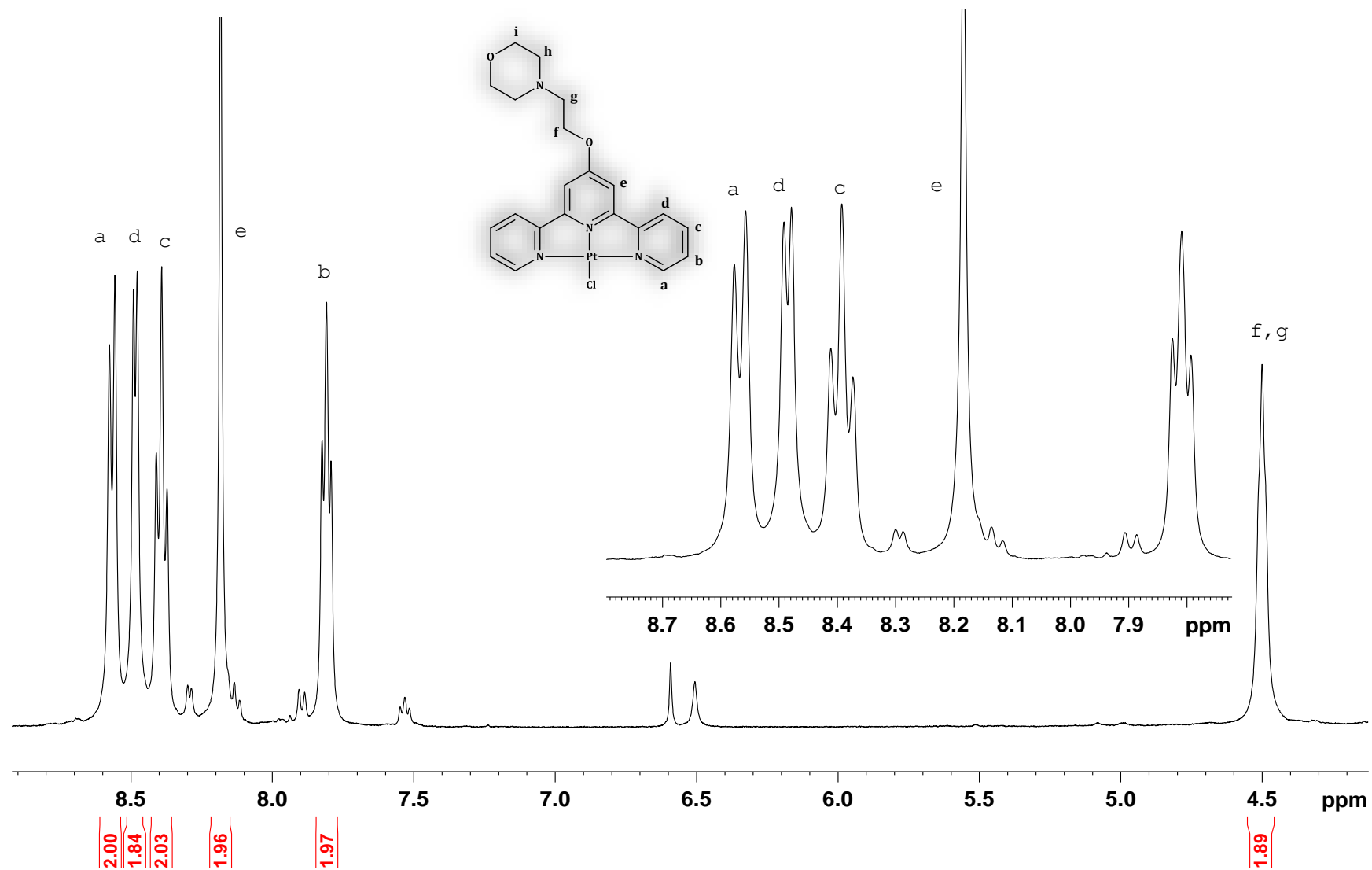


Figure A17: ^1H NMR spectrum of **C3S1** recorded in deuterated dimethyl sulphoxide ($\text{DMSO-}d_6$).

MIN-C3S1-MSc-13C-2018

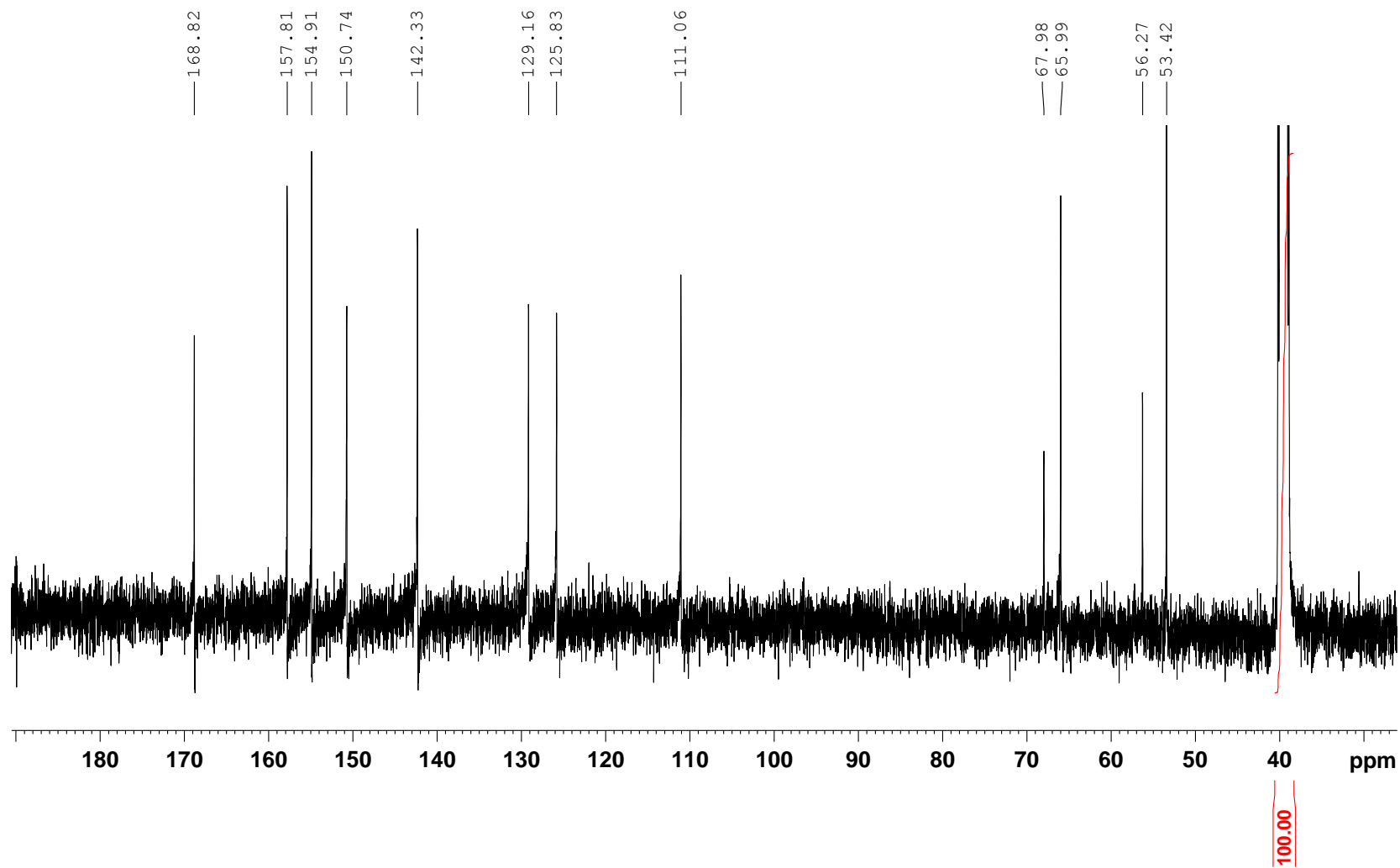


Figure A18: ^{13}C NMR spectrum of **C3S1** recorded in deuterated dimethyl sulfoxide ($\text{DMSO-}d_6$).

Elemental Composition Report

Single Mass Analysis

Tolerance = 5.0 PPM / DBE: min = -1.5, max = 50.0

Element prediction: Off

Number of isotope peaks used for i-FIT = 2

Monoisotopic Mass, Even Electron Ions

98 formula(e) evaluated with 1 results within limits (up to 20 closest results for each mass)

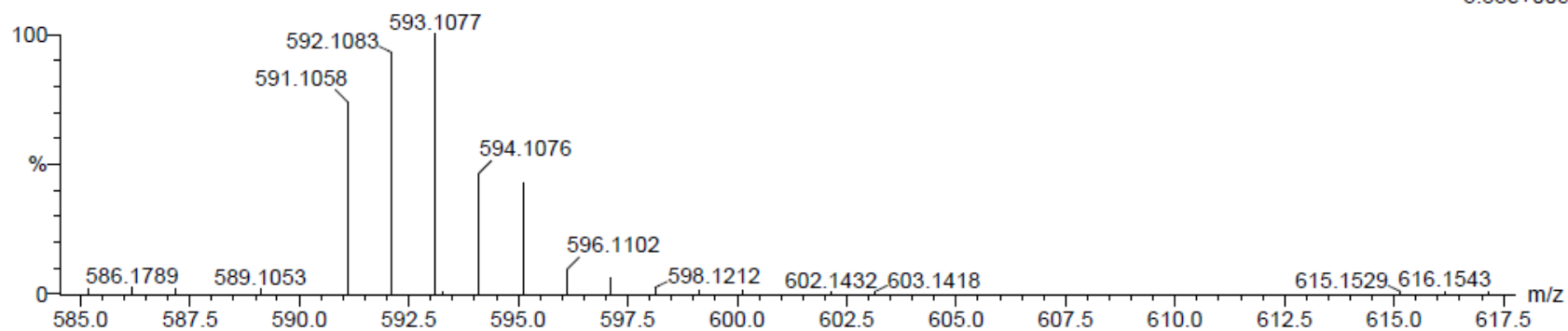
Elements Used:

C: 20-25 H: 20-25 N: 0-5 O: 0-5 Cl: 0-1 196Pt: 0-1

MIN-COOMorp-dmso 37 (1.214) Cm (1:61)

TOF MS ES+

3.83e+005



Minimum: -1.5
Maximum: 5.0 5.0 50.0

Mass	Calc. Mass	mDa	PPM	DBE	i-FIT	i-FIT (Norm)	Formula
593.1077	593.1081	-0.4	-0.7	13.5	42.3	0.0	C21 H22 N4 O2 Cl 196Pt

Figure A19: Mass spectrum of C3S1.

MIN-C4S1-MSc-1H-2018

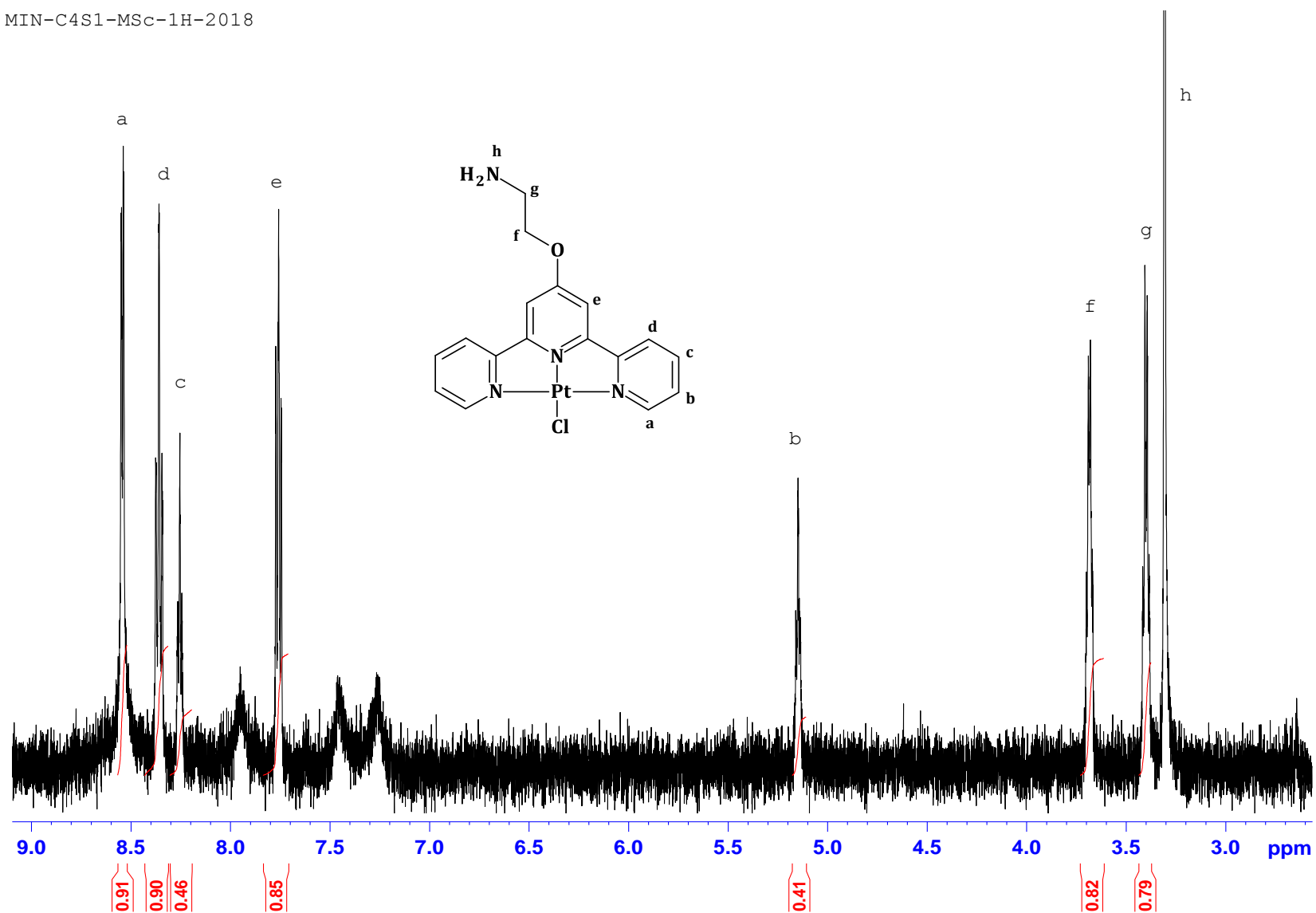


Figure A20: ¹H NMR spectrum of C4S1 recorded in deuterated dimethyl sulphoxide (DMSO-*d*₆).

Elemental Composition Report

Single Mass Analysis

Tolerance = 5.0 PPM / DBE: min = -1.5, max = 100.0

Element prediction: Off

Number of isotope peaks used for i-FIT = 2

Monoisotopic Mass, Even Electron Ions

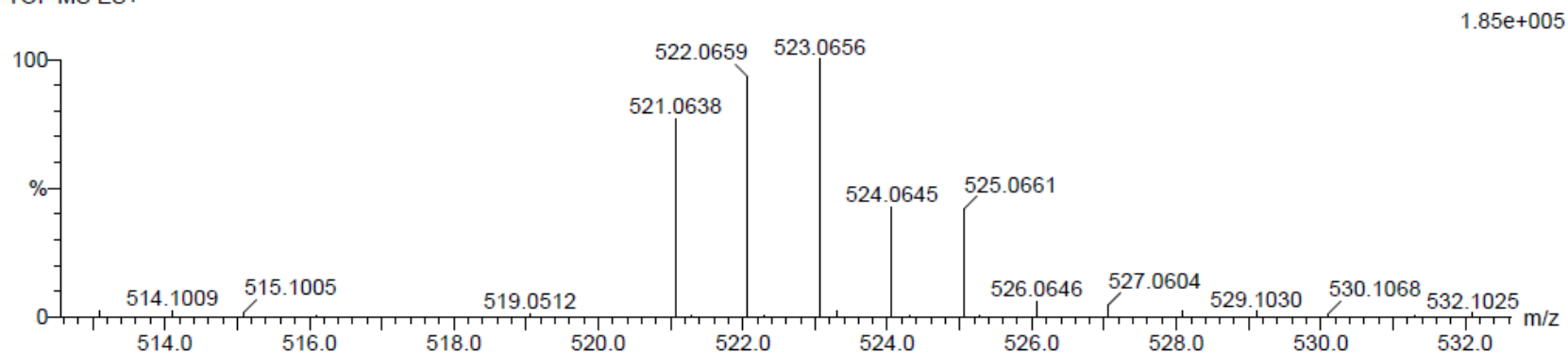
84 formula(e) evaluated with 1 results within limits (up to 20 best isotopic matches for each mass)

Elements Used:

C: 15-20 H: 15-20 N: 1-5 O: 0-5 Cl: 0-1 Pt: 0-1

MIN-C4S1-2P-DMSO 60 (1.990) Cm (1:61)

TOF MS ES+



Minimum:

-1.5

Maximum:

5.0

5.0

100.0

Mass	Calc. Mass	mDa	PPM	DBE	i-FIT	i-FIT (Norm)	Formula
------	------------	-----	-----	-----	-------	--------------	---------

522.0659	522.0660	-0.1	-0.2	12.5	90.7	0.0	C17 H16 N4 O Cl Pt
----------	----------	------	------	------	------	-----	--------------------

Figure A21: Mass spectrum of C4S1.

Appendix B - Kinetic and Thermodynamic Data

Table B1: Summary of selected wavelengths (nm) for the kinetic studies.

Complex	Incoming Nucleophile (Nu)			
	Im	1-MIm	Pyz	Histidine
C1S1	390	390	390	390
C2S1	390	390	390	390
C3S1	390	390	355	390
C4S1	380	380	454	380

Table B2: The averaged rate constants ($k_{\text{obs}}/\text{s}^{-1}$) for the substitution reaction of **C1S1** (5×10^{-4} M) withazole nucleophiles at various concentrations at 298.15K.

Nucleophile Concentration/mM	$k_{\text{obs}}/\text{s}^{-1}$			
	[Im]	[1-MIm]	[Pyz]	[His]
0.0025	0.004334	0.006695	0.001149	0.001951
0.0050	0.008870	0.012212	0.001881	0.003771
0.0075	0.012424	0.019060	0.002608	0.006145
0.0100	0.016801	0.026366	0.003206	0.007500
0.0125	0.021670	0.031520	0.003801	0.009233

Table B3: The averaged rate constants ($k_{\text{obs}}/\text{s}^{-1}$) for the substitution reaction of **C2S1** (5×10^{-4} M) withazole nucleophiles at various concentrations at 298.15K.

Nucleophile Concentration/mM	$k_{\text{obs}}/\text{s}^{-1}$			
	[Im]	[1-MIm]	[Pyz]	[His]
0.0025	0.009590	0.007500	0.001236	0.002455
0.0050	0.013075	0.015494	0.001980	0.004659
0.0075	0.017500	0.021565	0.002658	0.007015
0.0100	0.021650	0.029021	0.003272	0.008906
0.0125	0.026090	0.035620	0.003974	0.011330

Table B4: The averaged rate constants (k_{obs}/s^{-1}) for the substitution reaction of **C3S1 (5 x10⁻⁴ M)** with azole nucleophiles at various concentrations at 298.15K.

Nucleophile Concentration/mM	k_{obs}/s^{-1}			
	[Im]	[1-MIm]	[Pyz]	[His]
0.0025	0.003561	0.003930	0.001644	0.001167
0.0050	0.006242	0.006681	0.002416	0.002292
0.0075	0.008898	0.009792	0.003587	0.003409
0.0100	0.011273	0.013179	0.004431	0.004921
0.0125	0.013986	0.016310	0.005488	0.006122

Table B5: The averaged rate constants (k_{obs}/s^{-1}) for the substitution reaction of **C4S1 (5 x10⁻⁴ M)** with azole nucleophiles at various concentrations at 298.15K.

Nucleophile Concentration/mM	k_{obs}/s^{-1}			
	[Im]	[1-MIm]	[Pyz]	[His]
0.0025	0.008387	0.01019	0.0006566	0.0057091
0.0050	0.017450	0.01984	0.0009862	0.0118875
0.0075	0.024568	0.02760	0.0012643	0.0184071
0.0100	0.032515	0.03720	0.0015788	0.0264278
0.0125	0.041371	0.04822	0.0018793	0.0315611

Table B6: The averaged rate constants (k_{obs}/s^{-1}) for the substitution reaction of **C1S1 (5 x10⁻⁴ M)** with azole nucleophiles (7.5 x10⁻³ M) at different temperatures ranging between, **283.15 – 313.15 K**.

Temperature/K	k_{obs}/s^{-1} obtained at different temperatures			
	[Im]	[1-MIm]	[Pyz]	[His]
283.15	-	-	-	-
288.15	0.0045707	0.005938	0.001266	0.0031951
293.15	0.0079034	0.009128	0.001909	0.0043410
298.15	0.0124240	0.019060	0.002608	0.0061450

303.15	0.0182340	0.033140	0.003875	0.0079630
313.15	0.0247500	0.138550	0.007235	0.0104610

Table B7: The averaged rate constants ($k_{\text{obs}}/\text{s}^{-1}$) for the substitution reaction of **C2S1** ($5 \times 10^{-4} \text{ M}$) with azole nucleophiles ($7.5 \times 10^{-3} \text{ M}$) at different temperatures ranging between, **283.15 – 313.15 K**.

Temperature/K	$k_{\text{obs}}/\text{s}^{-1}$ obtained at different temperatures			
	[Im]	[1-MIm]	[Pyz]	[His]
283.15	-	-	-	-
288.15	0.007734	0.006614	0.000974	0.003486
293.15	0.012804	0.010583	0.001488	0.004890
298.15	0.021506	0.01859	0.002658	0.006515
303.15	0.244650	0.02984	0.003116	0.008426
313.15	0.142080	0.13446	0.004682	0.010603

Table B8: The averaged rate constants ($k_{\text{obs}}/\text{s}^{-1}$) for the substitution reaction of **C3S1** ($5 \times 10^{-4} \text{ M}$) with azole nucleophiles ($7.5 \times 10^{-3} \text{ M}$) at different temperatures ranging between, **283.15 – 313.15 K**.

Temperature/K	$k_{\text{obs}}/\text{s}^{-1}$ obtained at different temperatures			
	[Im]	[1-MIm]	[Pyz]	[His]
283.15	0.002027	0.002354	0.000612	-
288.15	0.003297	0.003662	0.000974	0.001480
293.15	0.005485	0.006169	0.001652	0.002292
298.15	0.008898	0.018116	0.002776	0.003409
303.15	0.015516	0.178741	0.004255	0.005273
313.15	-	-	-	0.007304

Table B9: The averaged rate constants ($k_{\text{obs}}/\text{s}^{-1}$) for the substitution reaction of **C4S1** ($5 \times 10^{-4} \text{ M}$) with azole nucleophiles ($7.5 \times 10^{-3} \text{ M}$) at different temperatures ranging between, **283.15 – 313.15 K**.

Temperature/K	$k_{\text{obs}}/\text{s}^{-1}$ obtained at different temperatures			
---------------	---	--	--	--

	[Im]	[1-MIm]	[Pyz]	[His]
283.15	-	-	0.0002483	-
288.15	0.009911	0.0016129	0.0004461	0.0077076
293.15	0.013496	0.0029601	0.0008045	0.0110312
298.15	0.024568	0.0043719	0.0012643	0.0184071
303.15	0.039177	0.0056224	0.0022680	0.0253061
313.15	0.087659	0.0091309	-	0.0524817

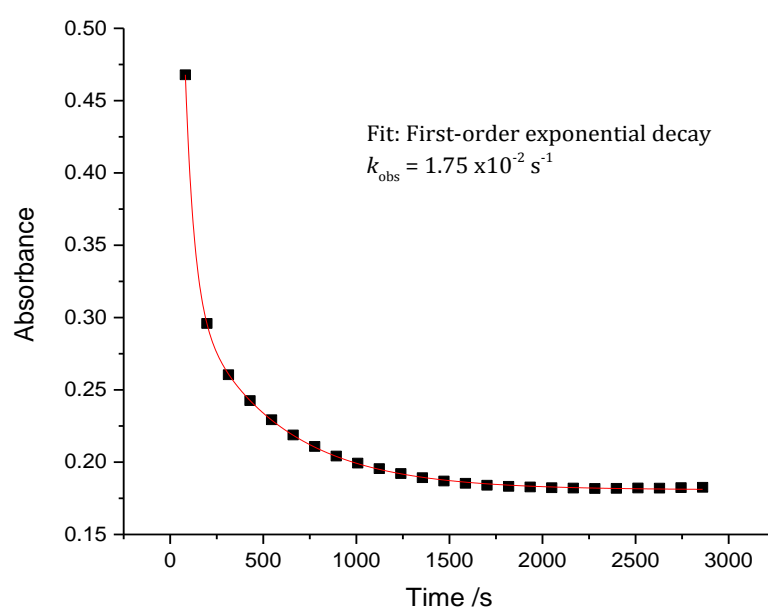


Figure B1: Absorbance spectrum of **C2S1** (2.5×10^{-4} M) and **Im** (5.0×10^{-3} M (30 fold)) obtained from Cary UV/Visible Spectrophotometry in ultrapure water ($I = 0.01$ M, 0.009 M LiCF_3SO_3 + 0.001 M LiCl) at 298.15 K.

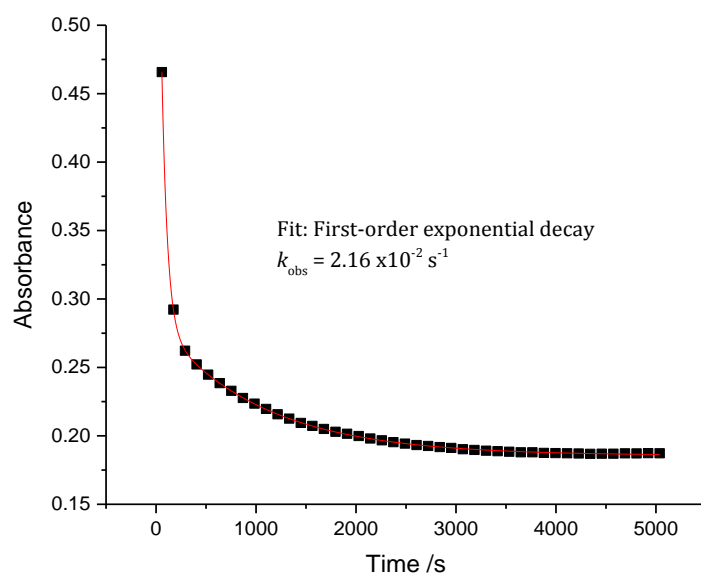


Figure B2: Absorbance spectrum of **C2S1** ($2.5 \times 10^{-4} \text{ M}$) and **1-MIm** ($5.0 \times 10^{-3} \text{ M}$ (30 fold)) obtained from Cary UV/Visible Spectrophotometry in ultrapure water ($I = 0.01 \text{ M}$, $0.009 \text{ M LiCF}_3\text{SO}_3 + 0.001 \text{ M LiCl}$) 298.15 K.

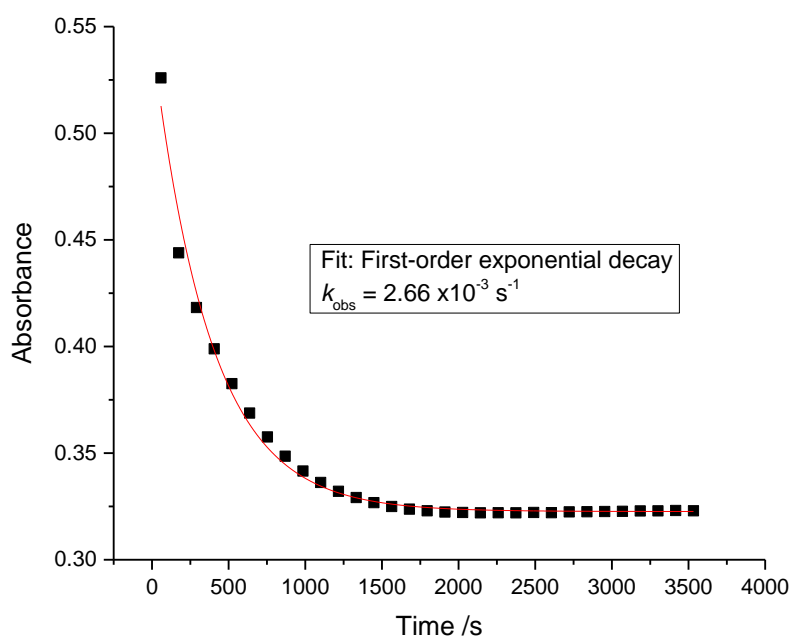


Figure B3: Absorbance spectrum of **C2S1** ($2.5 \times 10^{-4} \text{ M}$) and **Pyz** ($5.0 \times 10^{-3} \text{ M}$ (30 fold)) obtained from Cary UV/Visible Spectrophotometry in ultrapure water ($I = 0.01 \text{ M}$, $0.009 \text{ M LiCF}_3\text{SO}_3 + 0.001 \text{ M LiCl}$) 298.15 K.

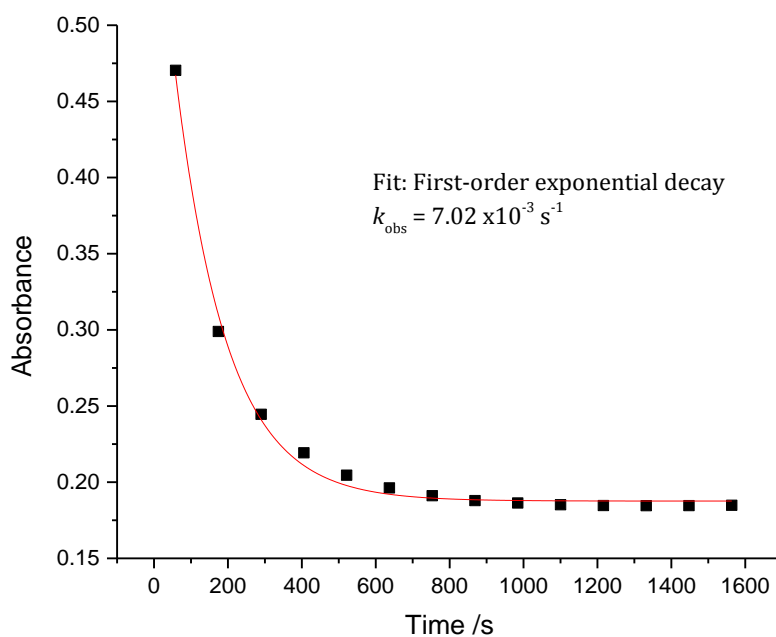


Figure B4: Absorbance spectrum of **C2S1** (2.5×10^{-4} M) and **His** (5.0×10^{-3} M (30 fold)) obtained from Cary UV/Visible Spectrophotometry in ultrapure water ($I = 0.01$ M, 0.009 M LiCF_3SO_3 + 0.001 M LiCl) 298.15 K.

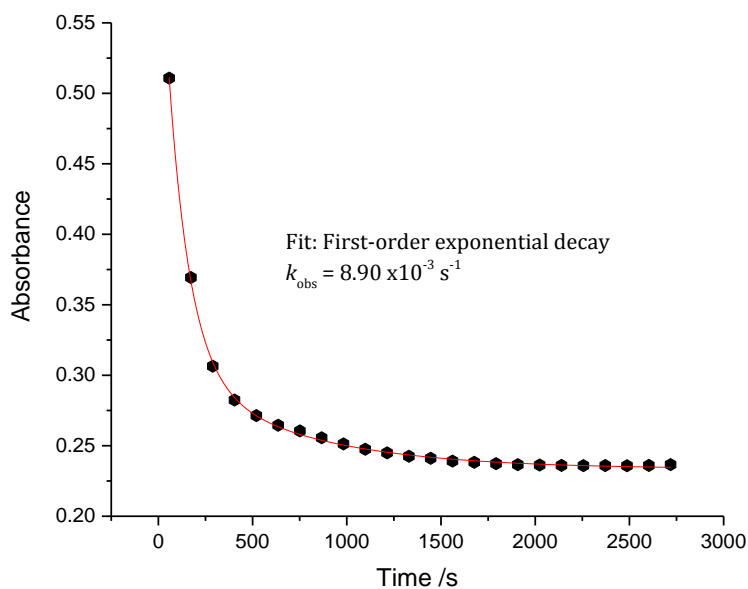


Figure B5: Absorbance spectrum of **C3S1** (2.5×10^{-4} M) and **Im** (5.0×10^{-3} M (30 fold)) obtained from Cary UV/Visible Spectrophotometry in ultrapure water ($I = 0.01$ M, 0.009 M LiCF_3SO_3 + 0.001 M LiCl) 298.15 K.

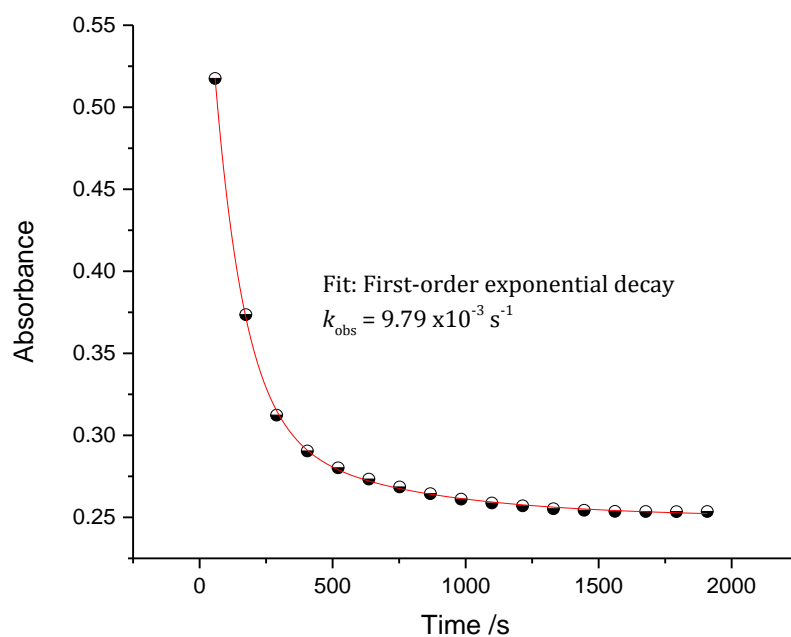


Figure B6: Absorbance spectrum of **C3S1** ($2.5 \times 10^{-4} \text{ M}$) and **1-MIm** ($5.0 \times 10^{-3} \text{ M}$ (30 fold)) obtained from Cary UV/Visible Spectrophotometry in ultrapure water ($I = 0.01 \text{ M}$, $0.009 \text{ M LiCF}_3\text{SO}_3$ + 0.001 M LiCl) 298.15 K.

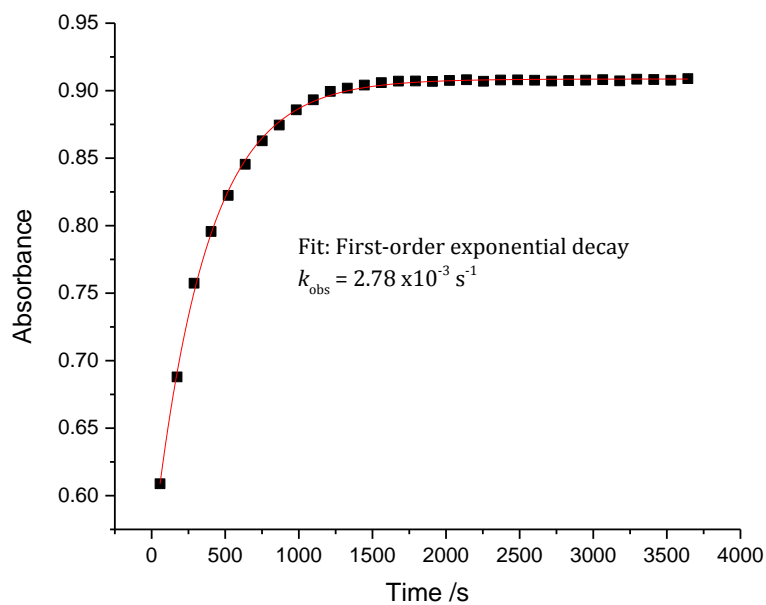


Figure B7: Absorbance spectrum of **C3S1** ($2.5 \times 10^{-4} \text{ M}$) and **Pyz** ($5.0 \times 10^{-3} \text{ M}$ (30 fold)) obtained from Cary UV/Visible Spectrophotometry in ultrapure water ($I = 0.01 \text{ M}$, $0.009 \text{ M LiCF}_3\text{SO}_3$ + 0.001 M LiCl).

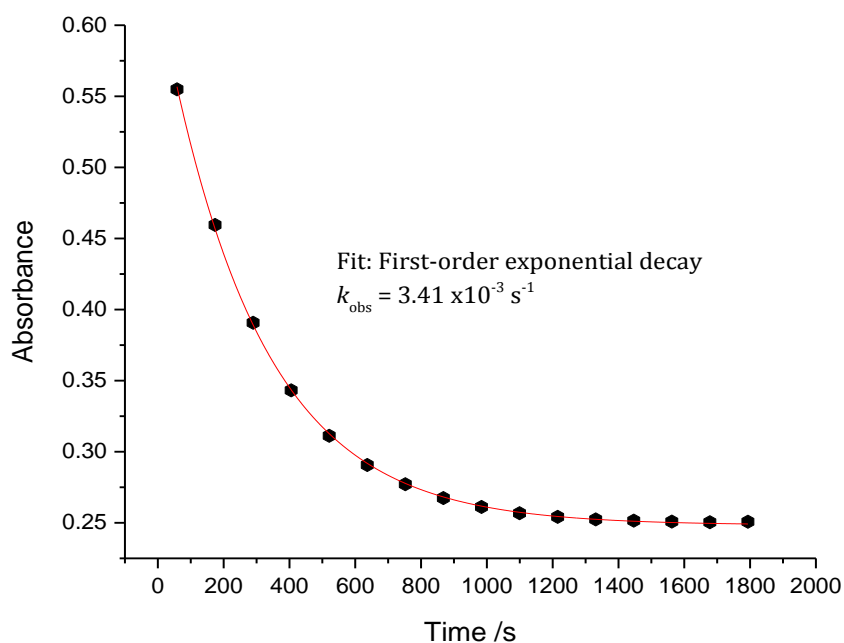


Figure B8: Absorbance spectrum of **C3S1** ($2.5 \times 10^{-4} \text{ M}$) and **His** ($5.0 \times 10^{-3} \text{ M}$ (30 fold)) obtained from Cary UV/Visible Spectrophotometry in ultrapure water ($I = 0.01 \text{ M}$, $0.009 \text{ M LiCF}_3\text{SO}_3 + 0.001 \text{ M LiCl}$).

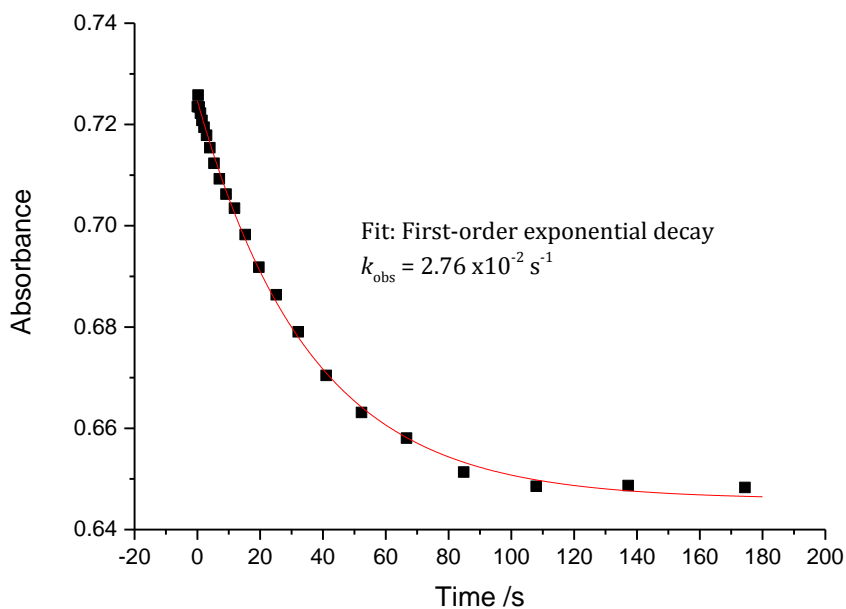


Figure B9: Absorbance spectrum of **C4S1** ($2.5 \times 10^{-4} \text{ M}$) and **1-MIm** ($5.0 \times 10^{-3} \text{ M}$ (30 fold)) obtained from Stopped-flow Spectrophotometry in ultrapure water ($I = 0.01 \text{ M}$, $0.009 \text{ M LiCF}_3\text{SO}_3 + 0.001 \text{ M LiCl}$) 298.15 K.

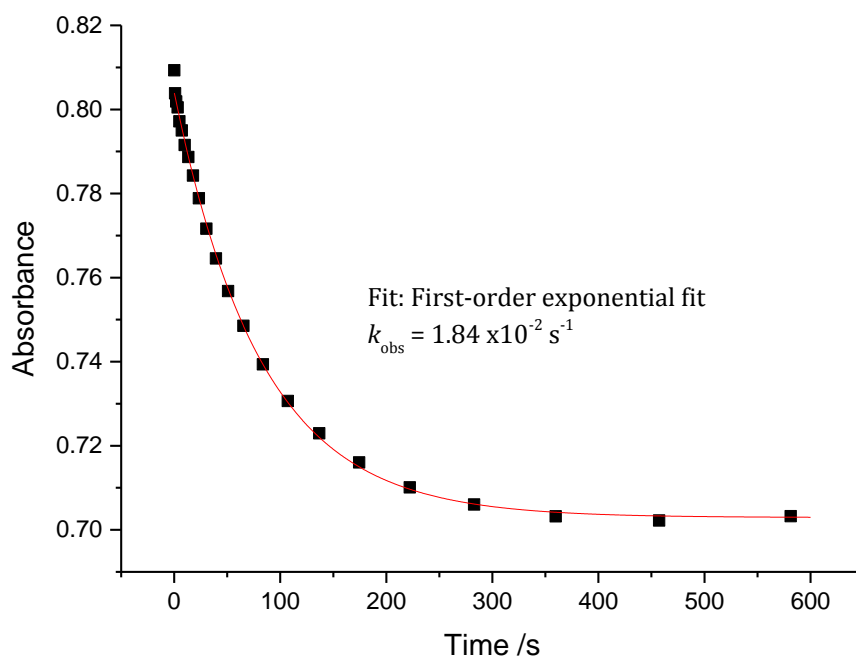


Figure B9: Absorbance spectrum of **C4S1** (2.5×10^{-4} M) and **His** (5.0×10^{-3} M (30 fold)) obtained from Stopped-flow Spectrophotometry in ultrapure water ($I = 0.01$ M, 0.009 M LiCF_3SO_3 + 0.001 M LiCl) 298.15 K.

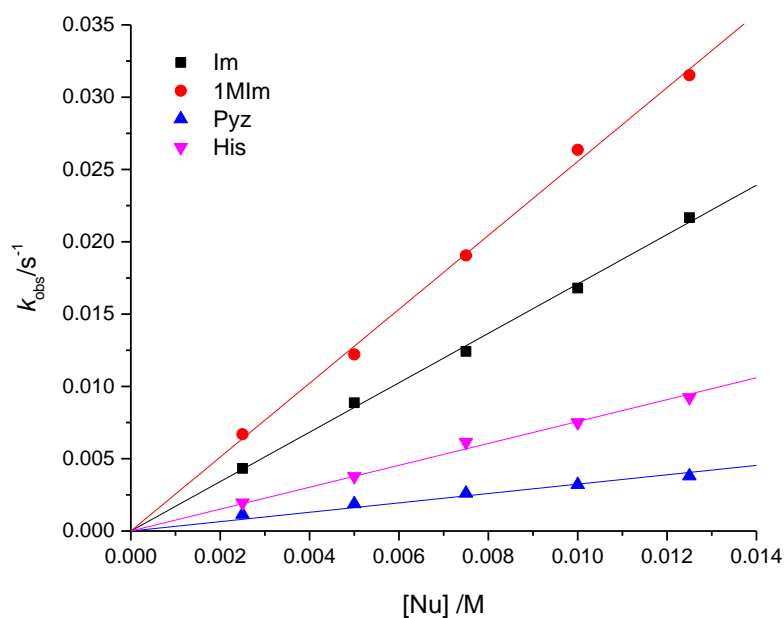


Figure B10: Dependence of the *pseudo* first-order rate constants (k_{obs}) on the concentrations of the azole nucleophiles for the chloride substitution from **C1S1** in ultrapure water solution ($I = 0.01$ M (0.009 M LiCF_3SO_3 + 0.001 M LiCl)) at 298.15 K.

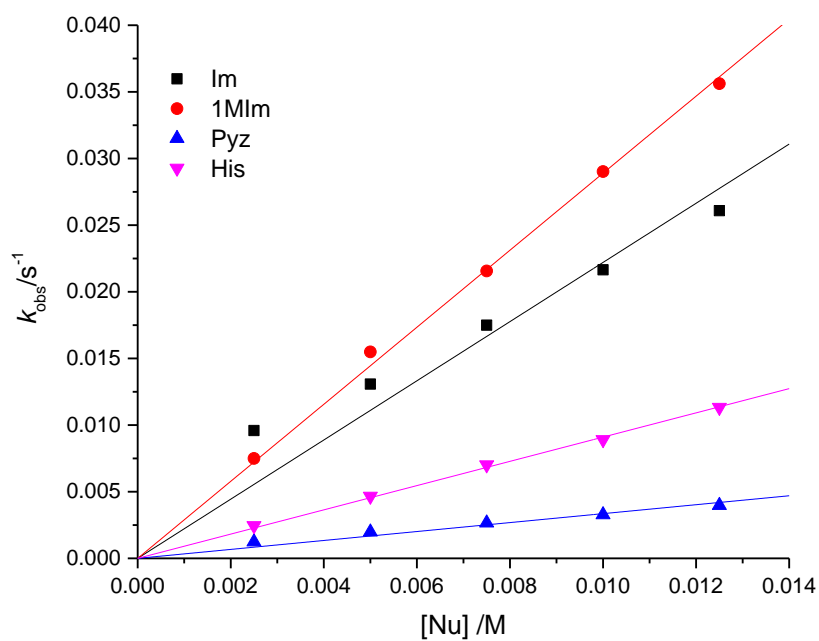


Figure B10: Dependence of the *pseudo* first-order rate constants (k_{obs}) on the concentrations of the azole nucleophiles for the chloride substitution from **C2S1** in ultrapure water solution ($I = 0.01 \text{ M}$ (0.009 M LiCF_3SO_3 + 0.001 M LiCl)) at 298.15 K.

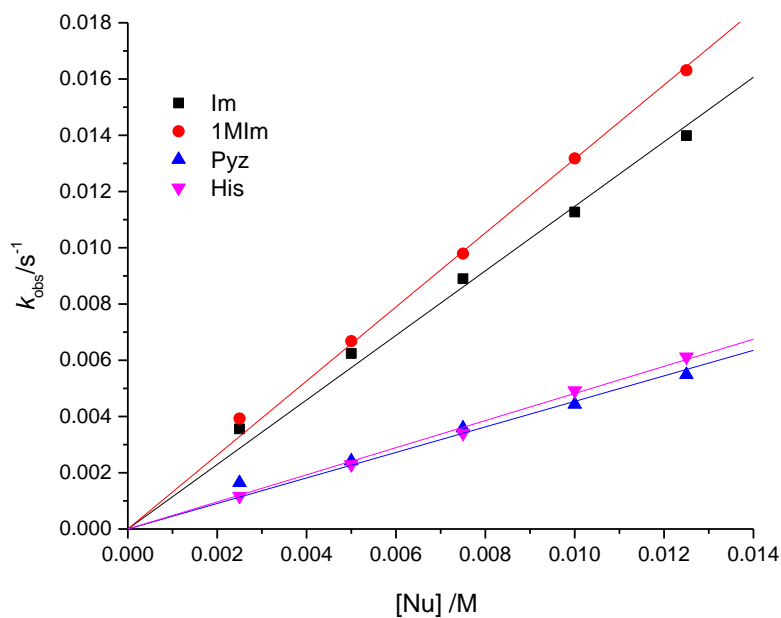


Figure B10: Dependence of the *pseudo* first-order rate constants (k_{obs}) on the concentrations of the azole nucleophiles for the chloride substitution from **C3S1** in ultrapure water solution ($I = 0.01 \text{ M}$ (0.009 M LiCF_3SO_3 + 0.001 M LiCl)) at 298.15 K.

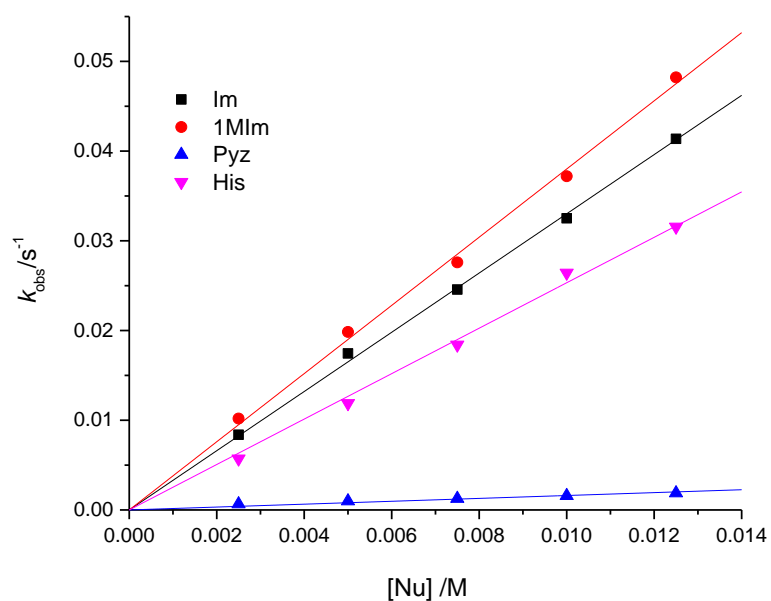


Figure B10: Dependence of the *pseudo* first-order rate constants (k_{obs}) on the concentrations of the azole nucleophiles for the chloride substitution from **C4S1** in ultrapure water solution ($I = 0.01$ M (0.009 M $\text{LiCF}_3\text{SO}_3 + 0.001$ M LiCl)) at 298.15 K.

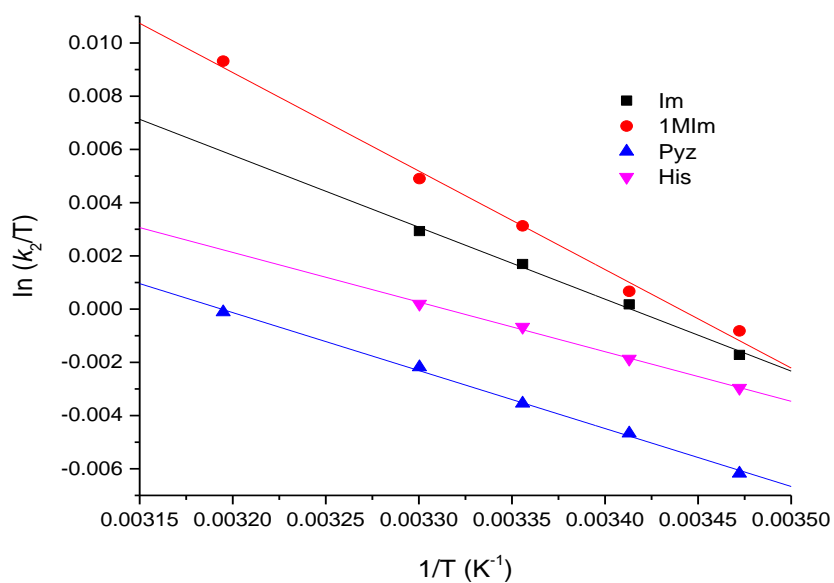


Figure B11: Eyring plot $\{\ln(k_2/T)$ against $1/T\}$ to obtain the activation parameters for the direct nucleophilic substitution reaction for **C1S1** with the four azole nucleophiles at various temperatures (ranging between 15 – 35 °C).

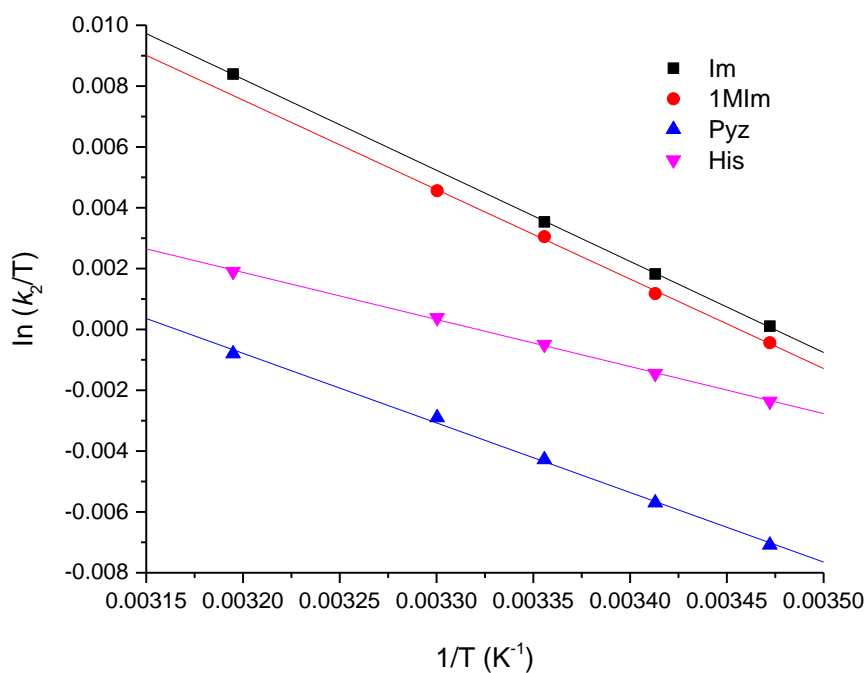


Figure B12: Eyring plot $\{\ln(k_2/T)$ against $1/T\}$ to obtain the activation parameters for the direct nucleophilic substitution reaction for **C2S1** with the four azole nucleophiles at various temperatures (ranging between 15 – 35 °C).

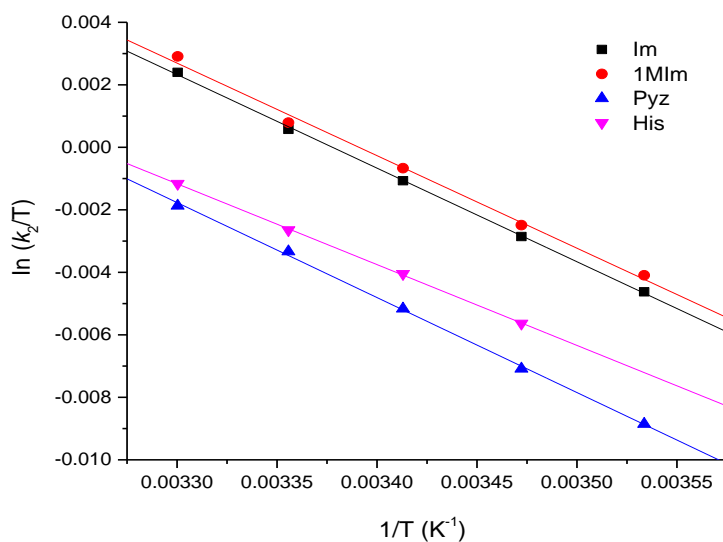


Figure B13: Eyring plot $\{\ln(k_2/T)$ against $1/T\}$ to obtain the activation parameters for the direct nucleophilic substitution reaction for **C3S1** with the four azole nucleophiles at various temperatures (ranging between 10 – 35 °C).

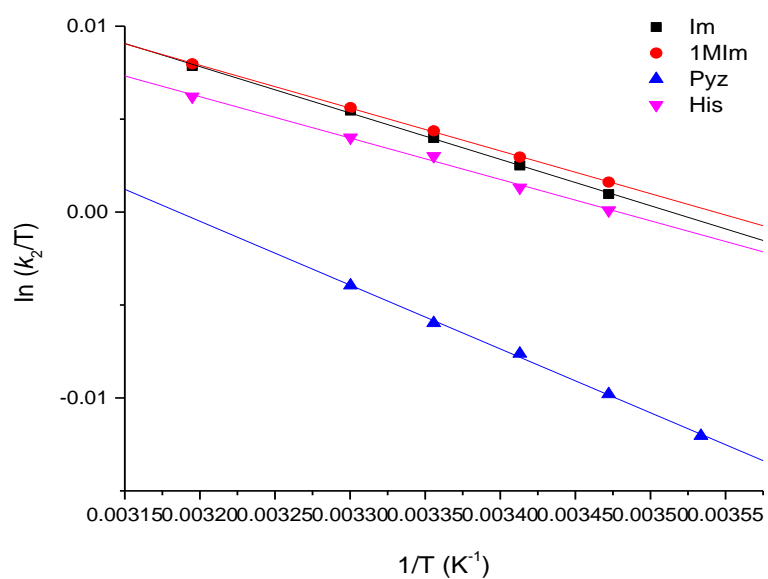


Figure B14: Eyring plot $\{\ln(k_2/T)$ against $1/T\}$ to obtain the activation parameters for the direct nucleophilic substitution reaction for **C1S1** with the four azole nucleophiles at various temperatures (ranging between 10 – 35 °C).